

DESIGN AND DEVELOPMENT OF A HIGH PRESSURE-HIGH TEMPERATURE  
WELLBORE SIMULATOR FOR INVESTIGATION OF THE IMPACT OF CYCLIC  
STRESSES ON THE INTEGRITY OF WELLBORE SECTIONS WITH CEMENT/CASING  
INTERFACES

By

**Zichao Lin**

A thesis submitted in partial fulfillment of the requirements for the degree of

Master of Science

in

Petroleum Engineering

Department of Civil and Environmental Engineering

University of Alberta

©Zichao Lin, 2021

## **Abstract**

An ideal cement job is expected to provide a perfect zonal isolation during the entire production life and even after the abandonment of the oil and gas wells. Variations of downhole stress conditions due to, for example, pressure cycles during the multistage hydraulic fracturing operations and temperature changes during the cyclic steam stimulation process, can affect the integrity of the cemented wellbore sections and, as a result, the zonal isolation may be lost. Investigation of the effects of downhole stress conditions and cement dehydration on the permeability of the cement matrix as well as the integrity of the cement/casing interface is, therefore, needed for a better understanding of why and how the zonal isolation may be lost under various downhole stress conditions, which would also be useful for the development of solutions to mitigate the associated formation fluid leakage problems.

Various blends of small-scale cement samples were prepared by using industrial procedures. Porosity and permeability of the cement samples were then measured by using standard testing protocols. After conducting initial screening tests, porosity measurement by drying was identified as the most appropriate method. Core flooding tests were conducted to measure the cement matrix permeability. A steady-state nitrogen permeability measurement of the wet cement sample was identified as the most suitable technique in this case.

A high pressure (43 MPa) and high temperature (120 °C) wellbore simulator was designed and constructed to investigate the integrity of the cemented wellbore sections under variable pressure and temperature conditions. The wellbore simulator is capable of measuring the permeability of the cemented casing sections (i.e. annular cement column between two casing sections) under cyclic temperature and pressure conditions. Potential leakage pathways due to micro-fractures

along the cement matrix and/or debonding along the cement/casing interfaces were visually inspected after conducting the permeability tests. Strength of the shear bonding between the inner casing and cement column was also measured.

Annular column of cement sections in the wellbore simulator was cured at 80 °C and 25 MPa for one week. Three groups of permeability measurements were conducted under constant pressure and temperature conditions. In the first and second groups of experiments, permeability measurements were conducted at constant pressures of 0, 10, 25 and 43 MPa while the temperature was kept constant at 80 °C and 50°C, respectively. The third group of tests was conducted to determine the effect of cement dehydration due to the time on the permeability of the cemented wellbore section under the same pressure and temperature conditions used in the first two groups of tests.

Based on the results of these initial experiments, three factors were identified as having the most significant effect on the permeability of the cemented annular (casing/cement/ casing) wellbore sections: i-) material (cement and casing) shrinkage/expansion caused by the temperature, ii-) casing shrinkage/expansion caused by the inner casing pressure change, and iii-) cement dehydration due to the nitrogen injection during each permeability measurement. The final permeability of the cemented annular section was controlled by the combined effects of these three factors.

Permeability of the cemented wellbore section was also measured under cyclic pressure (varying up and down between 3MPa and 43MPa) and constant temperature (50 °C) conditions. The permeability of the cemented wellbore section was measured after 12, 24, 36 and 50 cycles of pressure changes. Three groups of experiments were conducted under this category.

Comparison of results from the six groups of experiments conducted using the wellbore simulator revealed that once the debonding occurred at the cement/casing interface due to initial change in pressure and/or temperature, applying cyclic pressure did not significantly alter the permeability of the cemented wellbore section.

After finishing each group of permeability tests, cement to casing shear bonding strength measurements were also made. Visual observation of the casing surfaces indicated that the surface roughness conditions of the casings changed after each cement permeability test was conducted. The shear bonding strength increased (while the final permeability of the cemented wellbore section decreased) significantly with the increasing casing surface roughness. It was also found that the cyclic pressure tests caused a significant reduction in the cement to casing shear bonding strength and a corresponding increase in the final permeability of cemented wellbore sections.



## **Acknowledgement**

First and foremost, I would like to express my sincere gratitude to my supervisor, Dr. Ergun Kuru, for offering me the graduate research assistant position, priceless guidance and support during the project, making my research dream come true. His patience, motivation, immense knowledge and positive attitude towards the research will always be the bright lighthouse during my long way of sailing in the boundless academic ocean.

I would like to thank Dr. Simon Iremonger, Mr. Blair Fisher, and Mr. Jeff Spence for their professional guidance, positive input from the industrial perspectives, and profound discussions during the numerous project progress meetings.

This study has been conducted as part of the collaborative research project supported by the Natural Sciences and Engineering Research Council of Canada (NSERC) and Sanjel Energy Services (NSERC EGP 507672-16 Kuru, NSERC CRDPJ 531509-18 Kuru).

I am grateful to my committee members, Dr. Tayfun Babadagli, Dr. Huazhou Li, and Dr. Nobuo Maeda, for serving my M.Sc final exam.

My sincere thanks go to Mr. John F Czuroski, Mr. David Wang, and Mr. Lixing Lin for their technical support during the project. I would also like to express my gratitude to my colleagues and friends, Xinxiang (Jason) Yang, Hongbo (Rob) Chen, Yanxin (Sussi) Sun, Siqi Guo, Mingze Gao, Abdulla Abou-Kassem, and Scott Charabin, for their academic discussion and help during my life of pursuing M.Sc.

My heartfelt thanks go to my parents, Mr. Changping Lin and Mrs. Chenge Li, grandparents, Mr. Yuhuan Li, Mrs. Shuqin Jiang, Mr. Qingzhi Lin, Mrs. Zhiai Lin and my partner, Ms. Xinyi

(Joanne) Lai, for their love, prayers, understanding and encouragement in my life. They are the moonlight during the darkest night, a ray of sunshine during the cloudy days that keeps me running further unswervingly.

Last but not least, thanks to my Bengal cat, Mango, for the emotional support and accompanying me during the sleepless nights of the project.

# Table of Contents

Abstract .....	ii
Acknowledgement .....	v
List of Tables .....	x
List of Figures .....	xii
Chapter 1 Introduction .....	1
1.1 Overview .....	1
1.2 Statement of the problem .....	5
1.3 Objectives and scopes of the study .....	8
1.4 Contributions of the research .....	11
1.5 Organization of dissertation .....	12
Chapter 2 Literature review and background.....	15
2.1 Potential leakage pathways caused by cement failure in oil wells .....	15
2.1.2 Potential leakage through the interface between cement and casing.....	19
2.2 Permeability measurement techniques for the cement.....	22
2.2.1 Permeability measurement techniques for porous media .....	23
2.2.2 Gas steady state permeability on dried cement samples.....	25
2.2.3 Liquid steady state permeability on wet cement samples .....	28
2.3 Cement performance evaluation by using physical wellbore simulators.....	29
2.3.1 Large-scale wellbore simulators .....	30
2.3.2 Small-scale or bench type wellbore simulators .....	39
Chapter 3 Cement Porosity and Permeability Measurement .....	43
3.1 Summary .....	43
3.2 Introduction.....	44
3.3 Material and methods.....	48

3.3.1 Preparation of cement samples .....	48
3.3.2 Porosity measurement methods .....	53
3.3.3 Steady-state permeability measurement methods.....	57
3.4 Results and discussions.....	60
3.4.1 Flowrate and inlet pressure steady state criterion .....	60
3.4.2 Validation of the porosity measurements .....	61
3.4.3 Cement porosity by drying methods .....	63
3.4.4 Steady-state nitrogen permeability validation and data comparison .....	64
3.5 Conclusions.....	69
Appendix A Experimental Procedure .....	71
A.1 Cement sample preparation.....	71
A.2 Steady-state permeability measurement.....	83
Appendix B Procedure for porosity measurement by drying .....	89
Chapter 4 Design and Development of the Physical Wellbore Simulator for Evaluating Oil Well Cement Performance under In-Situ Pressure and Temperature Conditions .....	90
4.1 Summary .....	90
4.2 Introduction.....	91
4.3 The development process of the physical wellbore simulator system.....	92
4.3.1 The development of the wellbore simulator main body .....	93
4.3.2 The design of the wellbore simulator stand .....	113
4.3.3 The design of flowline .....	113
4.4 Results and discussion .....	115
4.5 Conclusions.....	123
Appendix C Protocol for operating the wellbore simulator system.....	124
Appendix D CAD drawing for the wellbore simulator system.....	132

Chapter 5 Assessment of the Permeability of the Cemented Wellbore Sections Under Elevated Temperature and Cyclic Pressure Conditions.....	137
5.1 Summary.....	137
5.2 Introduction.....	138
5.3 Materials, equipment, and methods .....	140
5.3.1 Validation of the newly designed physical wellbore simulator .....	140
5.3.2 Constant temperature and constant pressure experiment.....	143
5.3.3 Constant temperature and cyclic pressure experiment.....	146
5.3.4 Leakage pathway detect and cement removal .....	146
5.4 Results and discussions.....	147
5.4.1 Validation of wellbore simulator .....	147
5.4.2 Constant pressure and temperature experiments.....	148
5.4.3 Cyclic pressure and constant temperature experiments .....	154
5.4.4 Leakage pathway detection and shear bonding strength test.....	157
5.5 Conclusions.....	165
Appendix E Experimental procedure.....	167
E.1 Experimental procedure for the validation of the wellbore simulator.....	167
E.1.1 Experimental procedure for validating the pressure and temperature rating .....	167
E.1.2 Experimental procedure for cement removal validation .....	169
E.2 Procedure of mixing 1L ECOprime cement slurry for the wellbore simulator experiments	175
E.3 Procedure for constant temperature and constant pressure experiment .....	176
Chapter 6 Conclusions and Recommendations.....	178
6.1 Conclusions.....	178
6.2 Recommendations for the future work .....	181
Bibliography .....	183

## List of Tables

Table 2- 1 The prepared samples under different w/c ratios and finenesses (Based on Coleman and Corrigan, 1941) .....	26
Table 3- 1 Cement w/c ratio and calculated slurry density.....	49
Table 3- 2 Sample calculation procedure for Class G and G EXP shown in Figure 3-5.....	54
Table 3- 3 One of the flow rates calculations for G Abandonment dried sample .....	61
Table 3- 4 Porosity results for the cement measured by drying method .....	63
Table 3- 5 Measurement data for 1st and 2nd Scioto Sandstone.....	65
Table 3- 6 steady-state permeability measurement results for different samples by water and nitrogen .....	67
Table A- 1 Comparison of properties for PVC-P and PTFE materials ("PVC-P vs. PTFE: MakeItFrom.com," 2021) .....	76
Table 4- 1 Hoop Stress calculation for normal schedule pipes with maximum working pressure	97
Table 4- 2 Hoop Stress calculation for normal schedule pipes with 75% working pressure.....	99
Table 4- 3 Selected casing based on the maximum working pressure .....	99
Table 4- 4 Selected casing based on the 75% working pressure .....	100
Table 4- 5 Outer casing selection based on inner casing from table 4-3 and 4-4.....	100
Table 4- 6 Overall annulus gap and cement column length calculation based on the cement volume of 1 litter.....	101
Table 4- 7 Hoop stress calculation based on the field data.....	102
Table 4- 8 Hoop stress calculation for API P110 tubing 3.5in*0.375in .....	102
Table 4- 9 Hoop stress calculation for API P110 tubing 3.5in*0.254 .....	103
Table 4- 10 Work pressure calculation based on the field Hoop stress for API P110 3.5in*0.254in tubing .....	103

Table 4- 11 inner and outer casing, working pressure and Hoop stress summary for API tubing selection .....	104
Table 5- 1 Experiment order for three constant pressure constant temperature experiments.....	145
Table 5- 2 Average permeability results for the first constant pressure and constant temperature experiment.....	149
Table 5- 3 Average permeability results for the second constant pressure and constant temperature experiment .....	151
Table 5- 4 Average permeability results for the third constant pressure and constant temperature experiment.....	153
Table 5- 5 Average permeability results for the first cyclic pressure and constant temperature experiment.....	155
Table 5- 6 Average permeability results for the second cyclic pressure and constant temperature experiment.....	156
Table 5- 7 Average permeability results for the third cyclic pressure and constant temperature experiment.....	157
Table 5- 8 Shear bonding strength results.....	164

## List of Figures

Figure 1- 1 Main parameters causing annular gas migration (Modified from Bonett and Pafitis (1996)).....	2
Figure 1- 2 Potential leakage pathways (Modified from Celia et al. (2005)).....	3
Figure 1- 3 Unrepaired wells with SCVF, GM, or both in 2000-2019.....	4
Figure 1- 4 a) pure cement plug with 1in diameter and approximate 1in length. b) casing cement sample with 1in diameter and 1in length .....	9
Figure 1- 5 Wellbore simulator main body (left); cross-sectional view of wellbore simulator schematic (right) .....	9
Figure 1- 6 Small scale bulk cement sample and cement casing sample (Chapter 3) .....	13
Figure 1- 7 Large scale cement sample in the wellbore simulator and the wellbore simulator main body (Chapter 4) .....	13
Figure 2- 1 Potential cause for the failure of the cement system (from Viswanathan et al., 2008) .....	16
Figure 2- 2 Schematic of the test device for the Deformation and damage of cement sheath in gas storage wells under cyclic loading (Li et al., 2021).....	21
Figure 2- 3 Test device for evaluating the cement casing bonding integrity (Lamik et al., 2021).....	21
Figure 2- 4 Permeability results from Goode (1962).....	27
Figure 2- 5 Test equipment used in large-scale density evaluation by Carter and Slagle (1972). .....	32
Figure 2- 6 Schematic of large scale temperature evaluation apparatus by Carter and Slagle (1972).....	32
Figure 2- 7 Schematic of large scale dehydration evaluation apparatus by Carter and Slagle (1972).....	33
Figure 2- 8 Schematic of the gas flow model by Garcia and Clark (1976) .....	34
Figure 2- 9 Pressure simulator by Levine et al. (1979).....	35
Figure 2- 10 Schematic of test figure used to study gas leakage by Tinsley et al. (1980).....	36
Figure 2- 11 Schematic of test fixture for pressurized gas percolation and pressure-transmission tests by Sabins et al. (1982) .....	37
Figure 2- 12 Annular gas flow laboratory testing apparatus by Bannister et al. (1984).....	39



Figure 2- 13 Gas flow simulator by Cheung & Beirute (1985) .....	40
Figure 2- 14 Dynamic permeability apparatus by Drecq and Parcevaux (1988).....	41
Figure 2- 15 Wellbore-Simulation Apparatus by Zhang et al., 2018.....	42
Figure 3- 1 The trend of leaking wells in Alberta (Alberta Energy Regulator, 2021).....	45
Figure 3- 2 Potential leakage pathways in the wellbore barrier system .....	47
Figure 3- 3 a (left side) the high speed mixer used for small sample preparation; b (right side) the low speed mixer used for small sample preparation.....	51
Figure 3- 4 OFITE MODEL 350 porosimeter .....	53
Figure 3- 5 Mass change vs. time for G EXP and Class G cement plug samples .....	55
Figure 3- 6 Schematic for the porosimeter used in this study.....	56
Figure 3- 7 Klinkenberge correction for the dried G Abandonment sample .....	59
Figure 3- 8 Inlet pressure vs. time for dried G Abandonment sample.....	60
Figure 3- 9 Pressure vs time for the saturated G Abandonment plug sample.....	66
Figure A- 1 Cement blends used, from left to right, Class G, G EXP, G Abandonment, and REMEDIALmix EC.....	72
Figure A- 2 Measurement cup on the balance for small scale sample preparation .....	74
Figure A- 3 1in*1in PTFE mould for the cement sample.....	77
Figure A- 4 Semi transparent pipette used for injecting cement slurry to the mould for the preparation of small scale samples .....	78
Figure A- 5 Schematic for the samples in the curing cell for small scale sample preparation.....	79
Figure A- 6 Curing cell used for the preparation of small scale samples. ....	80
Figure A- 7 Setup before curing of small scale samples .....	81
Figure A- 8 Setup for removing the mould of the small scale sample .....	82
Figure A- 9 Sample storage for small scale cement plug samples .....	83
Figure A- 10 Schematic for the steady-state permeability measurement .....	84
Figure A- 11 Schematic for Hassler type core holder ("ASTM D4525 - 13e2 Standard Test Method for Permeability of Rocks by Flowing Air", 2021).....	85
Figure A- 12 Working mechanics of the bubble flowmeter (Solutions, 2021) .....	87

Figure B- 1 Schematic of sand bath for drying the cement .....	89
Figure 4- 1 wellbore simulator schematic.....	93
Figure 4- 2 Design cycle for the wellbore simulator .....	94
Figure 4- 3 1Cement curing cell with piston seal and flange seal .....	106
Figure 4- 4 Connection first design - holes drilled on flanges.....	107
Figure 4- 5 Drawing for the inner casing with applied pressure.....	108
Figure 4- 6 Drawing for the caps with applied pressure.....	109
Figure 4- 7 Overall set up of first design before simulation.....	111
Figure 4- 8 FEA safety factor for the first design.....	112
Figure 4- 9 Flowline Schematic for Curing Cement.....	114
Figure 4- 10 Flowline Schematic for Nitrogen Permeability Test.....	115
Figure 4- 11 FEA safety factor result for increasing the number of holes .....	117
Figure 4- 12 FEA safety factor result for increasing the size of holes .....	118
Figure 4- 13 FEA safety factor result for the final design .....	119
Figure 4- 14 FEA safety factor result for bolt-in design with Grade 60 iron .....	121
Figure 4- 15 FEA safety factor result for larger hole design with Grade 60 iron.....	121
Figure 4- 16 FEA safety factor result for wellbore simulator stand final design with ANSI 4130 steel .....	122
Figure 4- 17 Dimension of the stand with the simulation result.....	122
Figure C- 1 Bottom/Top Cap .....	125
Figure C- 2 Inner casing with surface labels .....	126
Figure C- 3 Longitudinal direction on the inner casing.....	126
Figure C- 4 1/4 HIP connection connected with wellbore simulator main body.....	128
Figure C- 5 1/4 in gland ("Taper Seal Connections   High Pressure Company", 2021).....	129
Figure C- 6 Female opening schematic ("Taper Seal Connections   High Pressure Company", 2021).....	129

Figure D- 1 Final CAD drawing for the wellbore simulator stand .....	132
Figure D- 2 Final CAD drawing for inner casing .....	133
Figure D- 3 Final CAD drawing for Teflon ring .....	134
Figure D- 4 Final CAD drawing for outer casing and flange .....	135
Figure D- 5 Final CAD drawing for caps .....	136
Figure 5- 1 Schematic for the set up of cement removal validation experiment .....	142
Figure 5- 2 Validation result of the wellbore simulator pressure rating .....	147
Figure 5- 3 Validation result of the wellbore simulator pressure and temperature rating .....	147
Figure 5- 4 Force applied for cement removal validation using loading frame.....	148
Figure 5- 5 Leakage detection result for the first constant pressure and temperature experiment .....	158
Figure 5- 6 Leakage detection result for the second constant pressure and temperature experiment.....	159
Figure 5- 7 Leakage detection result for the third constant pressure and temperature experiment .....	160
Figure 5- 8 Leakage detection result for the first cyclic pressure and constant temperature experiment.....	161
Figure 5- 9 Leakage detection result for the second cyclic pressure and constant temperature experiment.....	162
Figure 5- 10 Leakage detection result for the third cyclic pressure and constant temperature experiment.....	163
Figure E- 1 connected wellbore simulator system .....	167
Figure E- 2 Sealing of bottom surface for the outer casing of the cement removal test sample	169
Figure E- 3 High-speed mixer for large scale sample preparation .....	170
Figure E- 4 bottom holder for cement removal using loading frame .....	171
Figure E- 5 Overall setup for cement removal using loading frame.....	172
Figure E- 6 Hydraulic press setup.....	173
Figure E- 7 Overall setup for cement removal using the hydraulic press.....	174

Figure E- 8 Low-speed mixing system with water bath ..... 175  
Figure E- 9 Cement injecting process for wellbore simulator ..... 176

# Chapter 1 Introduction

## 1.1 Overview

Annular gas migration in cemented sections of the oil and gas wells has been recognized as one of the most severe problems in the petroleum industry (Al-Yami et al., 2009). Bonett and Pafitis (1996) explained the parameters that caused the annular gas migration through the cemented wellbore sections shown in Figure 1-1. All the parameters will finally result in the pressure imbalance between the gas-bearing formation and the cement, eventually causing the gas and other fluid to invade the annulus. Gas migration can cause problems ranging by severity, from a blowout in rare cases to the more common non-zero sustained casing pressure at the surface. Khalifeh and Saasen (2020) stated the importance of maintaining well control by using sufficient barriers in the well, and one of the critical barriers in the wellbore is the cement column. During the drilling of the well, production of the well and even after the abandonment of the well, cement needs to provide the proper zonal isolation function. The loss of zonal isolation of cement can result in severe economic loss, environmental pollution, and even loss of lives. Hefley et al. (2011) stated that the average cost for a Marcellus shale gas investment was \$7.6 million. The cost of a primary cement job is 5% of the total investment of the well. In comparison, an additional 12% cost of the entire well investment would be added if the cement remediation with squeezing was needed. Besides, the remediation job needs to follow the local policies and regulations and be approved by the regulators, which can be time-consuming (Bol et al., 1991). Furthermore, the remediation job, which commonly requires the perforation of the casing, can lead to further problems of zonal isolation.

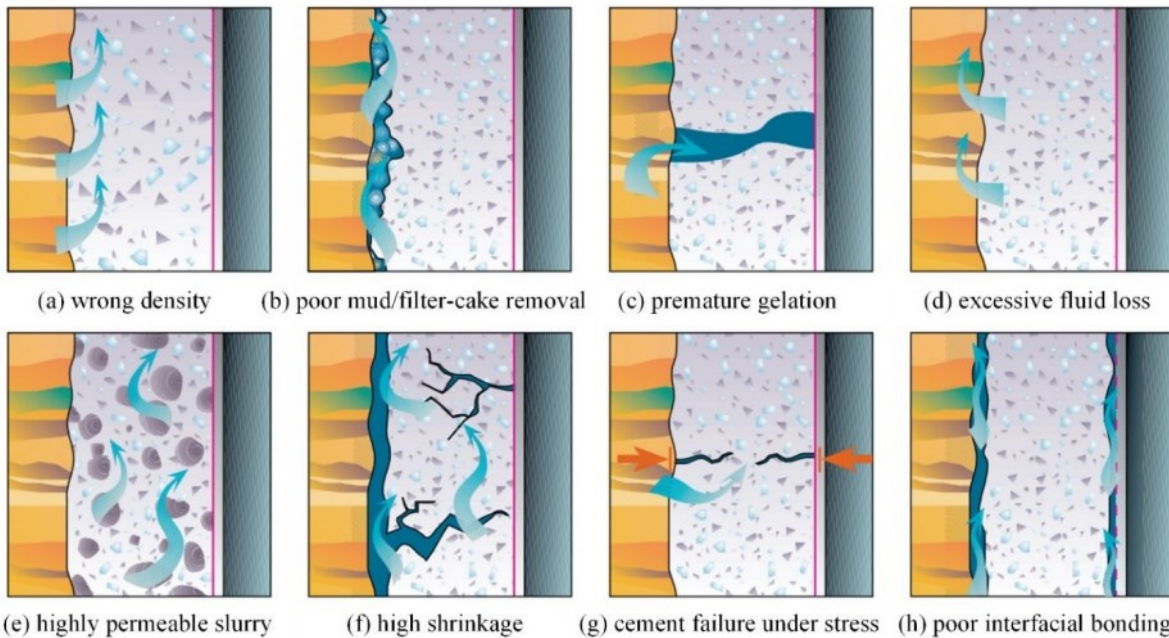


Figure 1- 1 Main parameters causing annular gas migration (Modified from Bonett and Pafitis (1996)).

Furthermore, even if the cement was appropriately placed initially, the bonding or the function of zonal isolation may be lost throughout time. The potential leakage pathways are summarized in Figure 1-2 (Modified from Celia et al. (2005)). The potential leakage pathways can be through the contact surface between cement and casing (1 and 2); through the cement matrix (3); through the fracture casing (4); through the fracture cement (5,); through the contact surface between the cement and formation (6). Through all these cases, once the gas flows through the pathway, the permeability of the overall system will be changed. These cases are also based on the perfect centralization of the casing. In the real world, the non-centralized casing can make the risk of failure even higher.

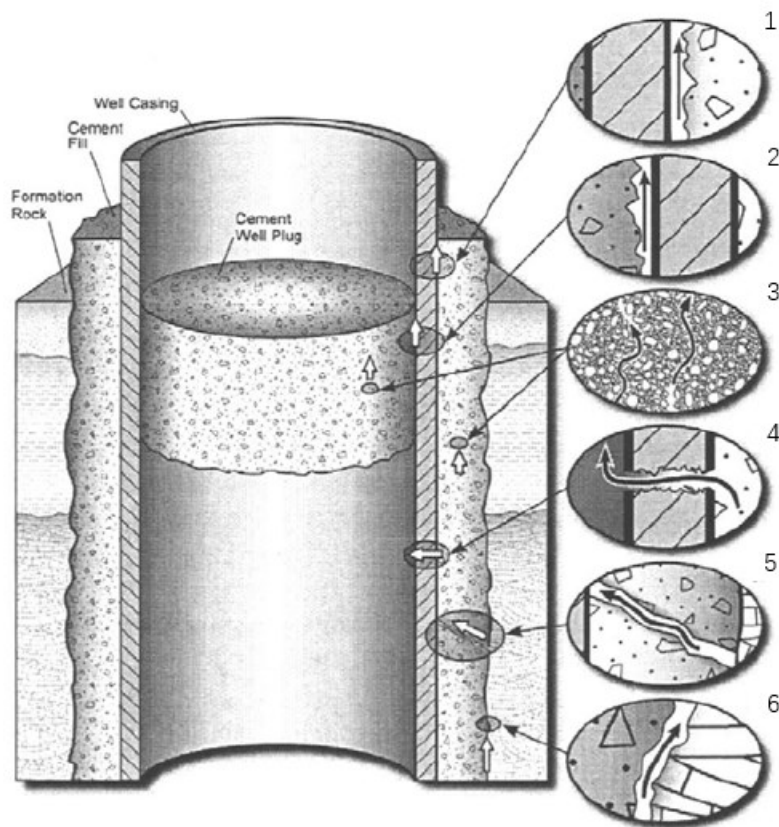


Figure 1- 2 Potential leakage pathways (Modified from Celia et al. (2005))

As a main component of natural gas and Greenhouse Gas (GHG), methane has a global warming potential of more than 70 times greater than carbon dioxide (CO<sub>2</sub>) over a 20-year period (Government of Canada, 2021) or 25 times greater than carbon dioxide over a 100-year period (Alberta Energy Regulator, 2021). Oil and gas sectors are the largest industrial methane emitters, contributing 44% of total methane emissions in Canada (Government of Canada, 2021). The gas leakage from the wellbore can be classified into two categories, Surface casing vent flow (SCVF) and gas migration (GM). SCVF is the gas, liquid, or both that come out on the surface inside the wellbore area. GM is detectable gas flow at the surface area outside the wellbore (Alberta Energy Regulator, 2021). From 2000 to 2019, the trend of unrepaired wells with SCVF, GM, or both increases, shown by Figure 1-3 (Alberta Energy Regulator, 2021). The Government

of Canada also states that fixing leaks can help to reduce the fugitive methane through upstream of the oil and gas sector (Government of Canada, 2020).

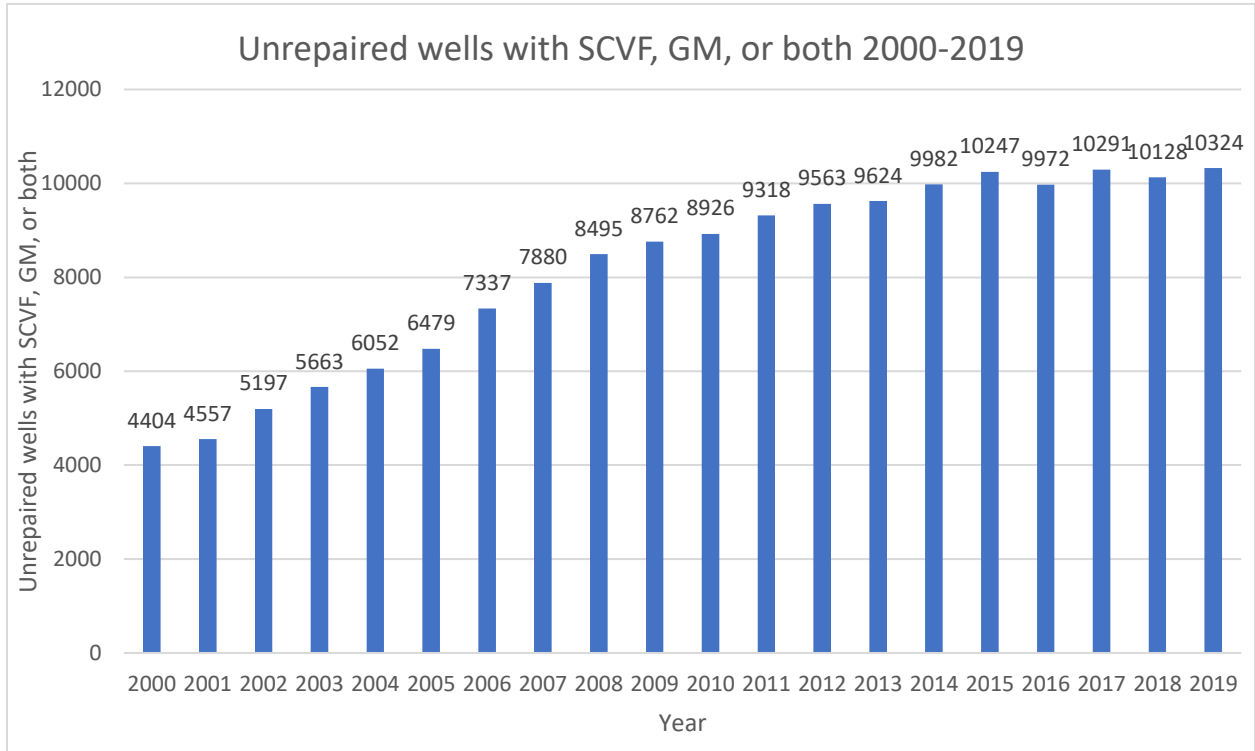


Figure 1- 3 Unrepaired wells with SCVF, GM, or both in 2000-2019



## 1.2 Statement of the problem

The interest in cement permeability has increased since the 1900s due to the increasing underground gas storage reservoirs (Goode, 1962). The permeability is considered as a key parameter for evaluating the durability and performance of the cement. Despite the importance of cement permeability, there is no API standard technique for measuring the permeability of the cement and few apparatus that can simulate the cement curing under in-situ temperature and pressure while measuring the permeability of the cement column under the cyclic load.

Considering all the gas migration cases described previously in Figure 1-2, the main reason for the gas migration can be identified as the overall non-zero permeability of the system. The system can be composed of pure cement, cement/casing, casing/cement/casing, casing/cement/formation, and cement/ formation combinations. For the pure cement system, only the cement matrix permeability is measured. However, in other systems, more than one component is involved. For example, two components are involved in a casing/cement system, cement and casing. Therefore, the measured permeability of such a system can be sourced from the cement matrix, the casing fracture, and the micro channels in the casing-cement interface. Therefore, determining the main source of permeability is a challenging task. Many previous studies only measured the permeability of the cement plug(s) (Ozyurtkan et al., 2013; Celia et al., 2005; Bauer, S.J. et al., 2019). The single cement plug permeability cannot precisely simulate the gas migration in the wellbore. In real life, there will be more than one element in the wellbore, although it is a good starting point to measure the permeability of the pure cement plug.

Moreover, to simulate the downhole conditions, the curing pressure and temperature should be close to the downhole conditions. Many previous experiments cure the cement under ambient pressure (Goode, 1962; Maharidge et al., 2016; Coleman & Corrigan, 1941) and under ambient temperature (Maharidge et al., 2016). Neither ambient pressure nor ambient temperature can represent the downhole conditions. As shown by Goode (1962), the different curing temperatures will affect the permeability of the cement. Therefore, it is essential to cure the cement under downhole conditions. However, it is not easy to achieve the High-Pressure High Temperature (HPHT) conditions in the lab. The apparatus needs to be carefully designed to withstand the

HPHT. One of the most recent wellbore simulators can reach up to 1500psi operating pressure (Li, Vandenbossche, Janssen & Iannacchione, 2018). However, 1500psi is still not high enough to simulate the downhole condition, for example, the Montney formation, which has more than 5000 psi reservoir pressure.

Besides, the shape of the cement can also be the factor that affects the permeability of the system. Therefore, if the cement between two casings (i.e., casing/cement/casing model) is investigated, the permeability measured from the pure cement plug prepared in a cylindrical mould cannot sufficiently simulate the casing/cement/casing condition as the cement prepared from a mould will be cylindrical shape rather than the hollow cylinder in casing/cement/casing.

Hydraulic fracturing became an industry standard and has been extensively used for the exploration of shale oil/shale gas resources, mainly because it is cost-efficient, very effective and safe (Energy, 2021). Nowadays, it is common to have 50 stages of hydraulic fracturing jobs depending on the formation. Due to the multiple pressure cycles used for multi-stage hydraulic fracturing jobs, cemented wellbore sections are exposed to a large amount of mechanical cyclic stresses, which may cause debonding of the annular cement column and, thus, increase the system permeability. Moreover, the refracturing of the previously hydraulically fractured reservoirs, may impose further mechanical stresses on the cemented wellbore sections, which might have been already damaged from the previous stimulation operations.

Besides the cyclic pressure load, the thermal stresses generated by injecting the cold or hot fluid downhole, such as cyclic steam stimulation, can also play a role in affecting the permeability of the cemented wellbore sections (Lavrov & Cerasi, 2013). Currently, few experimental apparatus are available to study the combined effects of the cyclic pressure and thermal load on the permeability of cemented wellbore sections while setting and curing cement under in-situ conditions.

Another critical parameter to investigate can be the type of cement. In many previous studies, such as Opedal et al. (2014), Bauer, S.J. et al. (2019), Coleman & Corrigan (1941), only the neat Portland cement was used. Although the neat Portland cement is a good starting point, it cannot simulate the most practical applications mainly because the neat Portland cement is not commonly used in the field applications due to the instability of the slurry leading to a settling of particles and reduced cement performance. In order to develop a more realistic experimental program,

commercial cement blends should be used to simulate the actual field applications as it has been rigorously engineered to provide known performance under downhole conditions.

Since the 1960s, many studies have developed physical wellbore simulators for evaluating the performance of cement under downhole conditions. These efforts can be categorized under two groups, large scale simulators (Carter and Slagle, 1972; Carter et al., 1973; Garcia and Clark, 1976; Levine et al., 1979; Tinsley et al., 1980; Sabins et al., 1982; Bannister and Lawson, 1985) and the small-scale bench-type simulators (Tinsley et al., 1980; Sabins et al., 1982; Cheung and Beirute, 1985; Rogers et al., 2004; Li, Vandenbossche, Janssen & Iannacchione, 2018). Large-scale simulators used relatively long cement columns for testing. The cement columns in the large-scale simulators typically have a length between 10 to 30 ft. These relatively long cement columns required significant storage space, and it was challenging to measure the properties of the cement consistently. Control of the curing temperatures, pressures and other parameters was difficult under most circumstances. For example, a very long time was needed for the whole cement column to reach uniform temperatures. Besides, the need for more cement material and the casing in most large-scale simulators could not be reused make the large-scale simulator very costly. Therefore, after the development of the first bench-type simulator, which was modified from an API fluid loss cell (Cheung and Beirute, 1985), the bench-type simulators became more and more popular due to their low cost and ease of handling. There are also some commercial HPHT cement hydration analyzers (CHAs), such as Model 7200 Cement Hydration Analyzer by Chandler Engineering (2015, 2017), the Fluid Gas Migration Analyzer #120-57 by OFI Testing Equipment (2014), and the Fluid/Gas Migration Analyzer TG-7150 by Shenyang Taige Oil Equipment (2017). The design of CHAs is still based on the modification of the API fluid loss cell. However, these commercial CHAs were mainly designed to study the gas migration potentials during the gel or transition phase of cement. From the commercial aspect, few apparatuses were designed to set and cure the cement under in-situ conditions while simulating the cyclic mechanical and thermal stress with the function of permeability measurement.

To summarize, currently, there is no API standard for measuring cement permeability. Although the small scale cement plug samples have been used for evaluating the permeability of cement in many studies, they still had the limitation of simulating the wellbore due to the lack of interface (i.e. cement/casing). As for the apparatus used for testing cement performance under downhole

conditions, few previous set-ups were capable of studying the influence of cyclic pressure and temperature loads on the permeability of the cement while setting and curing cement with in-situ conditions. Besides, fewer studies correlating the permeability of small-scale cement plug samples to the permeability of the cement prepared in the physical simulator.

### **1.3 Objectives and scopes of the study**

The primary objective of this research is to conduct experimental studies of the factors affecting the permeability of the cemented wellbore systems under simulated downhole conditions. Small-scale cement plug samples (Figure 1-4a) with 1in diameter and approximately 1in length were studied first to gain a basic understanding of the permeability of pure cement plugs and to establish suitable procedures for measuring cement porosity (i.e. by drying) and permeability (i.e. the steady-state method).

After the preliminary work, small-scale cemented-casing samples (Figure 1-4b) with 1in outer diameter and 1in length were prepared. The permeabilities of the small-scale cemented-casing samples were measured by using the technique developed from the first stage of the work. This was an intermediate step forward in testing cement properties under simulated downhole conditions since the casing was introduced as an additional constraint on top of the pure cement plug. Then, based on the experience gained from the previous two stages, a physical wellbore simulator (Fig.1-5) was designed and developed to study variables affecting the permeability of the cemented wellbore sections ( i.e. annular cement columns in between two casings) under simulated downhole conditions.

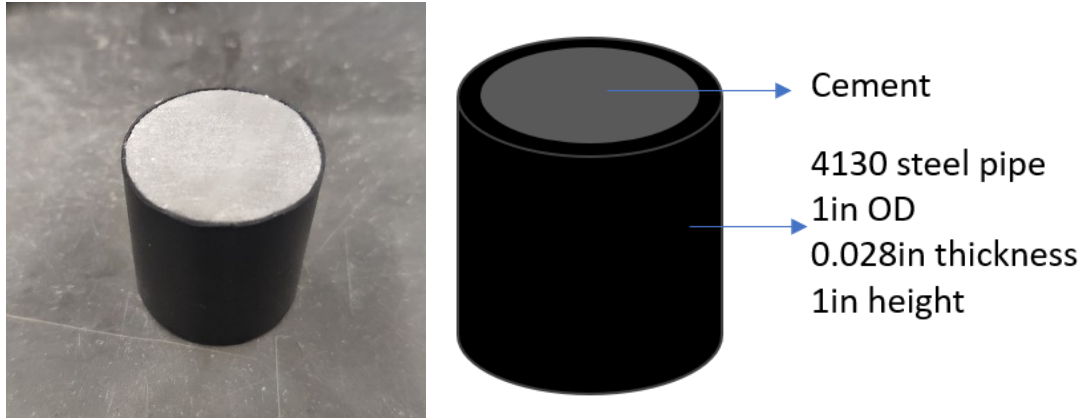


Figure 1- 4 a) pure cement plug with 1in diameter and approximate 1in length. b) casing cement sample with 1in diameter and 1in length

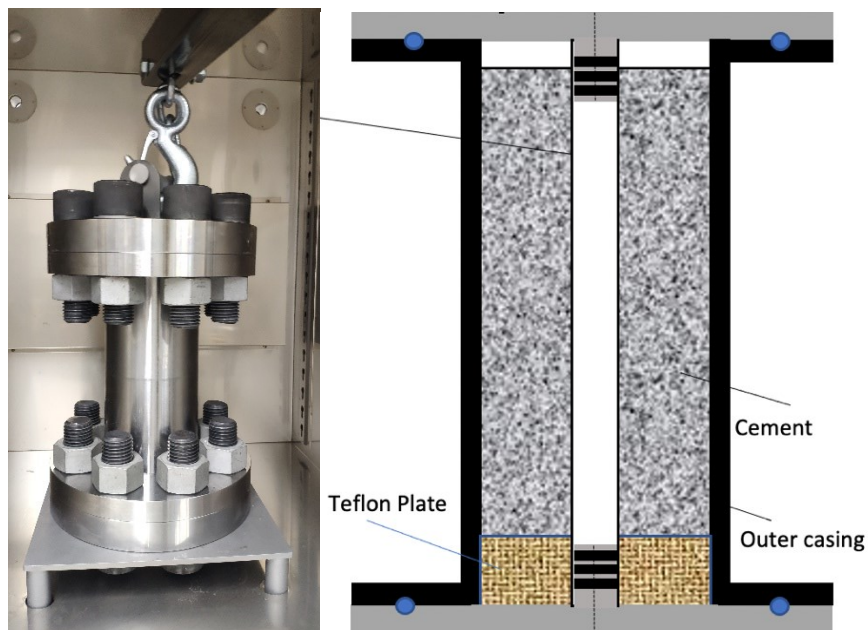


Figure 1- 5 Wellbore simulator main body (left); cross-sectional view of wellbore simulator schematic (right)

More specifically, the study has the following objectives:

- Develop the most suitable methods for preparing bulk cement samples, cemented-casing samples, and cemented wellbore sections using a physical wellbore simulator.

- Develop an optimized permeability measurement procedure to increase the efficiency of steady-state cement permeability measurement.
- Develop a suitable method for drying small scale cement samples.
- Determine a suitable cement porosity measurement method by comparing the results from porosity measurements using Boyle's law method and the porosity measurement by drying.
- Investigate the permeability of the various cement blends.
- Investigate the permeability variation caused by the cyclic mechanical and thermal stresses.
- Compare and understand the permeability difference caused by the size and shape of cement samples. (i.e. the small scale 1 in diameter sample versus the cement column inside the large scale wellbore simulator).
- Investigate the permeability difference caused by the component difference in the cement system (i.e. the increasing contact surfaces between cement and other objects).
- Design and develop a physical wellbore simulator that can cure the cement under downhole temperature and pressure conditions and simulate the cyclic load on cement with the function of permeability measurement.
- Describe the cement failure mechanisms (e.g. crack in cement matrix, micro annulus by debonding between cement and casing) by comparing the permeability variation among various cement systems (i.e. cement plug vs cemented casing sections) with the same cement blend under the same curing conditions.
- Determine the in-situ cement permeability by a newly developed physical wellbore simulator.

## 1.4 Contributions of the research

The main contributions of this research can be summarized under three groups: 1-) Develop procedures for optimizing and standardizing the permeability measurement process of bulk cement samples and cement casing samples; ii-) Design and develop a physical wellbore simulator that is capable of curing the cemented wellbore sections under downhole temperature and pressure and determining the permeability of the cemented wellbore sections under cyclic pressure and thermal loads; 3-) Determine the permeability of the cemented wellbore sections under constant temperature and pressure conditions as well as under constant temperature and variable (cyclic) pressure conditions.

More specifically, the main contributions are described as follows:

- Establish suitable methods for preparing bulk cement samples, cemented-casing samples and the cemented wellbore sections (i.e. annular cement columns between two casings).
- Provide a detailed description of the cement permeability measurement process using the steady-state method by water and Nitrogen.
- Standardize the cement porosity measurement process by comparing the results from Boyle's Law and by drying.
- Evaluate the feasibility of water permeability on the dry bulk cement sample, nitrogen permeability on the saturated bulk cement samples, and nitrogen permeability on the dried cement-casing sample.
- Conduct cement permeability testing under simulated downhole conditions, starting from the small scale bulk cement sample to the cement-casing sample and finally, to the physical wellbore simulator.
- Establish a unique procedure to compare the parameters that influence the permeability of cement.
- Investigate the influence of expansion agents and different cement blends on the permeability of cement.
- Investigate the impact of cement drying shrinkage on cement permeability.
- Detect the cement failure by comparing the permeability difference between different cement systems with the same cement blend under the same curing conditions.

- Design and develop a physical apparatus that can cure the cement under downhole temperature and pressure conditions and simulate the cyclic load on cement with the function of in-situ permeability measurement.
- Investigate the variation of the cement permeability due to change in sample size by comparing the small scale sample to the relatively large-scale wellbore simulator cement sample

## **1.5 Organization of thesis**

This MSc thesis is comprised of the following six chapters:

Chapter 1 provides a brief introduction to the investigated subject and an overview of the research. The statement of the problem is stated. The objectives and scopes of the research are summarized. The contributions of the research are also introduced.

Chapter 2 is the literature review. In this part, a comprehensive review of the available literature is conducted. The first section of this part will review potential leakage pathways caused by cement failure in oil wells, which explains why this research is conducted. In the next section, the permeability measurement techniques for cement were reviewed as cement permeability measurement is one of the main subjects of this thesis. The last section of this chapter is devoted to cement performance evaluation by using physical wellbore simulators. In this section, large-scale, bench type, and commercial wellbore simulators designed previously are reviewed because their development process, advantage and disadvantages provided an excellent background needed for developing the physical wellbore simulator in this study.



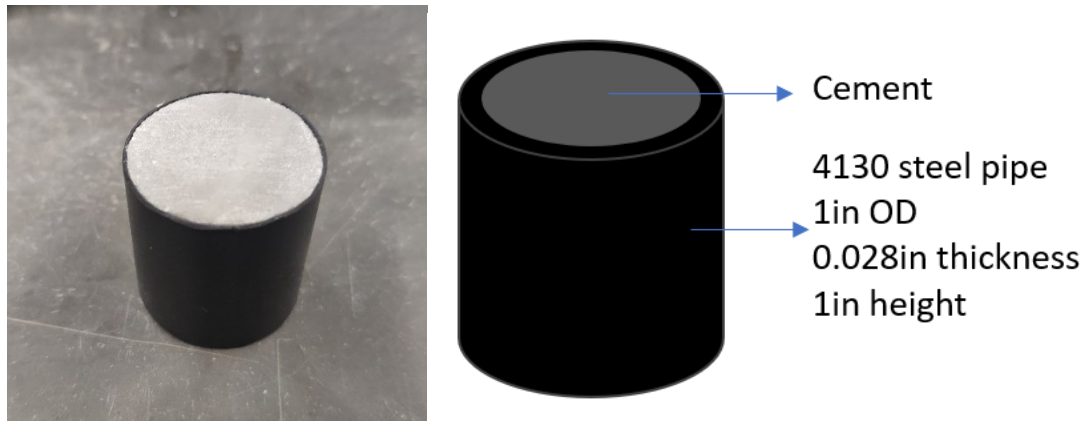


Figure 1- 6 Small scale bulk cement sample and cement casing sample (Chapter 3)

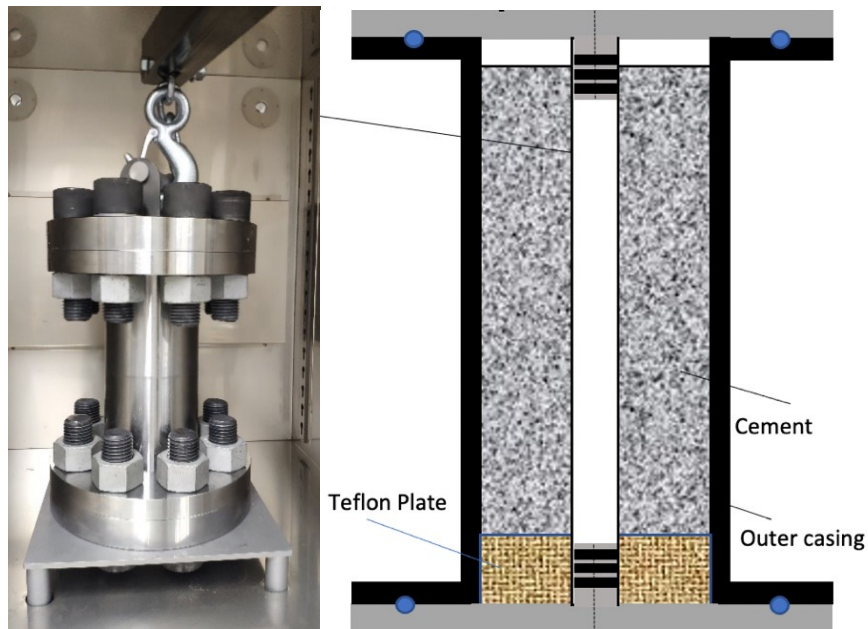


Figure 1- 7 Large scale cement sample in the wellbore simulator and the wellbore simulator main body

In chapter 3, a comprehensive study for measuring cement permeability is conducted. The small scale bulk cement sample and cement casing sample scaling down based on the field data with different cement blends, Class G, G EXP, G Abandonment, REMEDIALmix EC, are used. In this chapter, the porosity measurement methods by Boyle's law and drying are compared, and the optimal method of measuring the porosity is discussed. This chapter also standardizes the

procedure of permeability measurement on the cement samples using the steady state method by Nitrogen and water.

Chapter 4 described the design and development process of the physical wellbore simulator. This chapter discusses the procedure of choosing o-ring based on different sealing types. This chapter also described how the physical wellbore simulator designed is optimized based on finite element analysis (FEA). Besides, the design process of the flowlines connected with the wellbore simulator main body and their function are also discussed.

Chapter 5 provided the validation of pressure rating and temperature rating for the wellbore simulator. Furthermore, three sets of constant temperature and pressure experiments and three sets of constant temperature and cyclic pressure experiments were conducted. Furthermore, the method of detecting the leakage pathway of the gas in the wellbore simulator was demonstrated. After the leakage pathways were detected, the shear bonding strength test was conducted using a hydraulic press.

Chapter 6 provides the key conclusions of this study based on the results from previous chapters and recommendations for future research.

## **Chapter 2 Literature review and background**

The literature review chapter is composed of three sections. In the first part, a comprehensive review of the previous studies investigating the potential leakage pathways in cemented wellbore sections is provided. A good understanding of the potential leakage pathways helped us define one of the main objectives of this study, i.e. measurement of the permeability of the cemented wellbore sections under simulated downhole conditions. The second section of this chapter is devoted to the review of the previous studies on the experimental measurement of cement and some tight core permeabilities. The main methodology used in this research is adapted from the methods utilized in these previous studies. In the last section of the chapter, some previous work on designing and developing the physical apparatus to evaluate the cement performance is reviewed. These previous works provided valuable experience and guidance in designing the wellbore simulator designed and developed in this research by comparing the advantages and disadvantages of the previous works.

### **2.1 Potential leakage pathways caused by cement failure in oil wells**

The first and foremost goal of the cement job is to provide a complete and durable zonal isolation during the life of producing well and after the abandonment of the well. Based on the statistical data, about 15% of primary cement jobs fail, which costs the oil and gas industry USD 450 million annually for the cement remedial work (Newman & Wojtanowicz, 2001). Even though the cement is properly placed initially, the zonal isolation may still be lost over time. As it has an essential role in the wellbore barrier system, the failure of cement resulting from a sustained casing pressure (SCP) may cause significant economic loss, damage to the environment and the loss of lives. Bonett and Pafitis (1996) summarized the main parameters causing the annular gas migration due to the cement failure (Figure 1-1). Celia et al. (2005) summarized the potential leakage pathways in the cement systems (Figure 1-2). Viswanathan et al. (2008) summarized the potential failure of the cement system or wellbore barrier system (Figure 2-1). When the leakage pathways are formed, either in the cement matrix or along the

cement/casing, cement/rock interfaces, the permeability of the cement system will change. Therefore, permeability can be an effective indicator to assess the fluid flow inside the cement system (Baroghel-Bouny et al., 2009; Basheer et al., 2001; Luping and Nilsson, 1992). The potential reasons for the failure of the cement system can be summarized in two categories: Failure of cement body, failure of the interface between cement and formation rock or the casing wall.

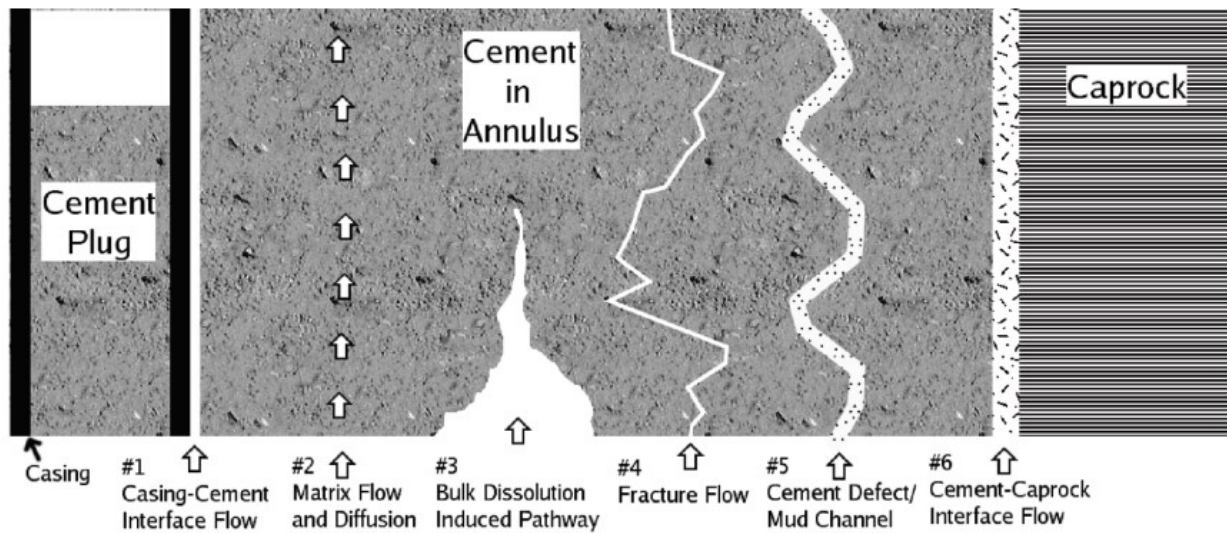


Figure 2- 1 Potential cause for the failure of the cement system (from Viswanathan et al., 2008)

The following sections provide the literature review of the detailed potential leakage pathways through cemented wellbore sections.

As mentioned in the previous section, permeability is an important indicator of the presence of fluid flow inside the cement system (Baroghel-Bouny et al., 2009; Basheer et al., 2001; Luping and Nilsson, 1992). Therefore, the measurement of the permeability of the cement matrix can be an important indicator for detecting the unwanted fluid flow through the cement. Guyvoronsky and Farukshin (1963) are one of the first researchers who introduced the concept of gas migration through the pore structure of set cement. After the introduction of the concept, the

cement matrix permeability was measured as 300 mD during the reduction of the hydrostatic pressure. The hydrostatic pressure will lose during the hardening process of the cement.

One of the earliest measurements of cement plug could be dated back to Coleman & Corrigan, (1941), where they studied the effect of fineness of the cement and the water-cement ratio on the volume and permeability of the cement. In this study, 96 test samples extracted from 16 bulk cement specimens (3 top samples and three bottom samples from each specimen) were prepared with different fineness and water-cement ratios. Permeabilities of the dried samples varied from 0.86 to 25.73 mD. Coleman & Corrigan (1941) thought that the high water-cement ratio would cause excessive free water within the cement slurry, further moving upward in the wellbore to create a water channel or water pocket, therefore, the high permeability in the cement.

Morgan & Dumbauld (1952) conducted wet cement permeability tests on the 'oil well cement'. The results showed that under 100psi pressure injection pressure, the water permeability was too low to be measured. However, by comparing the wet permeability data with the gas permeability data obtained from a dried sample, the authors concluded that the drying process of the cement would increase the permeability of the set cement. Therefore, even if the primary cement job is perfect, the leakage may still happen through the cement matrix if there is no water to keep the cement saturated under downhole conditions.

Goode (1962) conducted gas and water permeability tests on the dried and wet cement samples separately. He reported that the samples that contained a moderate amount of Bentonite seemed to have higher permeability values. Goode's results suggested that cement contamination by the drilling fluid (having Bentonite as a major component) could be one of the reasons causing the leakage through the cement plug. Goode (1962) also mentioned that except for the samples containing Bentonite, the permeabilities of cement samples decreased with ageing and temperature. Therefore, the proper curing time and temperature are essential to prevent or lower the possibility of fluid leakage through the cement matrix.

Ozyurtkan M. et al. (2013) used ARI, a natural magnesium complex with carbonate, as an additive to mitigate the gas permeability of oil well cements. The samples were prepared using Class G cement and cured for 1, 7, 28 day(s). Various samples were prepared containing 0%, 1%, 2%, 3% ARI, 0.4%, 0.7% viscosity controller, and 0.4%, 0.7% water loss controller. The study showed that adding 3% ARI into the class G cement developed an impermeable cement

matrix practically. The permeability through the cement matrix was reduced below the sensitivity of the permeability test apparatus by adding 5% ARI at the end of the curing period of 28 days under permeability experiment conditions of Ozyurtkan M. et al. They showed that the permeability or the leakage through the cement matrix could be reduced by adding the proper additives and curing for a suitable time. However, this paper did not directly answer the acceptable permeability value of the cement.

Another factor that may cause fluid leakage through the cement matrix is the downhole stress conditions. The stress can be mechanical stress, such as the one resulting from multi-stage fracturing or thermal stress, such as the ones experienced in SAGD wells and cyclic steam stimulation operations. They can be continuous stress or cyclic stress. These external stresses may create stress-induced fractures, which may further develop into interconnected leakage paths through the cement matrix and, eventually, cause cement permeability increase (Bonett and Pafitis, 1996; Skorpa and Vrålstad, 2018). Bauer et al. (2019) conducted an experimental study of the relationship between permeability and the deformation mechanisms using triaxial loading tests. The study showed that the strength of a neat cement increased with the increasing confining pressure. They also showed that flow paths are blocked slightly during initial axial loading for the two lower confining pressure tests. However, the favourably oriented-to-flow microcracks begin to open and connect. Finally, the microfracture formed, and the microfracture dominated the flow. In a recent study, Yang et al. (2020) used a set of cement samples under pre-peak and after peak uniaxial compressive stress. They measured the microfracture in the cement matrix by using SEM. They mentioned that fractures are isolated and not well connected to induce a significant change in permeability. However, this is not cyclic stress. The stress was only applied one time until it exceeded the UCS. Compared with the importance of cement integrity under various stresses, although the studies listed above have already started to explore this area, there is still very little attention paid to studying the relationship between the stresses and the cement matrix permeability.

## **2.1.2 Potential leakage through the interface between cement and casing**

This section provides a review of the literature related to the leakage through the interface between cement and casing. The cement in wellbore is typically bonded to casing and formation rock surfaces. As mentioned by Yang et al. (2021), the interface between the cement and formation is considered as a major potential leakage pathway in the wellbore barrier system and the physical properties of formation rock (e.g. density, porosity, surface roughness, etc.) rock influence the bonding between the cement and formation. However, our main focus is the bonding between the cement and the casing interface in this research. One of the main objectives of this research was to design and construct a physical wellbore simulator that would allow us to investigate the cement bonding between two casings (i.e. simulating casing-cement-casing system). Therefore, this section only presents a literature review relevant to potential leakage through the interface between cement and casing.

Baumgarte et al. (1990) and Bourgoyne et al. (2000) reported that the interface between cement and other components (i.e. casing and formation) in the wellbore barrier system has more possibility to have leakage than the cement matrix. This led to the concept of cement debonding. The term ‘debonding’ is used when the bond fails between cement/rock or cement/casing interface. In their classic book on cementing, Nelson & Guillot (2006) summarized the potential factors causing the debonding at the cement/casing and cement/rock interfaces in the cemented wellbore systems. They state that cement shrinkage by dehydration of the cement, the fluctuations of temperature and pressure, stimulation practices, casing movement when the subsidence occurs are the significant factors leading to debonding. In the wellbore, two criteria are often tested for the evaluation of zonal isolation. They are shear bonding and hydraulic bonding. The physical wellbore simulator built in this research can also test the hydraulic bonding and shear bonding of the cement casing interface. Evans and Carter (1962) conducted some of the earliest bonding tests to measure the shear-bond and hydraulic bond strengths of cement/casing and cement/rock interfaces. They used various casings and Class A cement in their study. Evans and Carter (1962) found a correlation between cement compressive strength and the shear bond strength. However, in their experiments, they did not apply any pressure in the inner casing and were not able to simulate the cyclic stress conditions as we experience today

in many wells due to, for example, the commonly used multistage hydraulic fracturing process. Carpenter et al. (1992) designed a cement-bond tester to test both the hydraulic and the shear bonds of the cement under the effect of different temperatures and admixes. Their results indicated that even with one thermal cycle between 300 to 355 Kelvin, the cement/casing shear bonding could significantly decrease. However, due to the limited pressure capacity of the tester, the water pressure could not reach a sufficiently high level to conduct the hydraulic bond test.

There has been more interest in studying casing-cement interfaces in recent years due to the increased interest in Carbon Capture and Storage (CCS) wells and the tighter regulations on SCVF. Plenty of studies focus on how the chemical reactions between  $CO_2$  and cement affecting the integrity of the bonding between cement and casings (Bachu and Bennion, 2009; Carey et al., 2010; Jung et al., 2013). However, the casing-cement wellbore barrier system is used in the CCS wells, the oil and gas production wells, and the gas storage wells. With advanced manufacturing techniques, the test apparatus can now provide more precise stress control. Therefore, the cyclic stress conditions can be simulated in the lab. Li et al. (2021) developed an apparatus (Figure 2-2) to test the deformation and the damage of cement sheath in between the formation and casing under triaxial cyclic load. It indicated that the internal damage of the cement occurred continuously under the cyclic load. The microfracture develops and finally forms the microfracture, leading to cement failure. In this test, there is more than one interface (cement/casing and cement/formation) on the cement. Therefore, it is hard to define the source of bonding failure. Furthermore, an apparatus was developed to test the cement/casing bonding integrity (Lamik et al., 2021). When placed the cement, the outer wall of the apparatus was covered with oil to produce only one cement/casing bonding interface. The uniaxial cyclic load was applied to the inner casing. The study indicated that the cement-casing bond shear strength is lower when the pre-cyclic load is applied. The larger the number of the pre-cyclic load applied, the larger the possibility of the cement-casing bonding failure will occur.



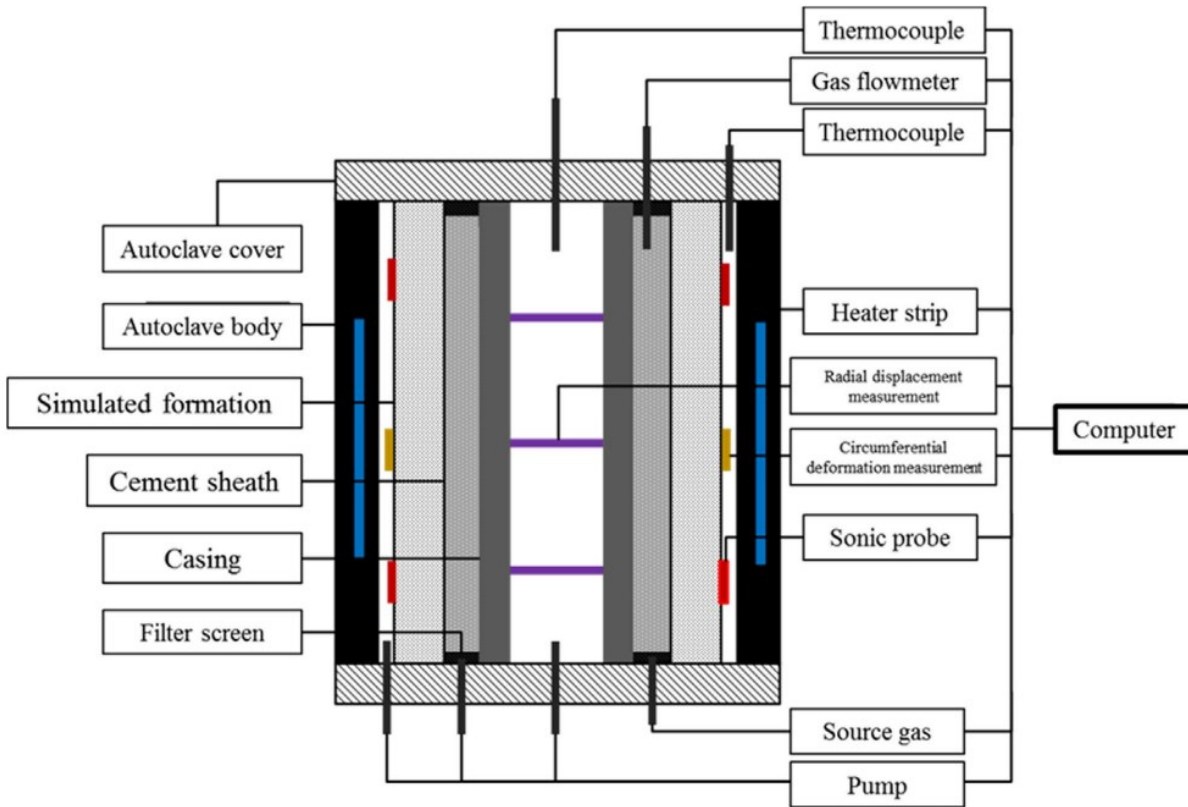


Figure 2- 2 Schematic of the test device for the Deformation and damage of cement sheath in gas storage wells under cyclic loading (Li et al., 2021)

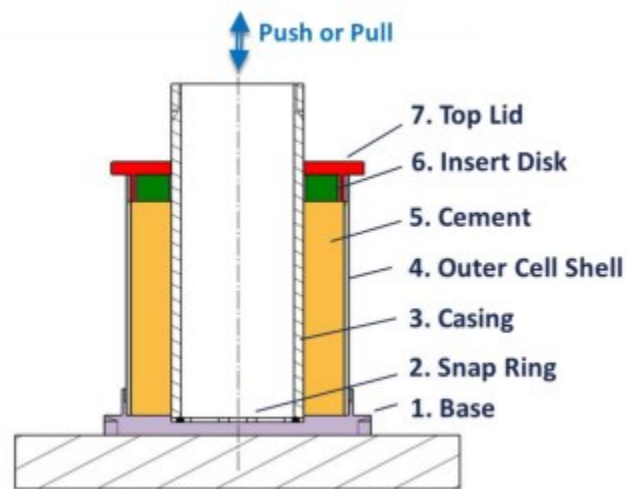


Figure 2- 3 Test device for evaluating the cement casing bonding integrity (Lamik et al., 2021)

Besides the experimental method to evaluate the bonding between cement and casing, micro-CT, SEM, and ESEM are the other way to observe the microfracture or the micro annuli between the cement and casing bond (Bentz et al., 1999; Scrivener et al., 2004; Torsæter et al., 2015; Yang et al., 2020). However, due to the duration of the scanning process of CT, the cement will dehydrate, and the properties of cement will change during the scanning process. For the SEM and ESEM, as the thin section samples are prepared, the cement casing samples are covered with epoxy resin. Therefore, the sample will have minor dehydration. However, some artificial fractures may be induced due to the cutting and polishing procedure when preparing the thin section samples. In this research, the experimental procedure is the main focus. Therefore, the Miro-CT, SEM, and ESEM are not introduced in detail.

## **2.2 Permeability measurement techniques for the cement**

The definition of porous media is the solid material containing pores. The pores are typically filled with fluid, and the skeletal part of the material is typically named ‘matrix’ (Ganji & Kachapi, 2015). Based on this definition, Portland oil and cement can also be considered porous media after curing. Therefore, the permeability measurement techniques used on the porous media can also be applied to cement theoretically. However, due to ultra-low permeability for the cement compared with sedimentary rock and no standard of permeability measurement for cement, some standard permeability measurement processes designed for the rock may need to be modified to measure the ultra-low permeability from cement. Even for the permeability measurement on cement, there are dry cement permeability measurements and permeability measurements on wet cement samples. This section is divided into three parts, the permeability measurement techniques on the porous media, the gas permeability measurement on the dried cement samples, the liquid permeability measurement on the wet cement samples.

### 2.2.1 Permeability measurement techniques for porous media

In this part, the generally used techniques for the porous media are reviewed. The permeability measurement methods for the porous media can be divided into two large categories, the steady-state methods and the unsteady state or the transient methods.

The steady-state method uses the equation of Darcy's law to determine permeability. Darcy first determined Darcy's law experimentally in 1856. Then Darcy's law was derived from Navier-Stokes equations via homogenization methods (Whitaker, 1986). After Darcy's experiment, Muskat first introduced the viscosity term into the equation. The equation can then be applied to the viscous fluid and is widely used in the oil and gas industry. The steady state method has a standard ASTM D4525-13e2 that can be followed. To be able to get the permeability, at least three major components in the system are needed. The coreholder to hold the core; the pressure transducer to measure the upstream inlet pressure of the fluid and to confirm whether the flow is under the steady state; the flowmeter to measure the flowrate. The Hassler-type specimen holder is suggested in the standard, which is also the most used coreholder for the permeability measurement. The bubble flowmeter is recommended as the performance of the bubble flowmeter is accurate under the low flow rate.

Depending on the fluid applied in the system, Darcy's equation for liquid is used to calculate the permeability for the liquid. For the gaseous fluid, Darcy's equation for gas is used. However, the permeability is not as liquid permeability for the gases, which is the same using different liquids. The gas permeability depends on the gas properties as the phenomena of slip need to be taken into account (Klinkenberg, 1941). However, Klinkenberg found that gas permeability is approximately the linear function of reciprocal mean pressure. Therefore, at the pressure of infinity large, the reciprocal mean pressure approaches zero, the liquid permeability can be obtained, independent of the fluid's properties. The Klinkenberg correction is critical under the permeability smaller than 0.01mD at low pore pressure differentials (Tanikawa and Shimamoto, 2009). For the cement, the biggest problem for the steady state method is the duration of the measurement by using water for the wet cement. Due to the ultra-low permeability of cement, the fluid is hard to get into the cement plug and hard to breakthrough. To be able to measure the permeability in the cement by water, precise control for the water flowrate is critical. Therefore,

many researchers started the gas permeability measurement on the porous media. However, the gas will displace the water inside the saturated sample, making it hard to obtain the gas permeability and, therefore, hard to perform the Klinkenberg correction. If the dried core is used to measure the gas permeability, the drying process may change the structure inside the core and cause errors for the permeability result. Due to the problems mentioned above, the transient method has been preferred in recent years. However, by a study, by controlling the flowrate precisely and designing the system appropriately, the steady-state method using water can be preferred to transient techniques (Boulin et al., 2012).

Moreover, a study compared the permeability result using the steady-state and transient methods for the same core plug. The sample was also sent to two commercial labs using two different unsteady state permeameters (Rushing et al., 2004). The result showed that the unsteady state technique consistently overestimates Klinkenberg's corrected permeabilities. The error of the unsteady state technique may be from fundamental problems with the methodology of the unsteady state technique as it is a systematic phenomenon. Therefore, the steady state method is preferred by the author in this study.

The unsteady-state methods will be briefly introduced in this paragraph as they are the permeability measurement techniques for the porous media. Still, they are not the main methods used in this study. Based on the time frame, the main unsteady state permeability measurement methods used are:

- The pulse decay method (Brace et al., 1968; Kwon et al., 2001; Carles et al., 2007; Giot et al., 2011) applies a pressure pulse at the end of upstream of the core. The pressure pulse will then decay over time. This pressure decay is used to calculate the permeability of the core.
- The oscillating pulse method (Kranz et al., 1990; Fisher & Peterson, 1992) sends a pressure wave through the core plug. The frequency and the amplitude of the pressure wave are constant. The change of the amplitude and phase between the sent wave and recorded downstream pressure are used to calculate the permeability.
- The GRI method (Luffel et al., 1993; Cui et al., 2009; Tinni et al., 2012) uses unconfined crushed rock and pressure pulse. The pressure decay over time is used to calculate the permeability. The method is mainly used in the permeability measurement for shale. This

method becomes popular because of the less time needed compared with the two other methods listed above.

To summarize, the steady-state permeability measurement techniques are chosen as the primary methodology in this study. It is simple to operate and can be directly corrected with the Klinkenberg correction. However, it can be time-consuming if the flowrate and the inlet pressure are not precisely controlled.

### **2.2.2 Gas steady state permeability on dried cement samples**

Guyvoronsky and Farukshin (1963) first introduce the concept of gas migration through the pore structure of set cement. The cement matrix permeability was then measured to be 300 mD during the reduction of hydrostatic pressure.

However, the earliest cement permeability data can be traced back to 1941, when Coleman and Corrigan designed an experiment process to study the effect of fineness and water-cement ratio on the volume and permeability of cement. Sixteen samples with different finenesses and water-cement ratios were prepared, shown in Table 2-1. Y means the sample was prepared and tested for permeability and vice versa. Six specimens were cut from each sample, three from the top and three from the bottom, to study the effect of precipitation of the cement. All samples were cured at room temperature 24 hours and 37.78 °C for another 48 hours in water under ambient pressure. The prepared samples were then dried under 100°C in a desiccator. However, the detailed procedures, inlet pressure, outlet pressure and confining pressure were not mentioned. The permeability test conducted by air was also not corrected for the Klinkenberg effect. Therefore, the reliability of the permeability result should be questioned.

Table 2- 1 The prepared samples under different w/c ratios and finesses (Based on Coleman and Corrigan, 1941)				
Fineness (cm <sup>2</sup> /g)	1890	1630	1403	1206
W/C Ratio				
0.35	N	N	Y	Y
0.40	Y	Y	Y	Y
0.50	Y	Y	Y	Y
0.60	Y	Y	Y	Y
0.70	Y	Y	N	N

In 1962, Goode measured the nitrogen steady-state permeability to study the effect of curing temperature, curing durations and the adding of Bentonite on the permeability of commonly used oil well cement. The cement used to prepare the samples are the Class A and Class C Portland cement. The additive was 4% Bentonite. The prepared samples were cured at 26.67, 37.78, 48.89, and 60 °c separately under ambient pressure for seven days in water. Another set of samples with the same conditions but cured for 28 days. The samples were then dried under 37.78°C (100°F) for 24 hours. The Nitrogen steady-state permeability measurement was conducted with the differential pressure between inlet and outlet of 340, 500, and 700 psi separately. The results were obtained using the gas Darcy’s equation and corrected by the Klinkenberg correction. The results are summarized in Figure 2-4. This procedure was pretty detailed. However, the confining pressure during the permeability measurement was not mentioned. The ambient pressure for curing cement cannot simulate the downhole curing condition for the cement. Besides, there may be some errors in Klinkenberg's correction by only using three points.

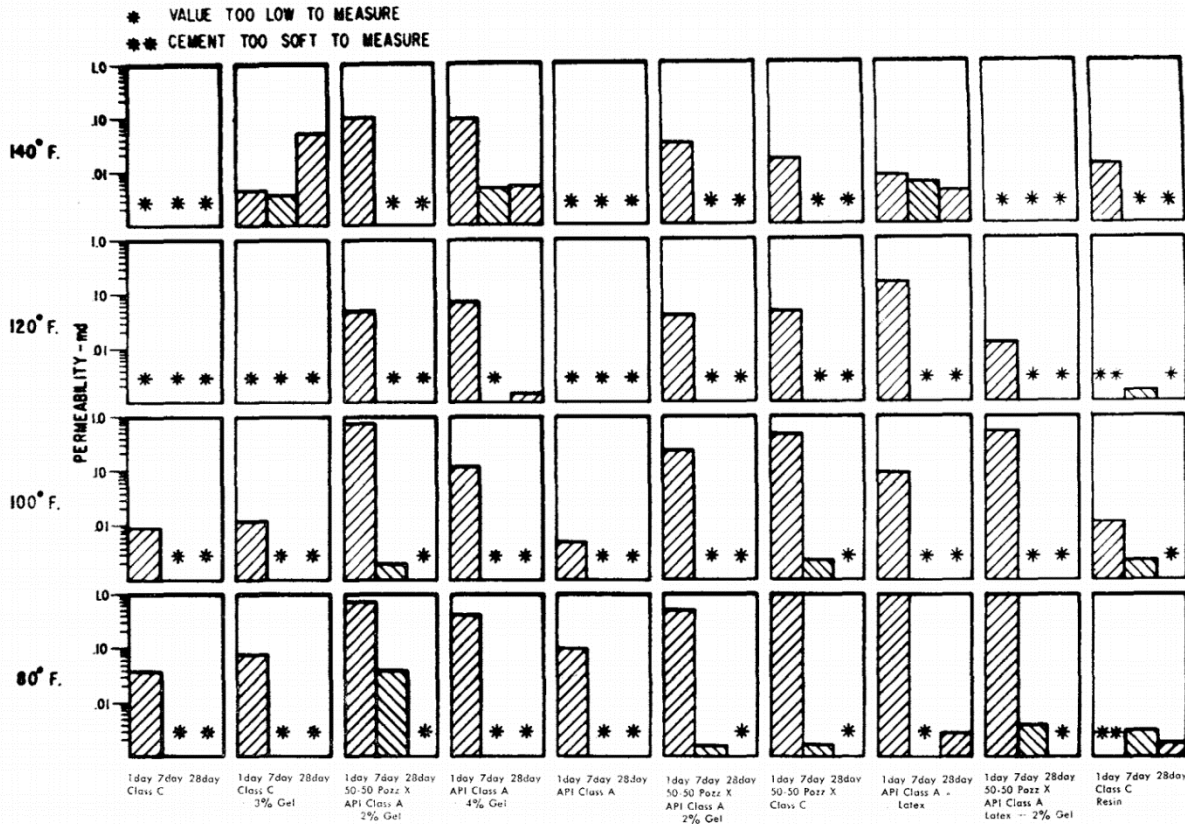


Figure 2- 4 Permeability results from Goode (1962)

In 2013, another nitrogen steady-state permeability measurement experiment was conducted by Ozyurtkan et al. The experiment was designed to study the mitigation of the oil well cement gas permeability. The variables in this experiment were the curing days, the additives. The samples were then prepared based on the combination of different variables. The curing durations were 1, 7, 28 days separately. The additives contained viscosity controller (0.4% and 0.7%), water loss controller (0.4% and 0.7%), ARI (0%, 1%, 2%, 3%) separately. For each condition, three samples were prepared to avoid the contingency of permeability deviation. Therefore, the total samples number will be  $3(\text{curing duration}) * 2(\text{VC}) * 2(\text{WLC}) * 4(\text{ARI}) * 3(\text{three samples for each case}) = 144$  samples. The w/c ratio for the samples was 0.44. Samples were cured under the desired duration, ambient pressure and temperature of 25°C. The confining pressure was 100psi. The inlet nitrogen pressure was between 0-110psi. Finally, the permeability was the average of the permeabilities from three samples. The permeability range obtained for all samples was 0-

0.31mD. However, the drying process in this experiment was not mentioned. The inlet pressure of 110psi was larger than the confining pressure, which may cause the nitrogen flow to bypass the side of the plug. The curing condition of 25 Celsius and ambient pressure was not able to simulate the downhole condition. Besides, due to the low inlet nitrogen pressure, the 0mD permeability here can only represent the impermeable under the pressure of 110psi. With the increase of inlet nitrogen pressure, there may be permeability through the plug.

Bauer, S.J. et al. (2019) further developed the experiment process by curing the cement under 50 Celsius degrees, the tensile stress of 383psi, and compression of 4525psi. The experiment was designed to study the permeability and deformation mechanisms during a triaxial test for the early-aged cement. The cement slurry used in this experiment was neat Class G cement with a w/c ratio of 0.45. The confining pressure was the variable. The experimental setup was also improved by applying the vacuum downstream of the plug and setting the nitrogen trap to trap the water from the outlet nitrogen gas. By this setup and applying of inlet pressure, 30.46psi under the confining pressure of 101.526psi, 304.579psi, and 2001.521psi, the permeability range of  $1.1E-4$  to  $5E-2$  mD was obtained. However, the permeability was not corrected for the Klinkenberg effect. Based on Tanikawa and Shimamoto (2009), under the permeability smaller than 0.01mD, at low pore pressure differentials, the Klinkenberg correction is critical. Besides, using the neat class G cement, which is not used on the field, the cement blend was hard to simulate the actual case.

To summarize, the experimental procedure can be improved by choosing class G and commercial cement, applying the curing conditions that can simulate real-life, specifying the drying process, applying the reasonable confining pressure, inlet and outlet pressure, correcting for the Klinkenberg effect if needed.

### **2.2.3 Liquid steady state permeability of wet cement samples**

The experimental setup for measuring the steady-state water permeability is straightforward. It contains at least three parts, the water pump to apply the inlet water pressure, the core holder to hold the plug, and the flowmeter to measure the flowrate. Despite the straightforward setup, the



tight rock and cement's water permeability was still hard to be obtained due to the time required to stabilize the water flow under low permeability (Hsieh et al., 1981). However, Boulin P.F. et al. (2012) showed that by precisely controlling the flowrate and inlet pressure, the steady-state method using water could be preferred to transient techniques.

Only a few studies focus on the steady-state water permeability measurement on the wet cement samples. Back in 1962, Goode measured the water permeability of Class A and Class C cement. However, the pressure difference between the inlet and outlet was only 100psi due to the limitation of the equipment. In 1997, Bache et al. studied characterizing the curing cement slurry properties, including the water permeability measurement. The permeability obtained was not helpful as the measured object was cement slurry rather than the wet cement plug. However, on the positive side, they used both a neat Class G blend and commercial blends, which improved the permeability measurement since it was closer to the actual case. Maharidge et al. (2016) proposed a more detailed procedure for measuring the permeability of the cement from slurry to set. The sample size was 1'' in diameter and 2'' in length. The w/c ratio was 0.44. However, the slurries were set under room temperature and ambient pressure. Besides, the flow rate was measured by the time for 1cc water loss. Therefore, the steady state was not guaranteed.

To summarize, besides the improvement needed from measuring gas permeability, the water permeability measurement process needs more precise control on the water flowrate and inlet pressure.

### **2.3 Cement performance evaluation by using physical wellbore simulators**

The gas migration problem is not a new topic but studying the physical process of the gas migration mechanisms is not easy as it is hard to simulate the downhole conditions. The statistical data shows that the oil and gas sectors are also the largest industrial methane emitters, contributing 44% of total methane emissions in Canada (Government of Canada, 2021). As cement is considered a critical component in the wellbore barrier system, the gas migration mechanism related to the oil well cement has become more and more critical since the 1960s,

especially after Carter and Slagle (1972) designed the first documented large-scale wellbore simulator to study the factors that influence the cement-column pressure distributions. From then, more wellbore simulators were designed to study the properties of cement, mainly focusing on the gas migration problems. Based on the size, the wellbore simulators can be classified into large-scale wellbore simulators and bench type or small-scale simulators. The large-scale simulators have a very long cement column, and some of them even use the actual casing to simulate the in-situ conditions. Due to these two reasons, the large-scale simulators are hard to move and require a lot of cement, making it challenging to mix this large volume of cement in the laboratory condition. It is also challenging to control the physical conditions inside the simulator, as some properties such as temperature and pressure need time to change under the large volume. The sealing of the system can also be a challenge in this case. Due to these disadvantages, the large-scale simulators were mainly designed between 1972-1983.

After 1983, the small-scale or bench type wellbore simulators took place and became the primary trend. Other apparatuses tried to study the cement/casing and cement/formation bondings rather than the gas migration. However, these apparatuses also gave this research a non-negligible direction on designing the wellbore simulator in this study. They can also be divided into the two categories mentioned above based on their size. Therefore, this section is divided into large-scale wellbore simulators and bench-type wellbore simulators. Until now, there is still no universal apparatus for testing the permeability of the cement while simulating the downhole conditions or the cyclic stresses. The standard for testing the permeability of cement from API still does not exist.

### **2.3.1 Large-scale wellbore simulators**

The designing purpose of the large-scale wellbore simulators is to simulate the downhole condition with a long cement column, typically around 10 to 30 ft. Due to this reason, the mixing of cement, the control of the system properties, and the system's mobility can be challenging. Also, due to these problems, large-scale wellbore simulators were typically produced in the

1970s and 1980s. This section reviewed the large-scale wellbore simulators from previous studies based on the time frame.

Carter and Slagle (1972) proposed the earliest documented large-scale simulator to study how the density, setting, dehydration, gelation, and bridging of the cement influenced the cement pressure under the downhole conditions. To simulate the close-to-reality conditions, a 2 7/8in tubing was mounted and centralized in a 7in N-80 casing with a 100md simulated formation constructed inside the casing. The 8 5/8in to 7in swages are attached to the 7in casing. The drilling fluid was first pumped and set. Then, the cement slurry was used to displace the drilling fluid. The device's schematic is shown in Figure 2-5, which was used to evaluate the effect of the cement density on the gas migration in the cement system. The device was further improved to add the function of studying the directional gas well completion. The evaluation of temperature on influencing the cement integrity was also designed and shown in Figure 2-6. This device can change the temperature in different positions of the string by using thermocouple probes. The high-temperature drill mud was first circulated and displaced by the mixed and heated cement slurries with a temperature lower than the drilling mud. They also developed the combined device (Figure 2-7) to simulate the dehydration process of the cement by combining the nitrogen reservoir with the simulated wellbore. The disadvantages of these devices are apparent. The volume of cement needed is up to 35.2 gals. The mixing of large volume cement is challenging under laboratory conditions. The casing string in this experiment is not reusable, making the experiment highly cost and time-consuming to prepare the simulator model. The heating process in this experiment uses the probe, which may not generate the heat evenly inside the system.

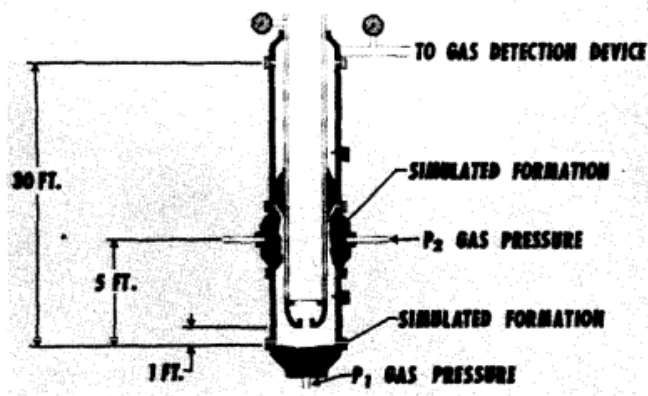


Figure 2- 5 Test equipment used in large-scale density evaluation by Carter and Slagle (1972)

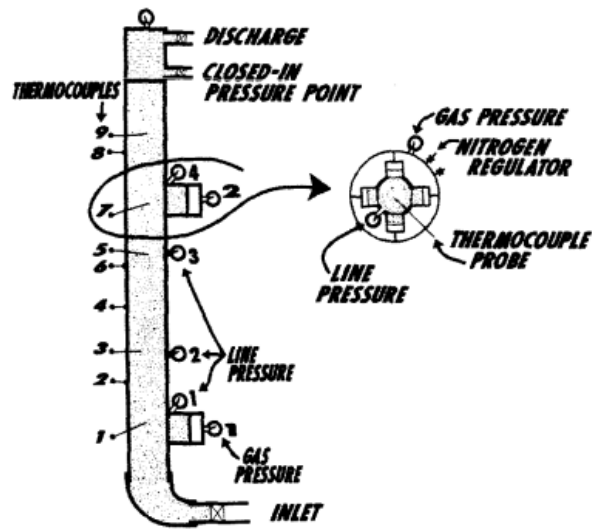


Figure 2- 6 Schematic of large scale temperature evaluation apparatus by Carter and Slagle (1972)

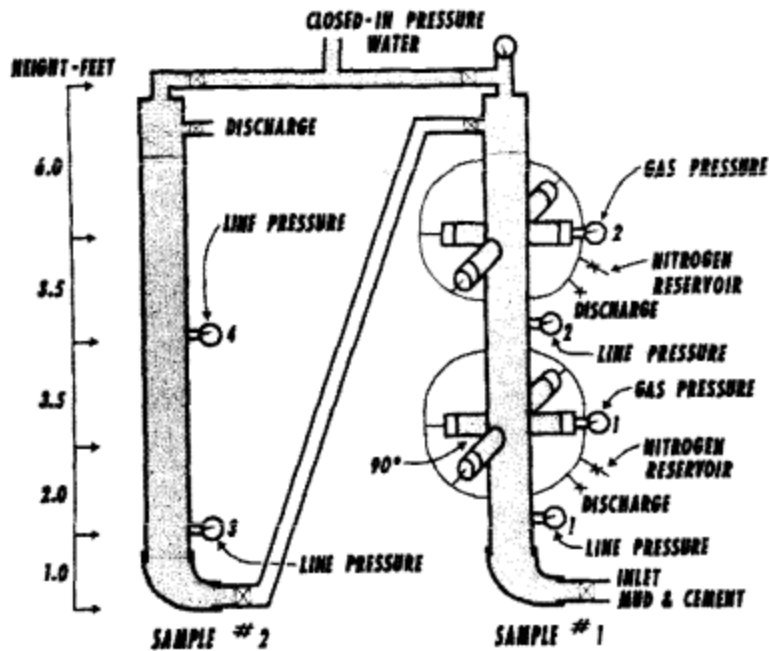


Figure 2- 7 Schematic of large scale dehydration evaluation apparatus by Carter and Slagle (1972)

After Carter and Slagle (1972), Garcia and Clark (1976) designed the device (Figure 2-8) to study the pressure change after the cement was initially set above the hole. The device simplified the cement sheath with a 2in pipe rather than the actual annular flow. The cement column length, in this case, is 20ft long with the cement volume of  $0.45 \text{ ft}^3$ . To simulate the cement initial set above the hole, the heating tape was placed in the midway of the pipe. When the pipe was heated midway, the cement in that part will be set earlier than the cement in other sections and thus isolated the cement below the early set cement. If the pressure drop occurred, the gas would flow across the aloxite plate, which had the function of isolating the gas supply from cement. The gas pressure was initially set the same as the cement hydrostatic pressure. Once the pressure dropped, the gas movement would be captured by the flowmeter at the bottom of the system. Overall, the structure of the wellbore simulator is simplified compared with Carter and Slagle (1972). Besides, less cement is needed, making the preparation process easier and quicker. However, the control on the temperature of the cement is rough. The heating tape cannot provide the precise heat exchange to the simulator. The temperature of other sections of the simulator is not under control. The simplified 2in the pipe may influence the result as the shape of the cement

is changed to cylinder rather than the hollow cylinder in the actual casing cement casing annular flow. Even with the reduced cement volume,  $0.45ft^3$  is still a large volume to be prepared in the laboratory. Moreover, the result is only qualitative. It only can tell if the gas migration happens rather than telling the result quantitatively.

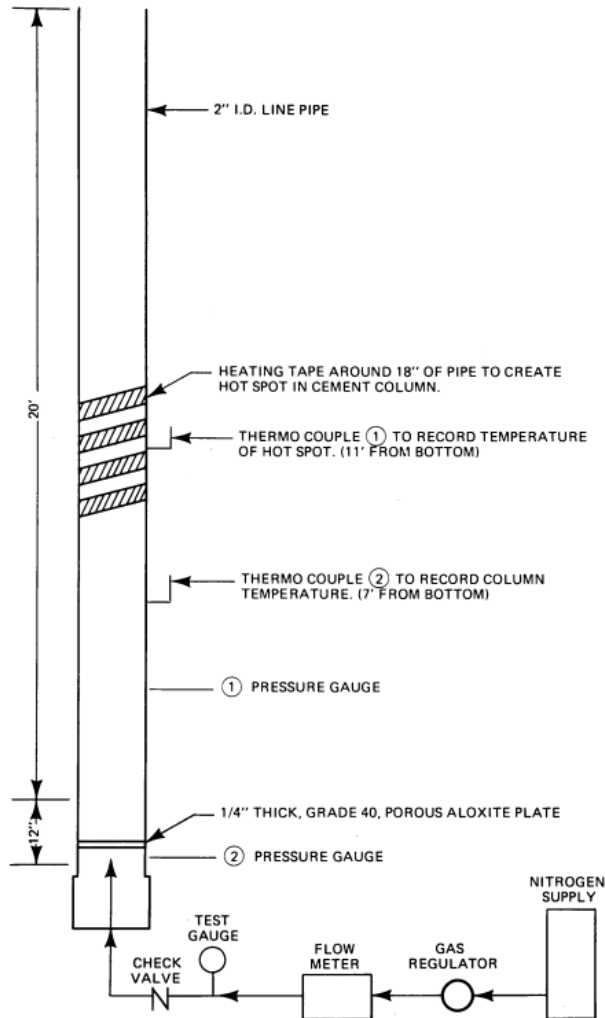


Figure 2- 8 Schematic of the gas flow model by Garcia and Clark (1976)

In 1979, Levine et al. designed a simulator (Figure 2-9) to study the changing of the hydrostatic gradient of the cement contributing to the annular gas flow. Compared with the previous two studies, the simulator had a 35ft water column at the top to simulate the overburden pressure on

the top of the cement column. The cement part was also submerged in a 150°F water bath for better heat exchange. The simulated cement shape was also a hollow cylinder rather than the simplified cylinder shape. However, 9.4gals cement is needed in this simulator. It did not mention if the wellbore simulator was scaled down from the actual wellbore size. The fresh water on the top may not apply enough overburden pressure on the cement to simulate the actual case.

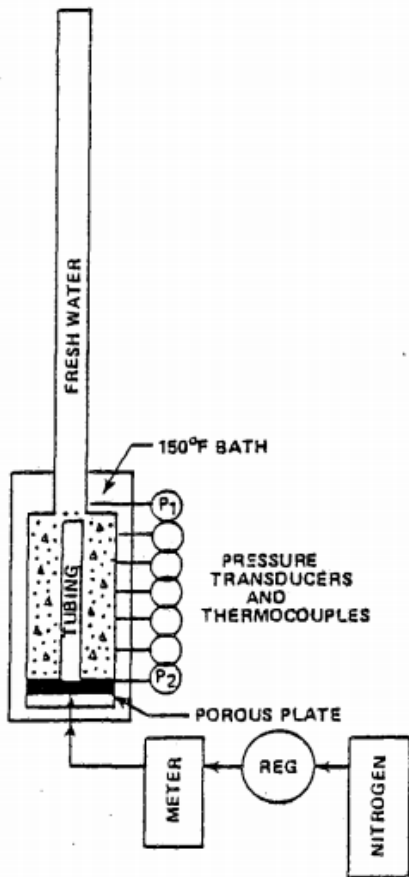


Figure 2- 9 Pressure simulator by Levine et al. (1979)

Furthermore, in 1980 Tinsley et al. proposed a newly designed simulator (Figure 2-10) to study the factor causing the annular flow after primary cementing. Compared with previous work, the improvement of this device is that the higher pressure, up to 1000psi, can be applied above the

cement column. The material outside the cement can be chosen between permeable and non-permeable material, which simulates the permeable formation and zero fluid loss conditions. However, the device needs 24gals cement, which is even more than the device designed by Levine et al., 1979. Besides, the system does not have a flowmeter to measure or control the migrated gas. The pressure applied on the top of the cement column is still not enough to simulate the actual case under the wellbore to some extent. Furthermore, it does not mention if the ratio between the inner pipe and the outer pipe is scaled based on the actual wellbore data.

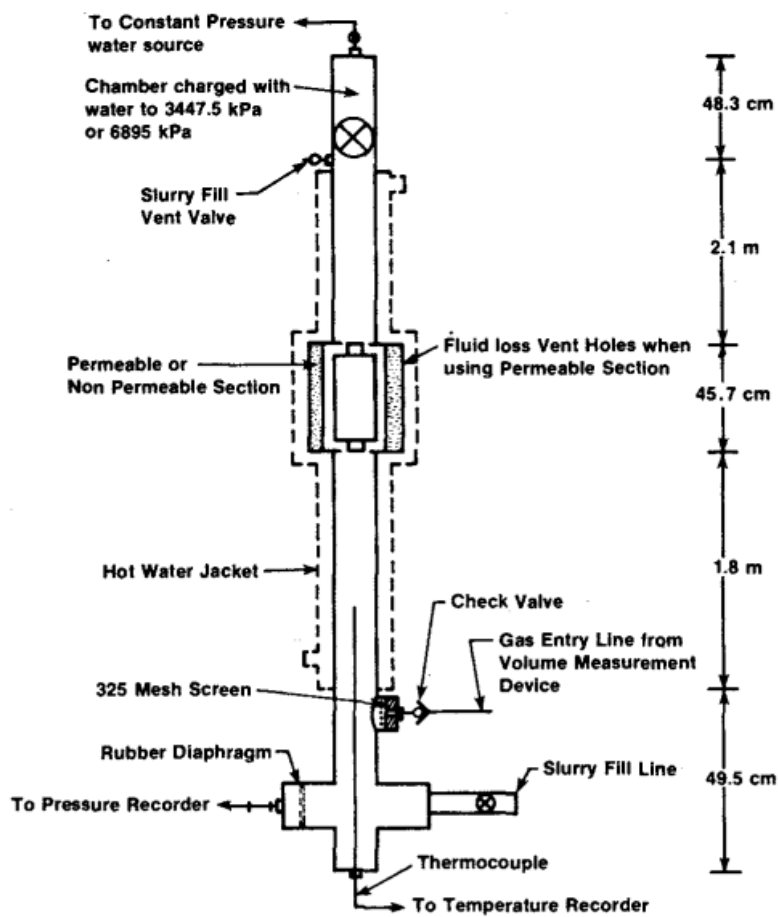


Figure 2- 10 Schematic of test figure used to study gas leakage by Tinsley et al. (1980)

In 1982, Sabins et al. designed a system (Figure 2-11) to study the transition time of the cement slurries to investigate the relationship between the transition time, static gel strength (SGS), and



percolation of pressurized gas. In this device, the function of simulating the wellbore irregularities was added by using the combination of three 2in ID pipes and three 1.5in ID pipes shown in the lower section of the device in Figure 2-11. Besides, the device also added the function of measuring the total gas flow volume by adding the gas trap section shown at the top of Figure 2-11. The system can also simulate fluid loss by removing the water from the fluid loss points. The volume of required cement was also decreased to 2.1gals. However, the 2in coiled pipes at the top were used to simulate the longer pipe in this device, but the tubing was not coiled in the actual case. The setup of the device was also complex, which made it hard to maintain.

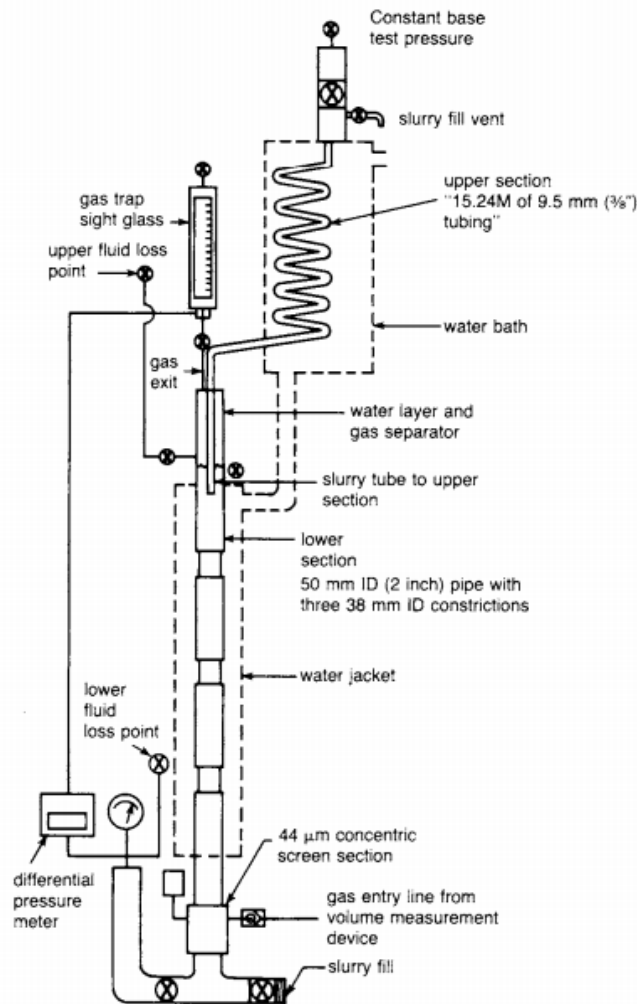


Figure 2- 11 Schematic of test fixture for pressurized gas percolation and pressure-transmission tests by Sabins et al. (1982)

A significant improvement on the large-scale wellbore simulator was made by Bannister et al. in 1984 when they designed a simulator (Figure 2-12) to study the annular gas flow of the cement from the invasion of gas into the cement slurries. Figure 2-12 shows that this wellbore simulator was the most advanced large-scale wellbore simulator among all the work discussed in this section. It is also the one closest to the modern small-scale simulator. It almost got rid of all the disadvantages listed previously. It had a simple setup. The 1in OD pipe was capped at both ends to be centralized in a 2in pipe. The water heat exchanger heated the whole system. The migrated gas had both controls of pressure and flowrate. The pressure and temperature of the whole system were tracked. The cement volume needed was reduced to 1.6gal. The temperature was adjustable between 100 to 300°F. However, the pressure applied to the top of cement was only 260psi. The paper did not mention if the diameters of the two pipes were scaled down based on the field data. Besides, the material of pipes was not mentioned.

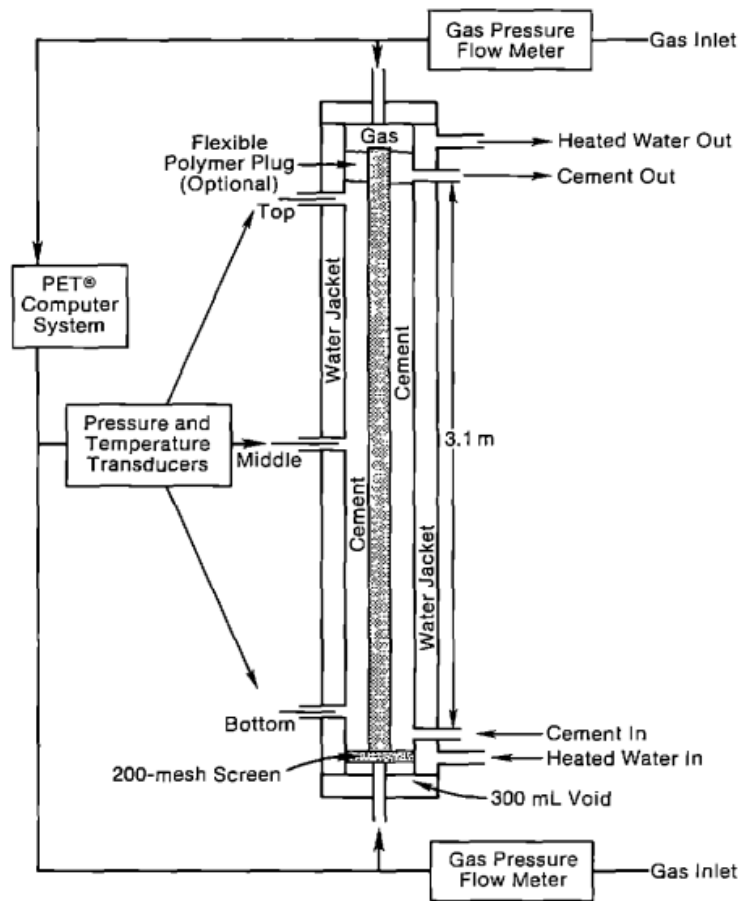


Figure 2- 12 Annular gas flow laboratory testing apparatus by Bannister et al. (1984)

### 2.3.2 Small-scale or bench type wellbore simulators

The small-scale wellbore simulators need less cement volume to operate, making the mixing of cement less challenging in laboratory conditions than the large-scale wellbore simulators. The volume of the bench-type wellbore simulators is also smaller, which gives the system higher mobility. The properties are also controlled easier due to the reduced volume of the system. The finely manufacturing of the bench-type wellbore simulator also gives a chance for the wellbore simulators to reach higher pressure and temperature capabilities.

Cheung & Beirute (1985) designed the first documented small-scale simulator (Figure 2-13) and improved it by Beirute & Cheung in 1990 by adding the filtrate valve for the filtration collection system. The main body of the simulator is a 10in long cell with the piston containing a 325mesh screen on the top to simulate the permeable formation. The mineral oil pressurized the top of the cement column. The pressure was recorded. The overburden pressure could be applied up to 1500psi. The nitrogen was injected from the bottom to generate the gas flow. The cement volume needed to operate the system was only 0.11 gal. However, for this device, the heat tape was used to heat the cell, which may not generate even heat. The cell could simulate the cement plug but could not simulate the annulus cement sheath.

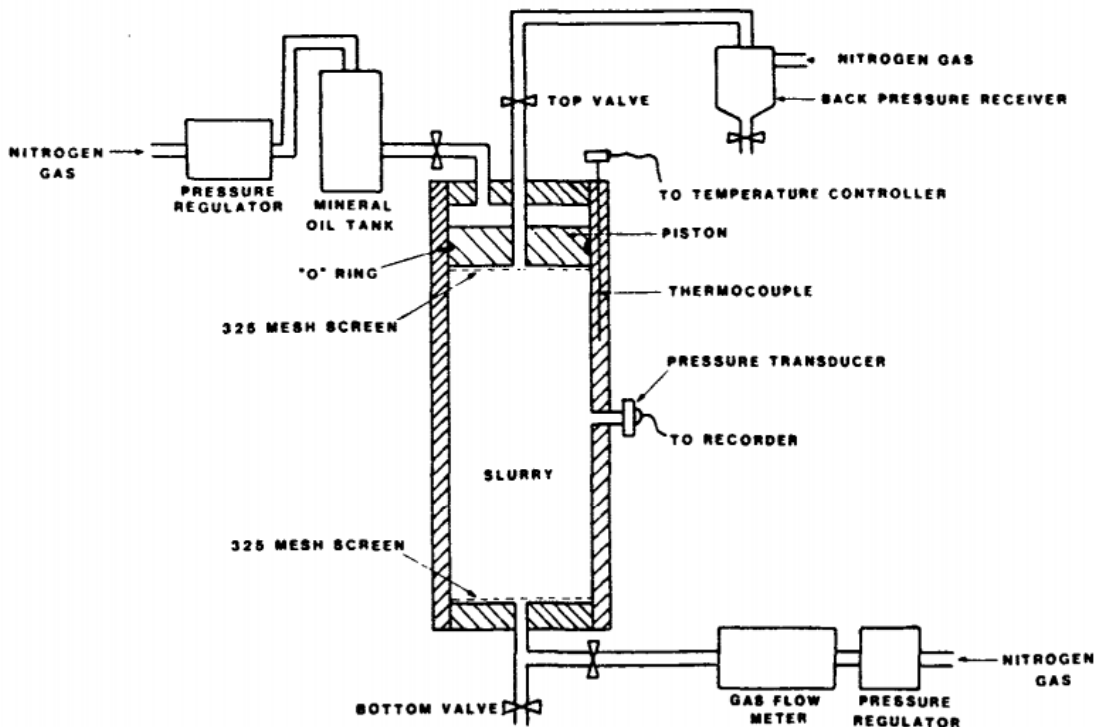


Figure 2- 13 Gas flow simulator by Cheung & Beirute (1985)

After that, in 1988, Drecq and Parcevaux designed an apparatus (Figure 2-14) by using dual cells for quantitative measuring the gas migration by dynamic permeability (gas conductivity) with the

other cell applying the hydrostatic to reduce the fluid loss effect on slurry pore pressure. The dynamic pressure cell was used to measure the gas conductivity. The hydrostatic pressure cell recorded the cement pore pressure reduction during the experimental period. The device provided an idea to separate the influence parameters rather than put all variables in a single cell. The device also provided a better way to heat the system, putting the cells in the thermostatic oven to heat evenly. However, even though both cells were put in the same oven with the cement prepared with the same procedure, operating two cells simultaneously still induced a significant variability to the experiment. Both cells could simulate the cement plug but could not simulate the annulus cement sheath.

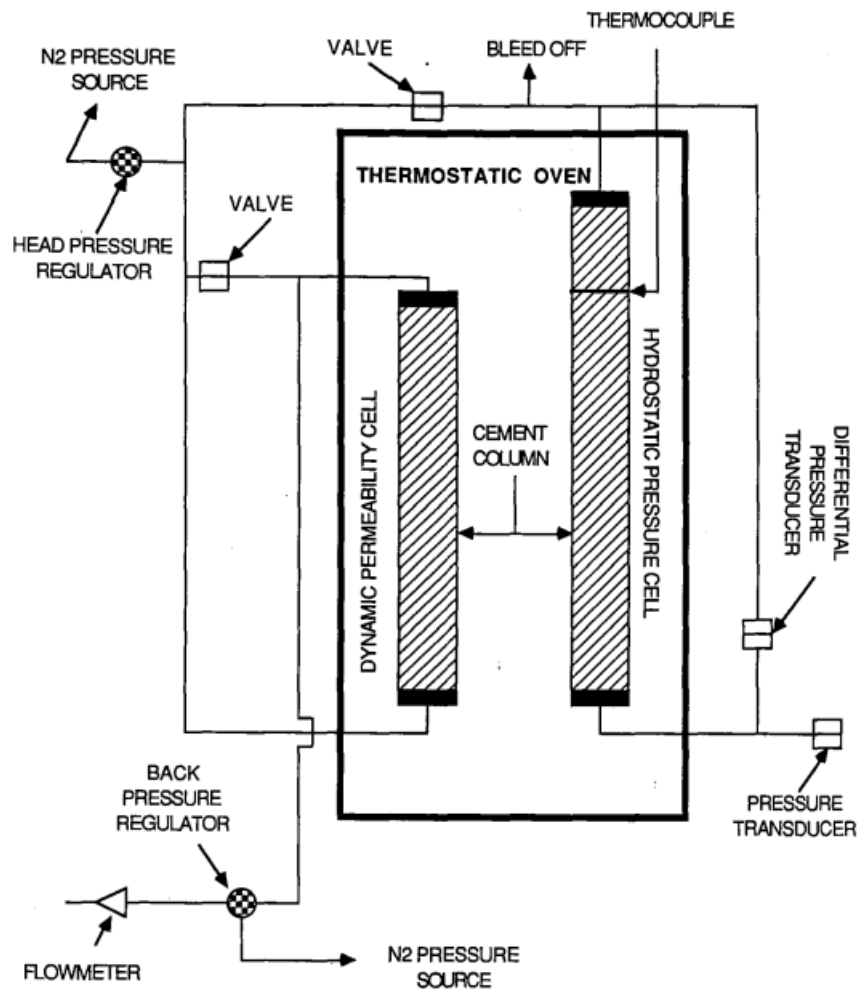


Figure 2- 14 Dynamic permeability apparatus by Drecq and Parcevaux (1988)

Furthermore, in 2018, Li et al. designed a wellbore simulator (Figure 2-15) after studying the pros and cons of the previous studies. The wellbore simulator had an inner casing OD of 5.5in and the pressure chamber ID of 9.75in. The piston was installed at the top to apply the overburden pressure. The artificial formation was put on the top of the sandstone to simulate two different permeability formations. A computer can record the temperature and pore pressure of the cement. However, the temperature probe was inserted into the cement, which may affect the integrity of the cement. Besides, the two different formations and the complex setup can lead to the artificial variability of the experiment. The system can be hard to maintain.

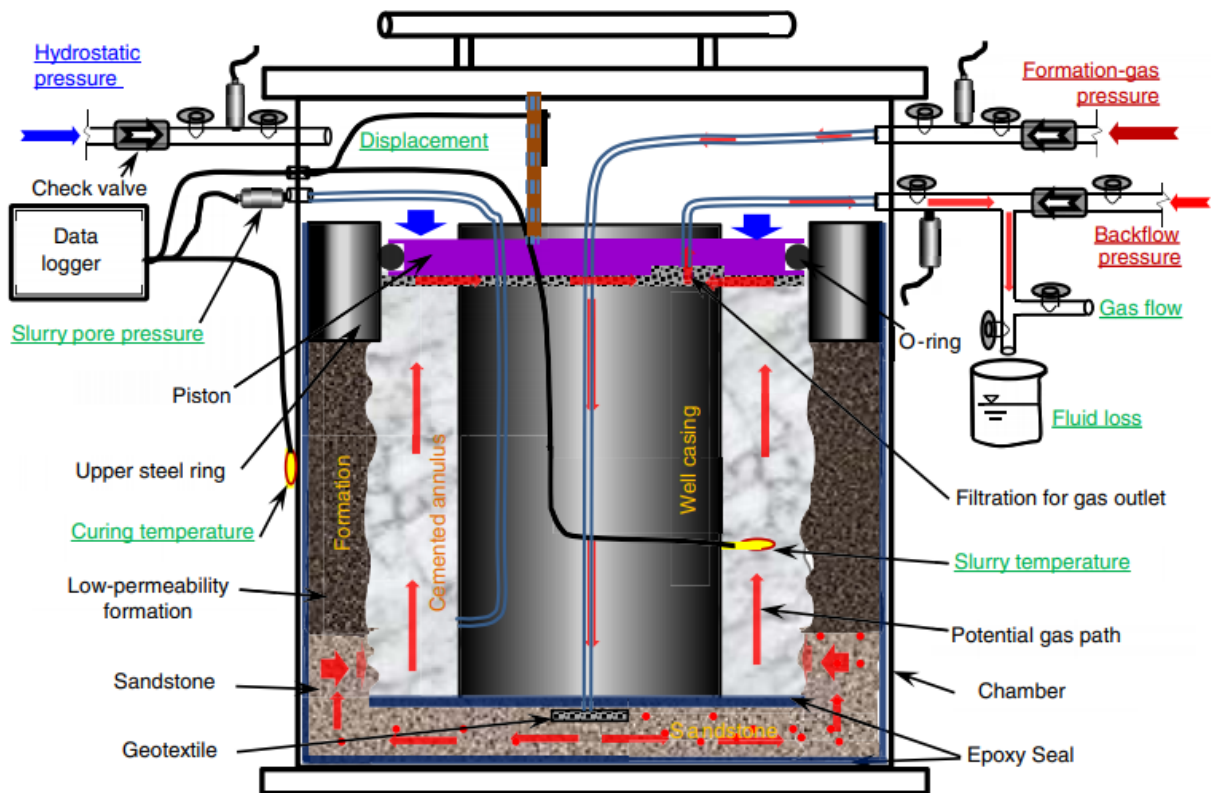


Figure 2- 15 Wellbore-Simulation Apparatus by Zhang et al., 2018

# Chapter 3 Cement Porosity and Permeability Measurement

## 3.1 Summary

The permeability of the cement is a critical parameter for evaluating the quality of the cement and the cause of the leakage from the well. However, due to the lack of API standards for curing and measuring the permeability of the cement, the permeability measurements in the previous studies were difficult to compare.

In this study, standardized procedures were developed for: i-) preparing the cement plug samples and cemented casing samples; ii-) measuring the porosity of the cement samples; iii-) measuring the permeability of the dried and wet (saturated) cement samples using nitrogen and water under steady-state conditions.

Cement porosity values measured using OFITE MODEL 350 porosimeter and the drying method were compared. Cement permeability values were measured by using four different methods: i-) Steady state nitrogen permeability measurement of the dried cement samples; ii-) steady state nitrogen permeability measurement of the saturated cement samples; iii-) the steady state water permeability measurement of the dried cement samples; iv-) the steady state water permeability measurement on the saturated cement samples.

Results show that:

- The drying method is a more accurate way to obtain the porosity of the cement samples.
- For the permeability measurement methods, the nitrogen steady-state permeability measurement for the dried and saturated samples and the water permeability measurement with precise flowrate control for the saturated samples are recommended. Among these three methods, the nitrogen steady-state permeability measurement of the dried sample gave the fastest results. The wet and dry Nitrogen permeability can obtain quantitative results, while the water permeability can only obtain the upper boundary. Nitrogen permeability measurement of the saturated samples can give the permeability results without significantly changing the cement structure compared to the dry nitrogen

permeability measurement. Besides, the wet Nitrogen permeability measurement has faster permeability measurement results compared with water permeability measurement.

- The drying process will change the structure of the cement sample, causing at least three orders of magnitude differences in permeability results. Therefore, the absolute permeability obtained by the nitrogen steady-state permeability measurement should be used with caution and only as a worst-case scenario permeability result.
- The larger total porosity does not necessarily yield to the larger permeability. There is no clear relationship between the total cement porosity and absolute permeability.
- The saturated neat Class G cement plug samples could have a permeability lower than 0.00007mD, far lower than the leakage criterion of 0.1md (Ozyurtkan et al., 2013). These results suggest that without the influence of external factors (e.g. in-situ stresses, chemical degradation by formation fluids, etc.), the cement itself can provide excellent zonal isolation even by using the neat Class G cement.

## **3.2 Introduction**

As the main component of natural gas and Greenhouse Gas (GHG), methane has a global warming potential of 70 times greater than carbon dioxide (CO<sub>2</sub>) over 20 years (Government of Canada, 2021) or 25 times over 100 years (Alberta Energy Regulator, 2021). The oil and gas sector is the most significant industrial methane emitter, contributing 44% of total methane emissions in Canada (Government of Canada, 2021). The gas leakage from the wellbore can be generally classified into two categories, surface casing vent flow (SCVF) and gas migration (GM). As shown in Figure 3-1, the trend of leaking wells with SCVF, GM, or both increased significantly between the years 2000 to 2019 (Alberta Energy Regulator, 2021). The Government of Canada also states that fixing leaks from individual wells can help to reduce the fugitive methane emission due to the activities of the upstream oil and gas industry (Government of Canada, 2020).



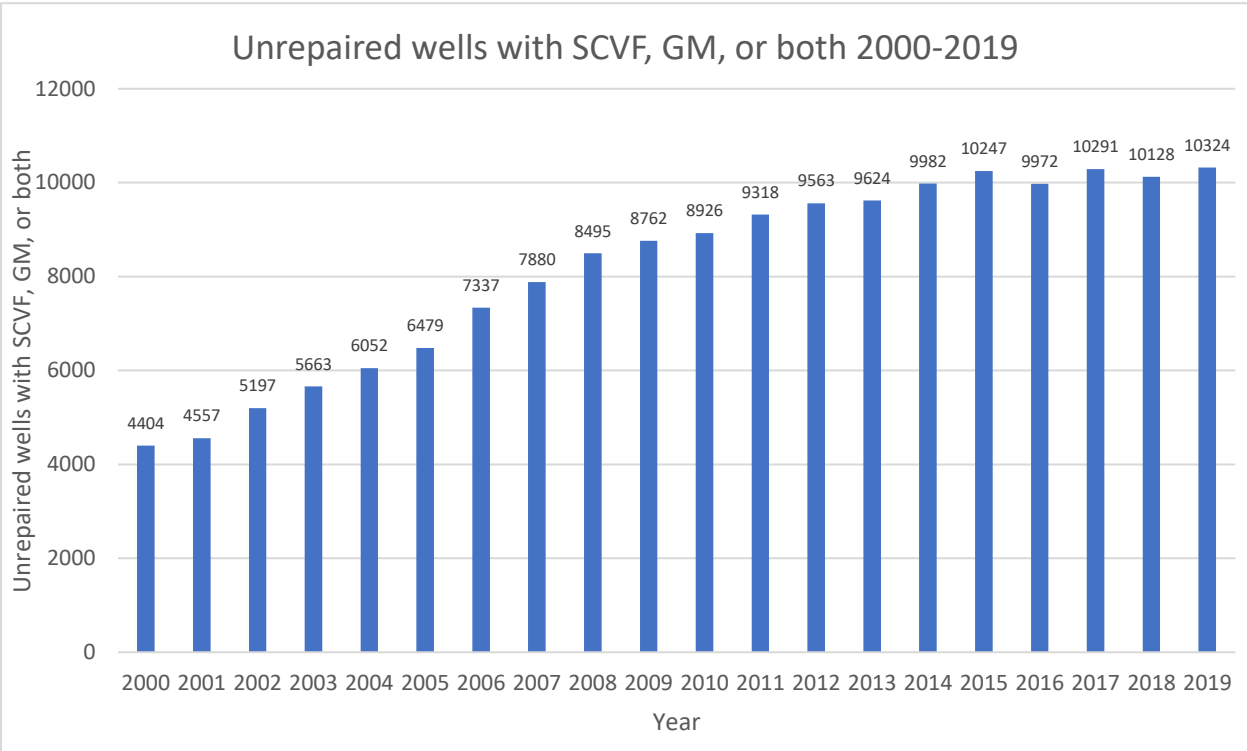


Figure 3- 1 The trend of leaking wells in Alberta (Alberta Energy Regulator, 2021)

As a critical component in the wellbore barrier system, the integrity of the cemented wellbore sections is essential to mitigate the gas leaking problem. The cement should provide zonal isolation during the entire production life of the well. The cement should also provide a gas leak-free well after plugging and abandonment of the well. About 15% of all primary cement jobs fail, and the resulting remedial cement job costs the oil and gas industry USD 450 million annually (Newman & Wojtanowicz, 2001). Even the cement is placed correctly at the beginning, the zonal isolations may still be lost over time.

The gas leakage through the cement can be treated as a fluid flow through porous media. The ability of a material to transmit the fluid is known as permeability. Therefore, when gas leakage happens in the cement system, it indicates that the cement has measurable permeability. Therefore, permeability can be considered as a critical parameter for evaluating the zonal isolation provided by cement. Although the importance of long-term integrity of the cemented wellbore sections has well been recognized, most wellbore cement research studies were limited

to the investigation of the cement plug permeability measurements. None of the previous research covered a whole range of investigations, including the very basic small cement plug measurements and the enhanced stage of large-scale cement system permeability measurements using a physical wellbore simulator that simulates the downhole conditions.

There have been numerous previous studies reporting only measurements of the permeability of the cement plug(s) (Ozyurtkan et al., 2013; Celia et al., 2005; Bauer, S.J. et al., 2019). Other studies (Carter and Slagle, 1972; Carter et al., 1973; Garcia and Clark, 1976; Levine et al., 1979; Tinsley et al., 1980; Sabins et al., 1982; Bannister and Lawson, 1985) have focused on the gas migration through the cement by using physical wellbore simulators. The cement plug permeability measurements could investigate the effects of very few variables as they simply involved curing the cement plug(s) and conducting the permeability test. Cement curing conditions and additives used for the cement formulations in these studies showed significant variations, leading to the different cement microstructures and, thus, different permeabilities. Also, the API standard for curing and measuring the permeability of cement does not exist. Besides, most of the curing conditions and the cylindrical shape of the cement samples were not accurately simulating the downhole conditions. The wellbore simulators can better simulate downhole conditions than the simple cement plugs. However, due to the complexity of setup and experimental procedures, some artificial variables could also be induced during these experiments. Therefore, the use of a more comprehensive approach, starting from the basic cement plug permeability measurement followed by the wellbore simulator permeability study for the cement, is needed to better understand the causes of the variation of cement system permeability under downhole conditions.

Celia et al. (2005) summarized the potential leakage pathways in a typical wellbore barrier system as shown in Figure 3-2. In the figure, '3' refers to the gas leakage through the cement matrix; '5' refers to the gas leakage through the cement fracture; '1', '2', and '6' refer to the gas leakage through the interface between the cement and other materials (i.e. casing and rock). Investigating the permeability of such a complex system will require comprehensive work covering the full range of investigations of cement plug to cemented wellbore sections, including cemented casings and cemented casing-rock annular sections. We start with the simplest and most straightforward case, permeability measurement of the pure cement plug. The permeability

result, in this case, will show the permeability of the cement matrix, which is the basic data needed for all other further studies.

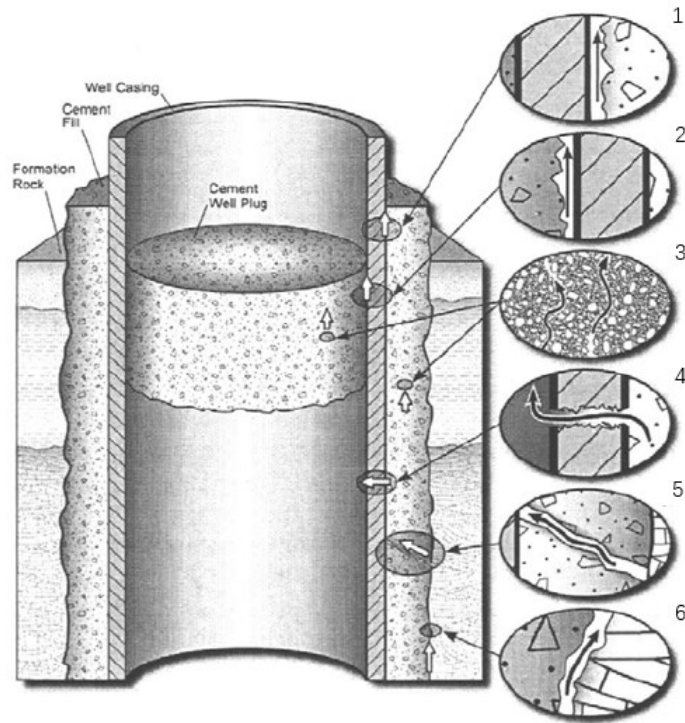


Figure 3- 2 Potential leakage pathways in the wellbore barrier system

This chapter presents standard procedures for preparing neat Class G, G abandonment, G EXP, and REMEDIALmix EC cement plugs and cement casing samples, measuring the porosity of the cement plugs and cement casing samples and measuring the permeability of cement plugs and cement casing samples. The methodology for conducting measurements in each case is presented in detail. Finally, the results and discussions are presented, and the chapter will end with conclusions.

### **3.3 Material and methods**

This part describes the sample preparation procedure for cement plug and casing cement samples. Besides, the cement porosity measurement methods used in this study are also described and compared. Finally, the description and validation of cement permeability measurement methods: water steady-state permeability measurement on wet samples, Nitrogen steady-state permeability measurement on wet samples, Nitrogen steady-state permeability on dry samples are proposed.

#### **3.3.1 Preparation of cement samples**

The preparation of cement samples includes the preparation of cement plug samples and cement casing samples. The cement blends involved in this study are described below:

- Class G without expansion agent (hereafter referred to as ‘Class G’) is the plain Class G cement without additives. The cement will have substantial free water and no fluid loss control. The slurry will likely show the sign of particle settling where the lower density cement will stay at the top. Due to these reasons, the cement is not pumped in the real world.
- Class G with expansion agent (hereafter referred to as ‘G EXP’) is the Class G with the temperature expansion additives. The cement will likely reduce the free water and particle settling by adding additives. This cement is also not used in the real world. The purpose of measuring this cement blend is to show the effect of temperature expansion additives on the permeability of the cement.
- Abandonment blend without expansion agent (hereafter referred to as ‘G Abandonment’) is a traditional cement blend widely used in the industrial and used for well abandonment. The blend has minimal free water, particle settling and controlled fluid loss. However, the blend is shown and tested to have bulk shrinkage.
- Abandonment blend with expansion agent (hereafter referred to as ‘REMEDIALmix EC’) is the new abandonment blend from Sanjel Energy Service. It is a real-world

commercial blend pumped in abandonment well. The blend has minimal free water, particle settling, and controlled fluid loss. The blend does not show bulk shrinkage after testing.

The water/cement ratio and calculated cement density are the two critical parameters before mixing the cement. The water-cement ratio gives the mass ratio of the cement to water. The calculated cement density gives the mixing quality of the cement slurry by comparing it with the measured cement slurry density. The exact numbers for these two parameters of each blend are listed in Table 3-1.

Table 3- 1 Cement w/c ratio and calculated slurry density

Cement Name	W/C Ratio	Calculated Slurry Density, kg/m <sup>3</sup>
Class G	0.4500	1901
G EXP	0.4479	1901
G Abandonment	0.4343	1901
REMEDIALmix EC	0.4498	1750

The calculated cement slurry density is another important parameter to know because it can indicate the mixing quality of the cement when compared with the measured density of the cement slurry. The theoretical density of the cement slurry is calculated based on the water-cement ratio or the weight of water and cement required. The general formula for calculating the slurry is listed below:

$$\rho_s = \frac{100}{\left[ \frac{c_s}{\rho_s} + \frac{[100 - c_s]}{\rho_l} \right]} \quad (\text{Equation 3 - 1})$$

Where

$\rho_s$  is the density of the slurry ( $kg/m^3$ )

$c_s$  is the weight concentration of the solids in the slurry (%)

$\rho_l$  is the density of the liquid ( $kg/m^3$ )

In our case, the liquid is the water. For the convenience of the measurement and calculation, 100g water is used to mix the cement slurry and the calculations. To simulate the scenarios on the fields, tap water is used for all the cases.

Three different rotation speeds should be used based on API 10A (American Petroleum Institute, 2002). While adding the cement blend, the mixer should be maintained at 4000rpm with a uniform rate of no more than 15 seconds. After adding all the cement, a mixing of 12000 rpm rotation speed should be held for 35 seconds. Then, a 30 minutes low speed, 150 rpm mixing process is followed.

In our experiment process, the combination of two mixers was used. The high-speed mixer (shown in Figure 3-3a) was a handheld mixer with a capacity of up to 12000 rpm. This mixer was used for 15 seconds and 35 seconds of high-speed mixing for all cement blends. Then, the mixture was immediately transferred to the low-speed mixer (shown in Figure 3-3b), which was adjusted to the rotation speed of 150 rpm for the 30 minutes mixing. The lid was put on the mixing container to avoid air intrusion.



Figure 3- 3 a (left side) the high speed mixer used for small sample preparation; b (right side) the low speed mixer used for small sample preparation

After mixing, the cement slurry is injected slowly into the mould. For the cement plug samples, the mould is 1in ID\*1in length PTFE. The reasons for choosing PTFE are listed in Appendix A, A.1.3 Cement mould selection, preparation and sealing of cement samples. For the cement casing samples, the mould is 1in OD\*1in length 4130 Steel. The reason for choosing 4130 rather than 4140, the material used to make the casing, is because of the accessibility of the 1in OD 4130 pipe. The core holder is built to measure the samples with 1in diameter. Besides, from the material's content, the only difference is in the carbon content (0.28-0.33% for 4130, 0.38-0.43%

for 4140). Therefore, 4140 steel will have higher hardenability and strength than 4130.

Therefore, 4130 is a better choice considering the accessibility and the similar material content.

Then, the samples are placed into the curing cell in the oven. To accelerate the cement curing for the Class G and G EXP samples, 50°C and 1500 psi were used. Ambient temperature, 1500psi, were used for G Abandonment and REMEDIALmix EC samples. The detailed steps and the picture of the apparatuses used are shown in Appendix A, A.1.4 Curing of the cement samples.



### 3.3.2 Porosity measurement methods

This study used two porosity measurement methods, porosity measurement by drying and porosity measurement by OFITE MODEL 350 porosimeter (Figure 3-4).

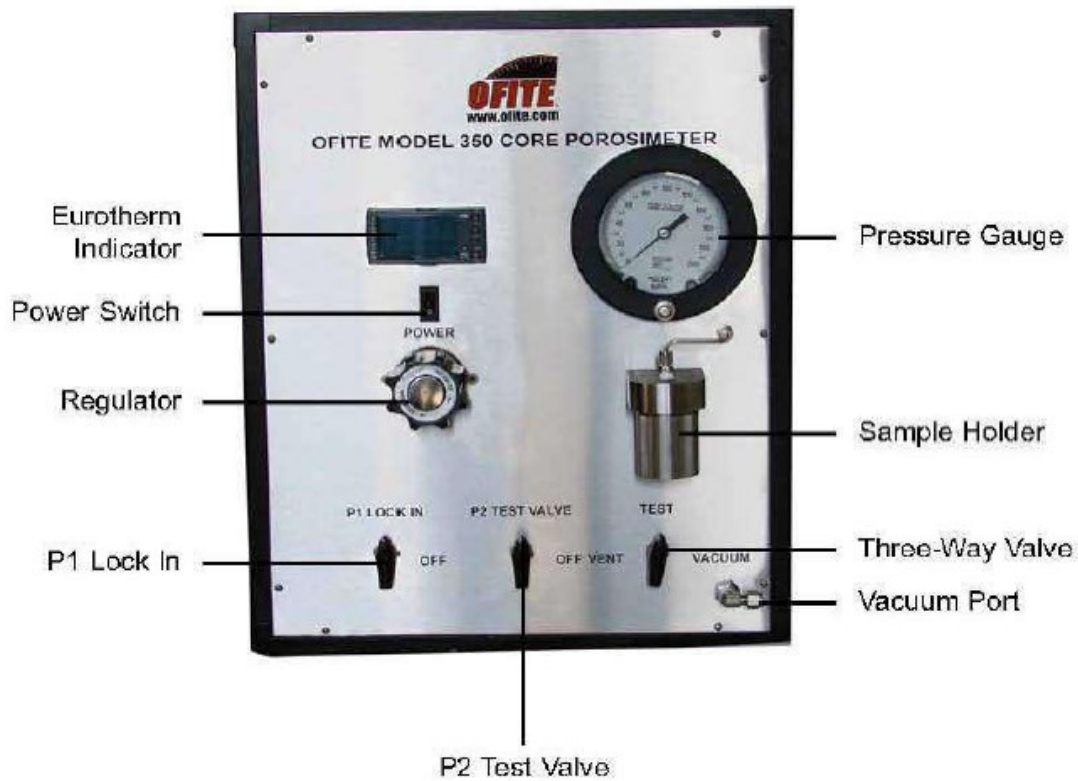


Figure 3- 4 OFITE MODEL 350 porosimeter

The porosity measurement by drying used the water loss in the cement sample to obtain the total porosity of the cement. After curing cement, the mass of the cement sample was immediately measured and recorded. The cement samples were then put into the oven at 60 Celsius by the sand bath. The mass for the cement samples was tracked and recorded at least once per day. The test was finished once the cement mass reached a relatively constant value or at least not changed for 24hours. The detailed operating steps for the drying process and the sand bath were described in Appendix B, Measurement of cement porosity and drying of cement. Figure 3-5 shows a sample mass change versus the time for the Class G and G EXP samples. The cement mass was

closely monitored at the first 8 hours as the mass changed rapidly during this period. The difference between the initial and final mass of the cement sample was calculated. Using the density of water under 21 Celsius (the lab room temperature), the volume of the lost water was calculated. This volume was assumed as the total pore volume. The bulk volume of the sample was easily calculated from the dimensions of the sample as the sample is cylindrical. Then, the pore volume divided by the bulk volume yielded the porosity of the cement sample. One of the sample calculation procedures for Class G and G EXP in Figure 3-5 is shown in Table 3-2.

Table 3- 2 Sample calculation procedure for Class G and G EXP shown in Figure 3-5

Dimension	G EXP	Class G
Diameter, D(cm)	2.6400	2.6300
Length, L(cm)	2.2533	2.2100
Bulk volume, Vb(cc)	12.3345	12.0059
Mass difference, delta m (g)	3.8800	3.8400
Pore volume, Vp (cc)	3.8878	3.8477
Porosity, $\phi$	0.3152	0.3205

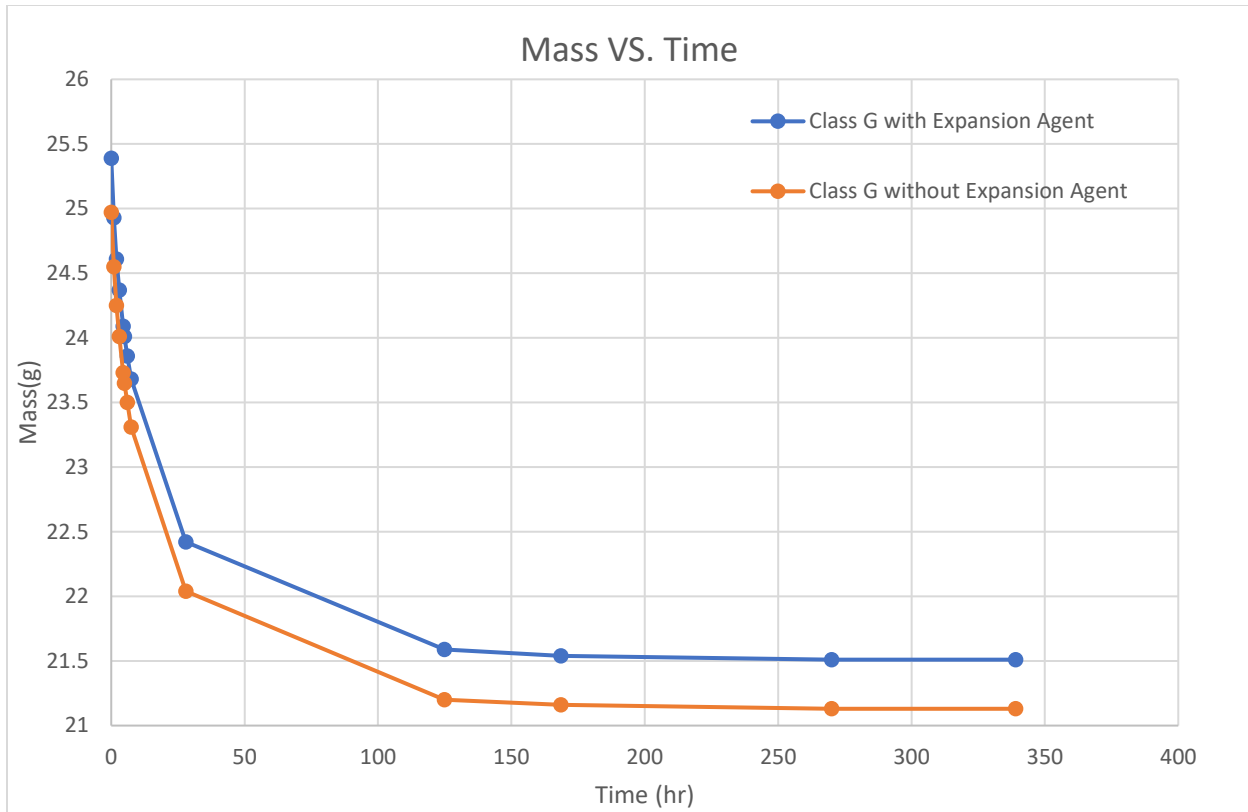


Figure 3- 5 Mass change vs. time for G EXP and Class G cement plug samples

Another method was to use the OFITE MODEL 350 porosimeter. The working theory of the porosimeter was based on Boyle’s law. The schematic of the porosimeter is shown in Figure 3-4. The porosimeter had two constant volume spaces, the reservoir and the sample chamber. The sample was placed in the sample chamber, and the desired nitrogen pressure was applied to the reservoir when the P2 valve was turned off. The nitrogen was with known volume and pressure in the reservoir chamber. Then, the P2 valve was switched on. The nitrogen moved from the reservoir to the whole system. Then, by using Boyle’s law shown by Equation 3-2, the volume of grain in the sample could be calculated by Equation 3-3. Then, the porosity could be obtained by Equation 3-4.

- $P_1V_1 = P_2 * (V_{reservoir} + V_{chamber} - V_{Grain\ in\ sample})$  (Equation 3 – 2)
- $V_2 - V_3 = (V_{reservoir} + V_{chamber}) - (V_{reservoir} + V_{chamber} - V_{Grain\ in\ sample}) = V_{Grain\ in\ sample}$  (Equation 3 – 3)
- $\frac{(V_B - V_{Grain\ in\ sample})}{V_B} = \emptyset$  (Equation 3 – 4)

Where,

$V_1 = \text{Reservoir volume (known constant)} = V_{Reservoir}$

$V_2 = \text{Reservoir volume} + \text{sample chamber volume (known constant)} = V_{Reservoir} + V_{Chamber}$

$V_3 = \text{Reservoir volume} + \text{sample chamber volume} - \text{grain volume in the sample} = V_{Reservoir} + V_{Chamber} - V_{Grain\ in\ sample}$

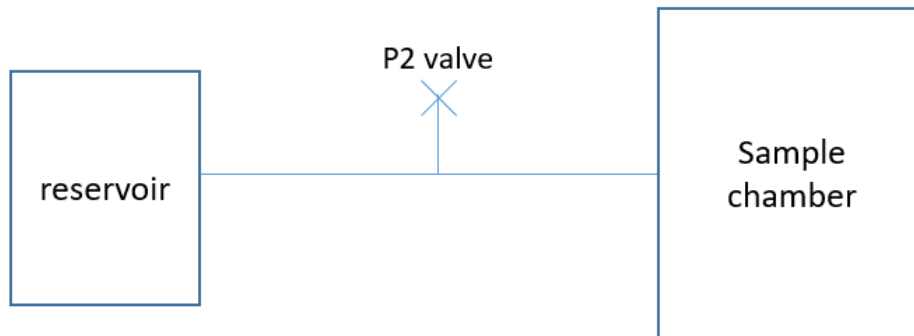


Figure 3- 6 Schematic for the porosimeter used in this study

### 3.3.3 Steady-state permeability measurement methods

This study used three steady-state permeability measurement methods: the nitrogen permeability measurement on the dried cement sample, the nitrogen permeability measurement on the saturated cement sample, and the water permeability measurement on the saturated cement sample. The water permeability on the dried cement sample was not used due to the effect of rewetting (Kjellsen & Jennings, 1996). As the re-wetting of the cement sample, the pressure will be hard to stabilize as the water will alter the permeability of the cement. After the experiments, the nitrogen permeability on the saturated cement sample was also not considered a suitable method. The nitrogen would displace the water in the cement, making the pressure hard to stabilize.

For both water permeability and nitrogen permeability, the schematics for the experiment setup and the detailed procedure of applying the pressure can be found in Appendix A, A.2.1 Steady-state water permeability measurement on cement samples, and A.2.2 Steady-state permeability measurement on cement samples by Nitrogen. This section described the Klinkenberg correction procedure for nitrogen permeability and the formula to calculate the permeability.

For the water permeability, the classic Darcy equation was used (Equation 3-5)

$$k = \frac{q\mu L}{A * \Delta P} \quad (\text{Equation 3 - 5})$$

Where,

q = the flowrate at the steady state, in  $cm^3/s$

k = the permeability of the sample, in darcies

A= the cross-sectional flow area, in  $cm^2$

$\Delta P$  = the pressure drop between the inlet and outlet, in atm

L = length of the sample, in cm

$\mu$  = the viscosity of the fluid, in cp

Precise fluid control is needed to measure the ultra-low permeability sample using water, although the equation is straightforward.

For the nitrogen permeability, the Klinkenberg correction was needed to obtain the absolute permeability for the cement using nitrogen. At least three nitrogen permeability values need to be measured under three different pressures. Then the nitrogen permeability was plotted versus the reciprocal of the average pressure between the inlet and outlet. Then, the intercept will be the absolute permeability. The calculation of the nitrogen permeability is shown by Equation 3-5, and the sample figure of Klinkenberg correction for the dried G Abandonment sample is shown in Figure 3-7.

$$k_a = \frac{2000p_a\mu q_a L}{(p_1^2 - p_2^2)A} \quad (\text{Equation 3 - 6})$$

Where,

$k_a$  = the nitrogen permeability, in mD

$p_a$  = atmospheric pressure, in atm

$p_1$  = upstream pressure, in atm

$p_2$  = outlet pressure, in our case atmospheric pressure, as the end was opened to the atmosphere

$L$  = length of the sample, cm

$\mu$  = the viscosity of nitrogen at 21°C (lab room temperature), cP

$q_a$  = gas flow rate at atmospheric pressure,  $cm^3/s$

$A$  = Cross-sectional flow area,  $cm^2$

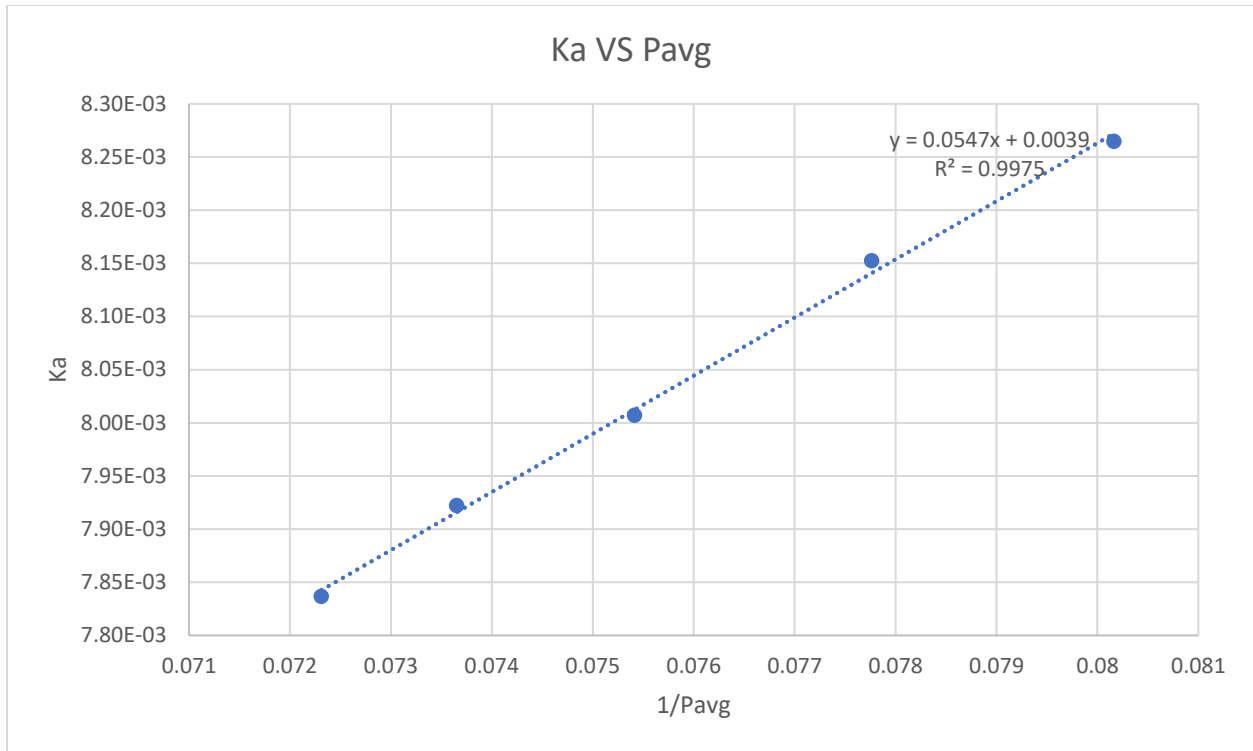


Figure 3- 7 Klinkenberge correction for the dried G Abandonment sample

For the detailed operating procedure, please check Appendix A.

### 3.4 Results and discussions

#### 3.4.1 Flowrate and inlet pressure steady state criterion

For the steady-state method, it is critical to have the criterion for steady-state inlet pressure and steady-state flow rate. The criterion of reaching the steady-state for the inlet pressure is based on the pressure vs time diagram. When the pressure reaches a relatively dynamic stable level for at least 5mins, the pressure can be assumed to be in a steady state. Figure 3-8 shows pressure data vs time for the G Abandonment sample, which was used to validate the permeability measurement process for the nitrogen permeability for the dried cement sample.

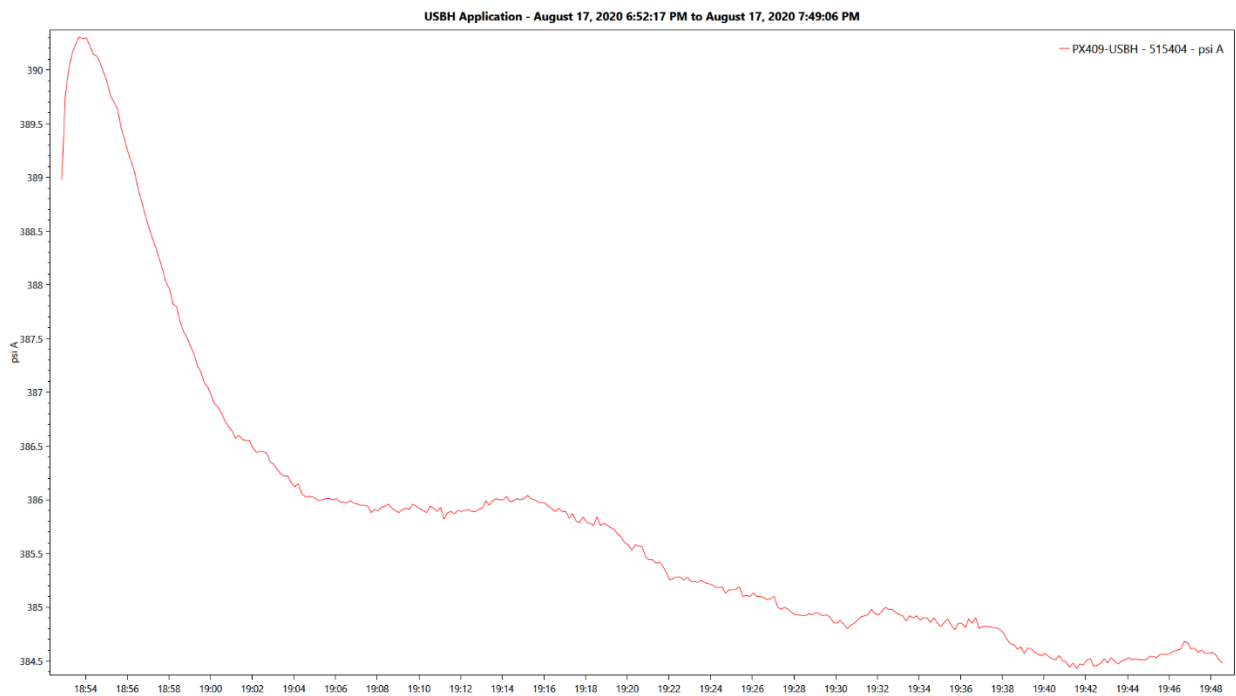


Figure 3- 8 Inlet pressure vs. time for dried G Abandonment sample

For the criterion for the flow rate reaching the steady-state, five measurements for the flow rate were conducted and recorded. Typically, the times to move the bubble to the 10cc, 20cc, 30cc, 40cc, 50cc were recorded. The time difference between the adjacent values was calculated. If the difference or the flow rate under each volume level was close, the flow rate was in a steady state.



Table 3-3 shows one of the flowrate calculation processes and the criterion to judge if the flowrate was under the steady state. As shown by table 3-3, the flow rate difference is less than 0.001 cc/s for the five-volume levels. Therefore, the flow is in a steady state.

Table 3- 3 One of the flow rates calculations for G Abandonment dried sample

Q, ml	t,s	q cc/s
10	25.3	0.395257
20	50.58	0.395413
30	75.86	0.395465
40	101.22	0.395179
50	126.32	0.39582

### 3.4.2 Validation of the porosity measurements

The porosity measurement by drying and the porosity measurement by porosimeter showed a considerable difference. The porosimeter gave the porosity result of 9.55% for the Class G sample, while the measurement by drying gave 39.45%. There is a 413% difference between the two methods. It also happened to the G EXP sample, whose porosity was 4.06% measured by porosimeter and 39.92% measured by the drying method. The difference between the result was 983%. Therefore, one of the methods should be wrong. Back to the working theory of the porosimeter, nitrogen gas was used to penetrate the pore of the sample to obtain the grain volume of the sample. The pressure needed to be high enough to penetrate the pores in the sample. However, the permeability measurement data showed that at least 200psi was needed to get the breakthrough in the Class G and G EXP dried samples. Due to this reason, the 70psi pressure applied by the porosimeter could not penetrate all the pores in the cement sample. Therefore, it will underestimate the porosity of the sample.

One G Abandonment sample was prepared and sent to the corelab after the measurement by drying to validate the drying method. The sample was stored in a sealed bag to avoid absorbing the water through the air. The porosity measured by the corelab was 30.1%, while the porosity

measured by drying was 37.15%. The difference between the porosity difference was due to the pressure difference. The corelab measured the porosity under 800psi, which was the confining pressure value for the permeability measurement, while the measurement by drying was conducted under ambient pressure. Therefore, the porosity result from the corelab should be larger than the result obtained by the drying method. However, this only gave qualitative confirmation of the result.

The two saturated Scioto sandstone samples were measured to obtain quantitative validation of the method. The results from two samples by drying were 18.50%, 18.36% separately, while the theoretical value was 16-18%. The error compared with 18% was lower than 2.7%. Therefore, the cement porosity measurement by drying can be a suitable method to estimate the porosity of the cement.

### 3.4.3 Cement porosity by drying methods

The porosity results for different cement are shown in Table 3-4.

Table 3- 4 Porosity results for the cement measured by drying method

Cement name	Curing condition	Porosity, %
Class G 1 <sup>st</sup> sample	1500psi 50°C	39.45
Class G 2 <sup>nd</sup> sample	1500psi 50°C	32.05
G EXP 1 <sup>st</sup> sample	1500psi 50°C	39.92
G EXP 2 <sup>nd</sup> sample	1500psi 50°C	31.52
G Abandonment 1 <sup>st</sup> sample	1500psi 50°C	37.15
G Abandonment 2 <sup>nd</sup> sample	1500psi ambient temperature	39.96
REMEDIALmix EC 1 <sup>st</sup> sample	1500psi 50°C	42.47
REMEDIALmix EC 2 <sup>nd</sup> sample	1500psi ambient temperature	43.62

From Table 3-4, even with the same cement blend and curing conditions, the difference for the porosity result can be more than 7%. The REMEDIALmix EC cured under 1500psi, and the ambient temperature had the largest porosity, while the G EXP sample had the lowest total porosity. The commercial abandonment blend, G Abandonment and REMEDIALmix EC had higher porosity compared with the other blend. Besides, the curing condition difference of 50 Celsius degrees did not have too much influence on the cement porosity compared to the result between the 1<sup>st</sup> and 2<sup>nd</sup> G Abandonment and REMEDIALmix EC samples.

### **3.4.4 Steady-state nitrogen permeability validation and data comparison**

The G Abandonment plug sample (G Abandonment 2<sup>nd</sup> sample) was prepared for permeability validation. The sample was cured under 1500psi and ambient temperature. The sample was dried in a sand bath at 60°C. The nitrogen steady-state permeability measurement was conducted, and the absolute permeability was measured as 0.0039mD for the sample. The sample was then sent to the corelab. The measurement condition was the same, 800psi confining pressure, five points steady-state nitrogen permeability measurement, and corrected by the Klinkenberg effect. The result from corelab was 0.0043mD. The sample was then measured for the second time to check if the shipment would create a significant error. The second measurement result was 0.0046mD. The difference between the results was acceptable, which validates the nitrogen permeability measurement on the dried cement sample.

For the nitrogen permeability measurement on the saturated sample, the Scioto sandstone was used. However, as shown by Table 3-5, the applied nitrogen flow displaced more than 50% fluid in the core. Due to this, the pressure was hard to reach the steady state. Besides, by comparing the permeability of samples one and two, the permeability was negatively related to the liquid left in the sample. As 4.44% less liquid is left in the sample, the difference in the permeability could be 50%. Therefore, the nitrogen permeability measurement on the wet sample was not a suitable method.

Table 3- 5 Measurement data for 1st and 2nd Scioto Sandstone

<b>Sample</b>	<b>S1</b>	<b>S2</b>
Dry Mass, g	27.97	27.99
Mass After Saturation, g	30.4	30.4
Saturated Pore Volume, cc	2.394089	2.374384
Sample Diameter, cm	2.546	2.544667
Sample Length, cm	2.542	2.542667
Bulk Volume, cc	12.94143	12.93127
Calculated Porosity	18.50	18.36
Theoretical Porosity	16-18	16-18
Mass After Permeability test, g	29.05	28.93
Mass loss, g	1.35	1.47
Solution left%	44.44	39.00
Permeability, mD	0.3554	0.7175

The water permeability measurements on the saturated G abandonment plug and G Abandonment casing cement samples were conducted. The pressure vs time figure (Figure 3-9) for the G Abandonment sample showed that the pressure kept increasing till the limit of the equipment without any breakthrough. No fluid was collected from the outlet side. These also happened to the G Abandonment casing cement sample. However, using the flow rate and the maximum pressure, the upper boundary of the saturated cement permeability could be obtained.

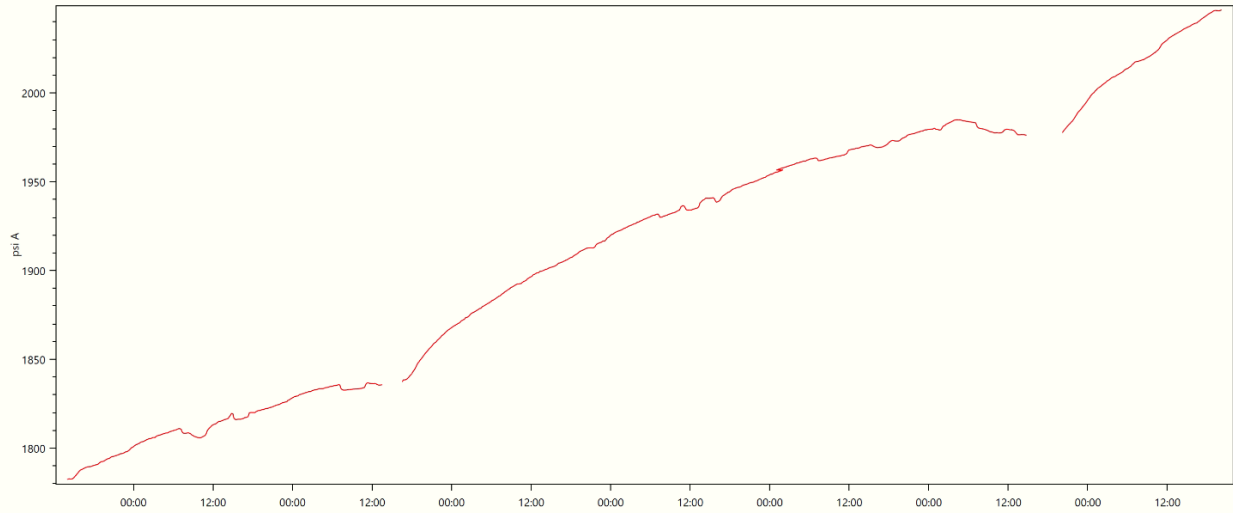


Figure 3- 9 Pressure vs time for the saturated G Abandonment plug sample

### 3.4.5 Steady-state permeability measurement result

The table (Table 3-6) below summarizes the steady-state permeability measurement results for different samples by water and nitrogen.

Table 3- 6 steady-state permeability measurement results for different samples by water and nitrogen

Cement Type	Curing Condition	Sample Condition	Fluid	Porosity	Permeability, mD
G	1500Psi 50C	Dried	N2	32.05	0.0078
G	1500Psi 50C	Saturated	N2	N/A	7.00E-05
G Exp	1500Psi 50C	Dried	N2	31.52	0.0055
G Exp	1500Psi 50C	Saturated	N2	N/A	N/A under 905 psi
G Abandonment	1500Psi Ambient	Dried	N2	39.96	0.0039
G Abandonment 2 <sup>nd</sup> measurement	1500Psi Ambient	Dried	N2	39.96	0.0046
Casing G Abandonment	1500Psi Ambient	dried	N2	37.28	Higher than 131 mD, not accurate due to the transducer error
G Abandonment	1500Psi Ambient	Saturated	N2	N/A	N/A under 2211 psi
G Abandonment	1500Psi Ambient	Saturated	Water	N/A	Lower than 5.27E- 6
Casing G Abandonment	1500Psi Ambient	saturated	Water	37.28	lower than 2.35E-5 mD
REMEIDALmix EC	1500Psi Ambient	Dried	N2	43.62	0.0037
REMEIDALmix EC	1500Psi Ambient	Saturated	N2	N/A	N/A under 2197 psi

By comparing the cement sample's permeability with the cement samples' total porosity, there is no clear relationship between the total porosity and the permeability. The permeability of the REMEDIALmix EC was the lowest, while the total porosity of the sample was the highest. This may be due to the lack of connected pores to form the leakage pathway. The pores in the REMEDIALmix EC and G Abandonment do not connect. Therefore, it is also hard to obtain the permeability result using nitrogen for the saturated cement sample. Compared with the nitrogen permeability on the saturated cement sample, water permeability could be better. It will give the upper boundary of the cement permeability, which is approximately zero permeability in our case. Although the gas permeability measurement on the dried sample can yield qualitative results, the drying process will alter the cement structure and cause a high permeability difference between the saturated sample and the dried sample. However, the nitrogen permeability measurement on the saturated cement sample can reasonably simulate the drying process of the cement. It also gave us the permeability without altering too many structures in the cement compared with the measurement on the dried samples. Furthermore, it gave a faster measurement compared with water permeability measurement.



### 3.5 Conclusions

In this study, the standardized procedures for preparing the cement plug samples and cement casing samples, measuring the porosity of cement samples, and measuring cement permeability by steady-state methods using water and nitrogen for both dried and saturated samples were presented.

The nitrogen steady-state permeability measurement provided quantitative absolute permeability and total porosity results for the dried cement samples of non-commercial use cement blend, Class G, G EXP, and commercial use abandonment blend, G Abandonment REMEDIALmix EC.

The water steady-state permeability measurement gave the upper boundary of the permeability for the saturated cement samples. Based on the results of the investigations from this chapter, the following conclusions can be offered:

- Compared with the OFITE MODEL 350 porosimeter, though it takes more time, the drying method is a more accurate way to obtain the porosity of the cement samples. By increasing the max applied pressure of the porosimeter, the porosity measurement result may be more accurate.
- The nitrogen steady-state permeability measurement of the saturated cement sample was a proper way to simulate the drying process of the cement. After the cement is placed downhole, the cement will lose water as time goes on. During wet Nitrogen permeability measurement, the water in the cement plug will also be lost. The technique also allowed to measure permeability without significantly altering the cement microstructure compared with the measurement of the dried samples. Furthermore, it resulted a faster measurement compared with water permeability measurement. Therefore, this technique was used for future permeability measurements using the physical wellbore simulator.
- As for the permeability measurement methods, the nitrogen steady-state permeability measurement of the dried samples and the water permeability measurement with precise flowrate control of the saturated samples are recommended. Between these two methods, the nitrogen steady-state permeability measurement on the dried sample is faster and can obtain quantitative results. However, the drying process will change the structure of the

cement sample, causing at least three orders of magnitude differences in permeability results. Therefore, the absolute permeability values obtained by the nitrogen steady-state permeability measurements should be used with caution and should only serve as worst-case scenario permeability results.

- The water steady-state permeability measurement of dried cement samples was unsuitable for measuring the permeability. The water steady-state permeability measurement on dried cement samples causes the rewetting of the cement sample, which makes it difficult for the injection pressure to stabilize.
- The larger total porosity does not cause the larger permeability. There is no clear positive or negative relationship between the total porosity and absolute permeability.
- Water permeability of the saturated neat Class G plug samples could be lower than 0.00007mD, far lower than the leakage criterion of 0.1md (Ozyurtkan et al., 2013). This indicated that without the influence of the external factors, by appropriately setting the cement, the cement itself can provide excellent zonal isolation even by using neat Class G cement.

For future work, external factors such as the geometric scaling effect of the cement sample, the cyclic temperature and mechanical stress can be considered when measuring the cement permeability. The flow rate control can be further improved by using the precise Quizix pump, which can help obtain the steady-state water permeability for the saturated cement samples. Furthermore, by measuring the nitrogen permeability of the wet cement samples under different saturation levels, the relationship between the liquid saturation and the permeability can be obtained, which would make the nitrogen permeability measurements of the saturated sample more realistic.

# Appendix A Experimental Procedure

## A.1 Cement sample preparation

The cement materials, mixing procedure, mould preparation, and the curing procedure of the hardened cement paste samples are described in the following sections.

### A.1.1 Cement material

Four cement blends shown in Figure A-1, neat Class G, Class G cement with Expansion Agent, Abandonment Cement without Expansion Agent, and Abandonment Cement with Expansion Agent, are studied in this section. Neat Class G cement, shortened as Class G, is rarely used in fields as it has no fluid loss control compared with other cement blends and therefore will have substantial free water and show some signs of the particle settling with the low-density cement on the top. However, it can provide an excellent baseline for the performance of other cement. By comparing different cement blends with Class G, the effect of additives and/or cement formula can be known. Besides, Class G is widely used and studied for academic purposes. Therefore, the properties of Class G are widely understood, which makes Class G an excellent validation blend and a good start point for the comprehensive experimental study of the performance of the cement. Class G Cement with Expansion Agent, shortened as G EXP, is a Class G based cement with low-temperature expansion additives to reduce the free water and settling of the cement slurry. This blend is not used in the real world. However, G EXP can give an excellent way to investigate the effect of low-temperature expansion additives on the permeability of the cement by comparing G EXP with Class G. Abandonment Cement without Expansion Agent, named as G Abandonment, is a traditional abandonment blend that is used in industry. It has minimal free water and particle settling with controlled fluid loss. However, based on the field test of this cement blend, it shows bulk shrinkage. By comparing G Abandonment and Class G, the performance of the abandonment formula can be demonstrated. Abandonment Cement with Expansion Agent, shortened form as REMEDIALmix EC, is a new

Class G-based abandonment blend, which is pumped on well abandonments. It has minimal free water, particle settling, and controlled fluid loss.

Moreover, based on the field test result, it did not show significant bulk shrinkage. The permeability comparison between the G Abandonment and REMEDIALmix EC will demonstrate the effect of expansion additives. In contrast, the comparison between the G EXP and REMEDIALmix EC can show the impact of the abandonment formula.



Figure A- 1 Cement blends used, from left to right, Class G, G EXP, G Abandonment, and REMEDIALmix EC

### **A.1.2 Cement mixing procedure**

After knowing the cement blend, the first step of experimental sample preparation is mixing cement. Water cement ratio, w/c ratio, and the weight ratio of water divided by cement are essential parameters for cement mixing. Before mixing, water and cement are weighed separately in the 316stainless steel cup on balance to the two digits after the decimal shown by Figure A-2, following the required water-cement ratio (w/c ratio). Table 3-1 shows the water-cement ratio needed for each cement blend.

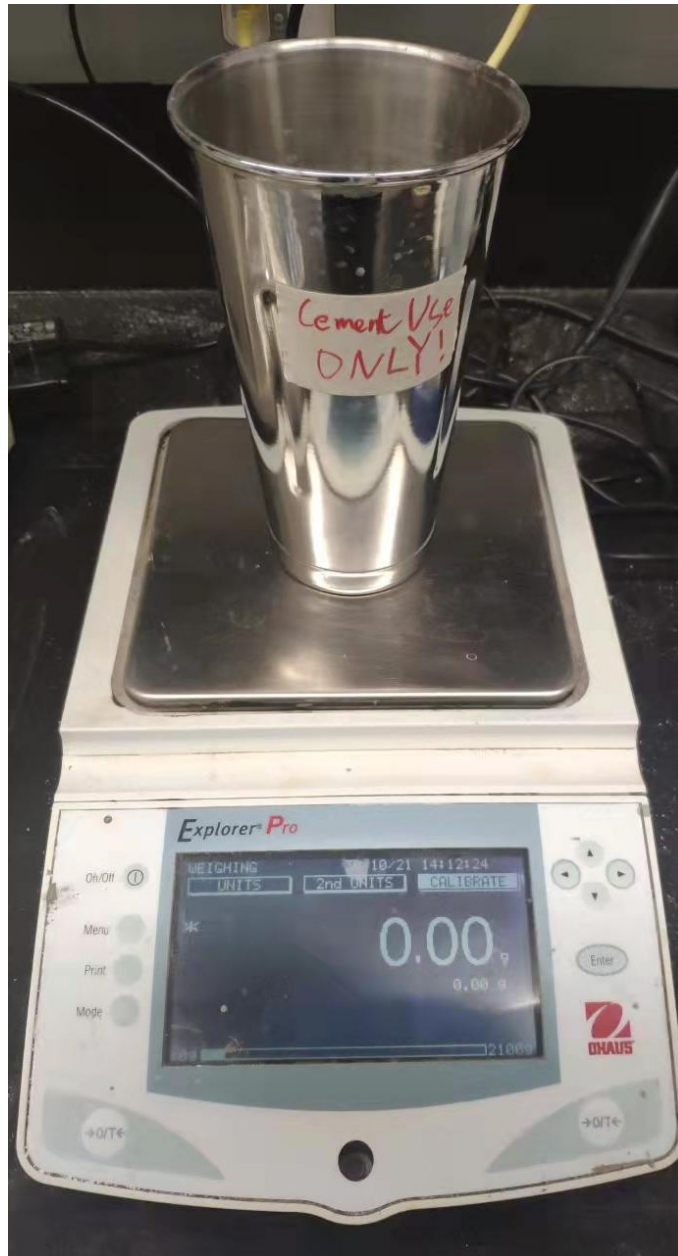


Figure A- 2 Measurement cup on the balance for small scale sample preparation

Three different rotation speeds should be used based on API 10A (American Petroleum Institute, 2002). While adding the cement blend, the mixer should be maintained at 4000rpm with a uniform rate of no more than 15 seconds. After adding all the cement, a mixing of 12000 rpm rotation speed should be held for 35 seconds. Then, a 30 minutes low speed, 150 rpm mixing process is followed.

In our experiment process, the combination of two mixers is used. The high-speed mixer (shown in Figure 3-3a) is a handheld mixer with a capacity of up to 12000 rpm. This mixer is used for 15 seconds and 35 seconds of high-speed mixing for all cement blends. Then, the mixture is immediately transferred to the low-speed mixer (shown in Figure 3-3b), adjusted to the rotation speed of 150 rpm for the 30 minutes mixing. The lid is put on the mixing container to avoid air intrusion.

### **A.1.3 Cement mould selection, preparation and sealing of cement samples**

High temperature chemical-resistant slippery PTFE tube is used to make the mould. The reason for choosing the PTFE material is described below:

Compared with metal material, PTFE is easy to cut and easy to customize the length of the mould upon the requirement of the sample. It can be cut simply by a saw, while the metal material requires the laser cutter or EDM line cutter, which is time-consuming for preparing one sample and hard to customize the length of each sample upon the changing of requirements. Besides, the cement will develop a strong bond during the curing with the stainless steel material. Due to this reason, it will be very challenging to remove the cement plug from the mould, while, for the PTFE mould, the mould can be removed by cutting a gap in the longitudinal direction of the mould.

The comparison of PTFE and PVC-P material properties are shown in Table A-1:

Table A- 1 Comparison of properties for PVC-P and PTFE materials ("PVC-P vs. PTFE: MakeItFrom.com," 2021)

Material	PVC-P	PTFE
<b>Mechanical Properties</b>		
Elongation at break,%	180	75-300
Ultimate tensile strength, MPa	16	Upto 25
<b>Thermal Properties</b>		
Max Temperature, °C	75	260-270
Melting Onset, °C	190	330-340
Thermal Conductivity, W/m-K	0.17	0.24-0.65
Thermal Expansion, $\mu\text{m}/\text{m-K}$	160	110-120
<b>Unclassified Properties</b>		
Density, g/cc	1.4	2.1-2.3
Water adsorption after 24 hours,%	0.45	0.0093-0.050

As shown by Table A-1, from the mechanical properties, the ultimate tensile strength of the PTFE is higher than that of PVC-P, which means PTEF is stronger than PVC-P in terms of tensile failure. In addition, PTFE has a higher temperature capacity than PVC-P. Max temperature is one of the critical parameters for choosing the material for the mould as the curing of the cement requires the mould and cement to be placed under the required temperature. Besides, the thermal expansion of PTFE is lower compared with PVC-P, meaning that the PTFE material will have less size-changing under the temperature. Due to this reason, by using PTFE, the diameter of the cement plug obtained from the mould will be closer to 1in than that of using PVC-P under the same 1in ID.

Furthermore, the thermal conductivity of the PTFE is also higher, which means the PTFE mould tends to pass the heat easier to the cement, making it easier for cement to reach the curing condition from its initial state. For other properties, PTFE has a higher density which will help the sample settle at the bottom of the curing cell when adding water to the curing cell before



applying any pressures. Also, PTFE has more negligible water adsorption than PVC-P, demonstrating that the curing cell will reach the stable pressure level easier by using PTFE materials as the water volume in the curing cell will change less.

The mould cut by a saw from the long PTFE pipe had an inner diameter of 1in and a length of 1in ideally. However, there are some errors in the mould's length due to the hand-cutting process. After cutting, sandpaper and a scissor are used to remove the burr around the PTFE mould and smooth the mould's edge. The finished PTFE mould is shown below:

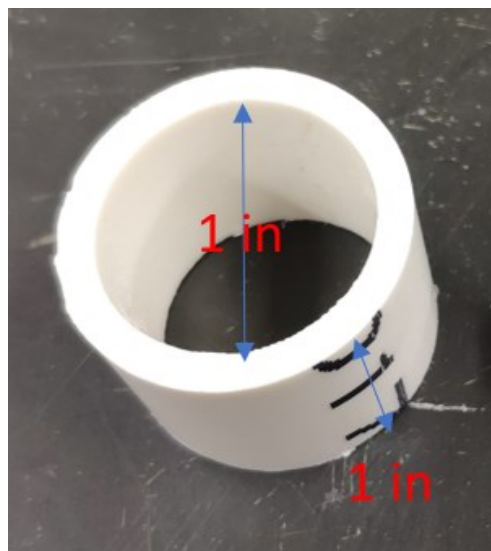


Figure A- 3 1in\*1in PTFE mould for the cement sample

The electrical tape is used to seal the bottom surface of the mould. After the preparation of the mould, the desired cement slurry is injected into the mould by a semi-transparent plastic pipette (shown in Figure A-4). Then, a cable tie is used to gently stir the cement slurry inside the mould to get rid of the air bubble. Next, electrical tape is used to cover the top surface of the mould. The mould containing cement slurry is then put into the cement curing cell (the schematic shown by Figure A-5).



Figure A- 4 Semi transparent pipette used for injecting cement slurry to the mould for the preparation of small scale samples

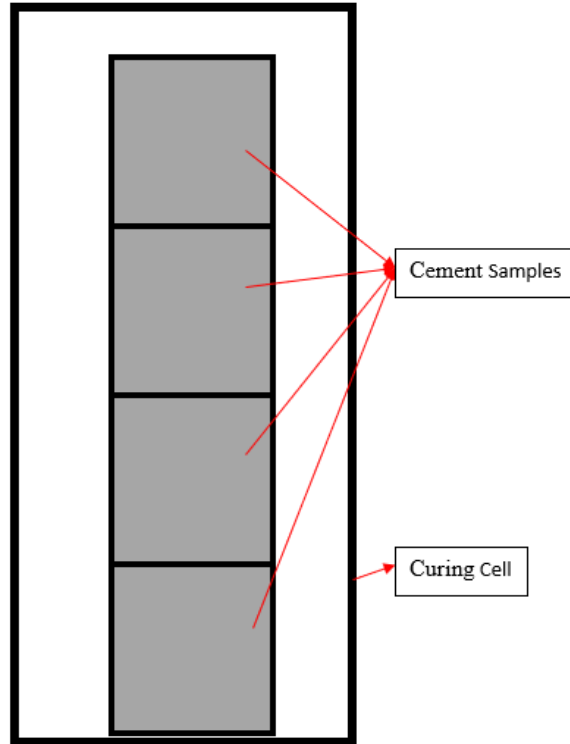


Figure A- 5 Schematic for the samples in the curing cell for small scale sample preparation

#### **A.1.4 Curing of the cement samples**

To accelerate the cement curing for the Class G and G EXP samples, 50°C and 1500 psi are used. Ambient temperature, 1500psi, are used for G Abandonment and REMEDIALmix EC samples. The apparatus used for cement curing is shown in Figure A-6 below:



Figure A- 6 Curing cell used for the preparation of small scale samples.

The curing cell with samples is placed in the oven. The curing cell is connected to the 1/8in Swagelok tubing, further connecting with the ISCO water pump. To have the flat top surface for the cement samples, the curing cell is placed vertically, with the moulds inside the cell also placed vertically, shown in Figure A-7.



Figure A- 7 Setup before curing of small scale samples

For applying pressure to the curing cell, the steps below are followed:

1. Both the top valve and middle valve on the curing cell are opened.
2. The water is added to the curing cell from the middle valve.
3. Close the water pump once the water is observed coming out from the top valve.
4. Close the top valve and gradually increase the water pressure by operating the ISCO pump connected with the middle pump until the pressure setting is 1500psi.
5. Record the pressure and volume changed from the pump every 24 hours.

6. Turn on the oven and set the temperature to 50°C for Class G, G EXP samples and ambient temperature for G Abandonment and REMEDIALmix EC samples.
7. Wait for seven days to finish the curing of cement samples. During this one week, the temperature, pressure, and volume of water are monitored daily.

After curing, the samples are taken out and wrapped with a wet cotton towel to avoid dehydrating the cement plug. A table clamp then holds the sample in the longitudinal direction shown by Figure A-8. Next, a saw is used to cut the PTFE mould. When the cut is nearly touching the cement plug, stop the saw and crack the PTFE mould with the flat screwdriver. Next, the PTFE mould is removed, and the cement plug is weighed on the balance. The weight of the plug is recorded to the two digits after the decimal. The sample is then wrapped with a wet cotton towel and stored in sealed plastic bags (Figure A-9) to prevent dehydrating and contacting air.

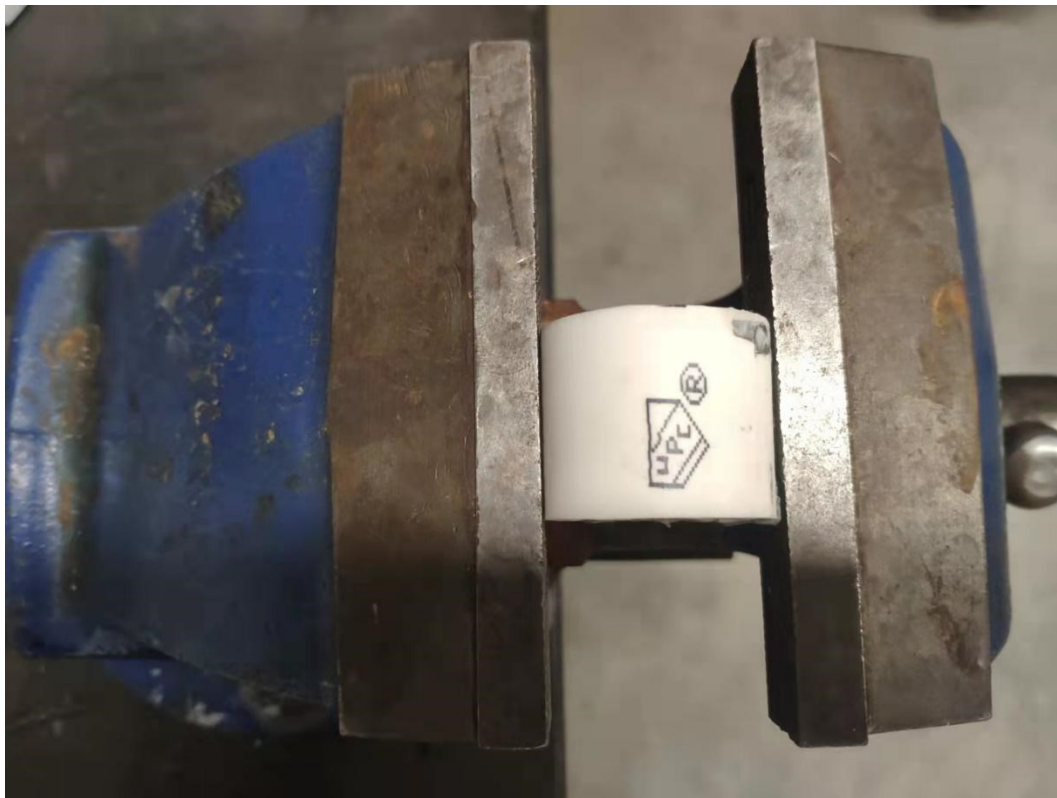


Figure A- 8 Setup for removing the mould of the small scale sample

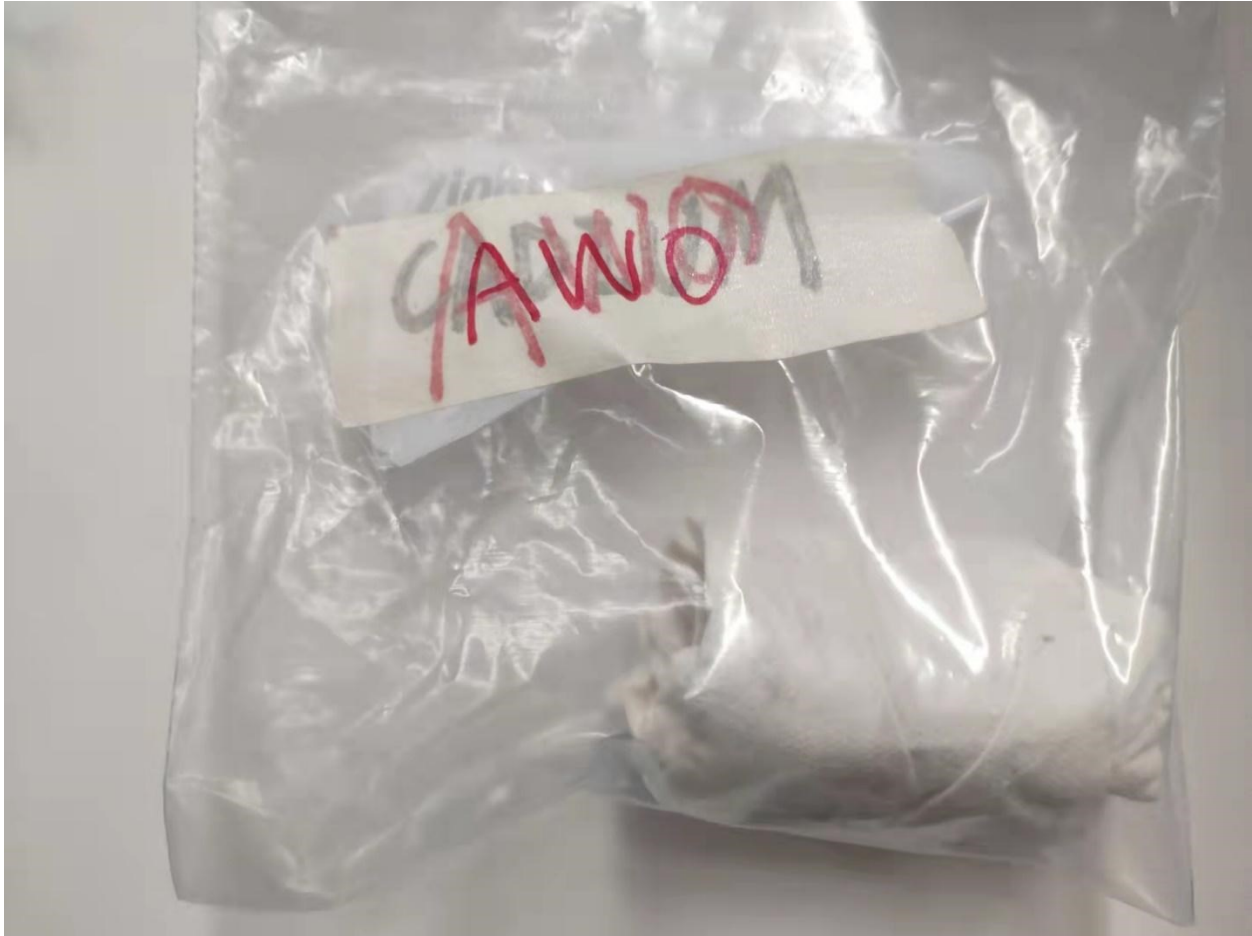


Figure A- 9 Sample storage for small scale cement plug samples

## **A.2 Steady-state permeability measurement**

In this section, the procedure of steady-state permeability measurement of the cement samples is demonstrated. The steady-state permeability measurement for the cement samples is then divided into water permeability on the saturated cement sample, Nitrogen permeability on the saturated cement sample, and Nitrogen permeability on the dried cement sample. The procedure of drying cement will also be described after the steady-state permeability measurement procedure.



### A.2.1 Steady-state water permeability measurement on cement samples

The cement samples are considered the fully saturated cement sample just after the curing process, as the curing process is conducted under the static water pressure of 1500psi. The storage of cement is also considered no fluid loss because the weight of the cement samples after storing has the same weight compared with the cement samples just after the curing. The experimental setup is shown in Figure A-10

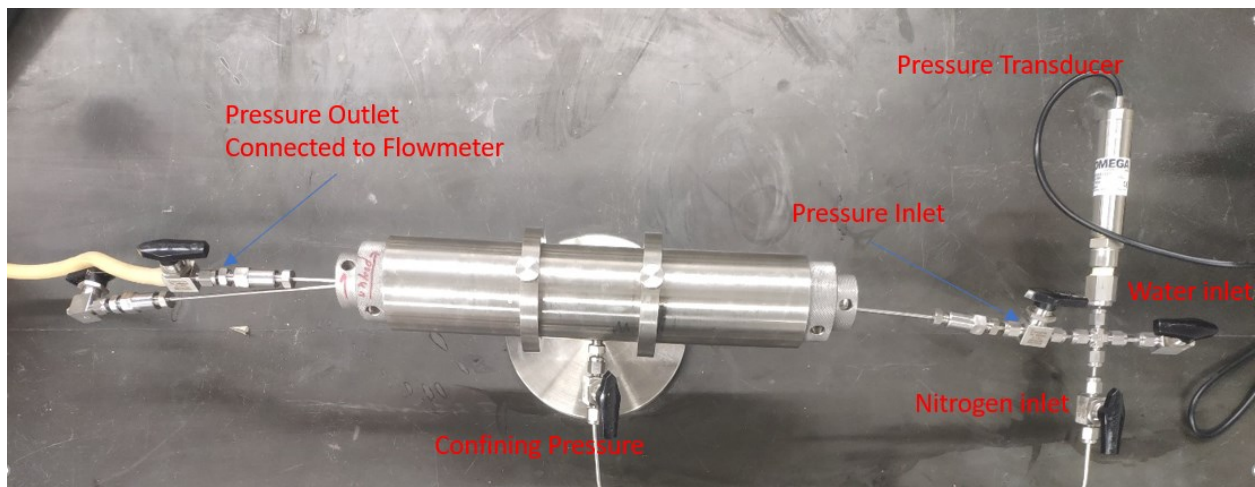


Figure A- 10 Schematic for the steady-state permeability measurement

The schematic shows that two valves are at the left side of the 1in Hassler-type core holder shown in Figure A-11. The top valve marked by the blue arrow is used for the nitrogen permeability measurement, further connected to a bubble flowmeter. The bottom valve is used for the water permeability test. The confining pressure valve is further connected with the ISCO 260D syringe pump with max pressure 7500psi ("260D Syringe Pump", 2021). The water inlet is connected to another water pump, the ISCO 100DX Syringe Pump. This pump has a higher working pressure, 10000psi, and can achieve a lower flow rate, 0.00001cc/min. Other parts will be discussed under the Nitrogen permeability section, as they are related to the Nitrogen permeability test. The steps of operating the system for the steady-state water permeability measurement are described below.



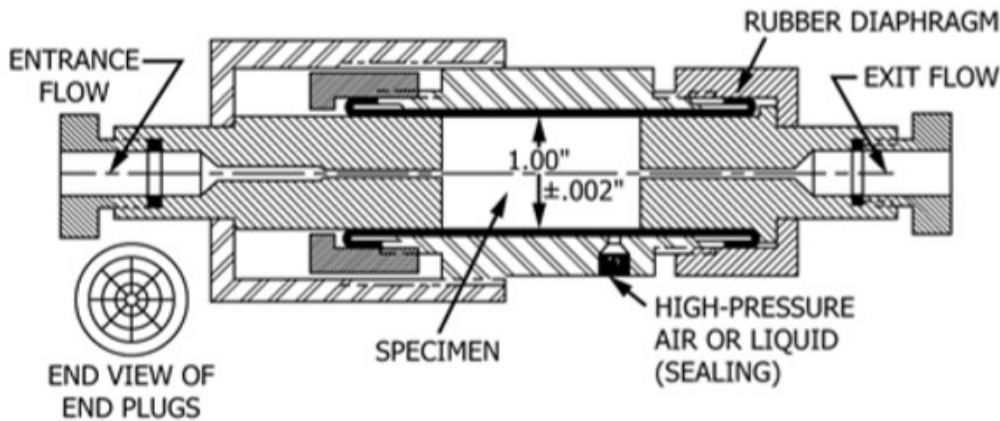


Figure A- 11 Schematic for Hassler type core holder ("ASTM D4525 - 13e2 Standard Test Method for Permeability of Rocks by Flowing Air", 2021)

The procedure is created based on ASTM D4525 13E2, as there is no standard procedure for measuring the cement permeability approved by either API or ASTM. Besides, the constant flowrate method is used in the study.

1. Wrap the cement sample with electrical tape to protect the rubber sleeve from scratching by the edge of the cement sample. In addition, by wrapping with the electrical tape, the diameter error of the cement plug caused by the thermal expansion of the PTFE mould while curing can also be corrected, making the cement sample's diameter closer to 1in.
2. The cement sample is inserted into the rubber sleeve.
3. The entrance flow and exit flow cap on the core holder are closed. Make sure both sides are attached to the sample.
4. 50psi confining pressure is set to investigate the sealing of the overall confining flowline and to fix the sample, entrance flow cap and exit flow cap from moving. While applying the confining pressure, push the entrance and exit cap towards the cement sample to insure the inlet and outlet surfaces are attached to the cement sample.
5. The confining pressure is increased to the desired level. However, the confining should not exit 2500psi, the max working pressure for the Swagelok connection used in the system.
6. Check the inlet valve connected with the nitrogen tank and ensure the valve is closed.
7. The inlet valve connected with the ISCO 100DX Syringe Pump is opened.

8. The flowrate is set to the desired level. The difference between inlet water pressure and the confining pressure should not be lower than 100psi to avoid the water flow in the rubber sleeve overcoming the confining pressure and causing the error on the measured cement permeability.
9. The inlet pressure is monitored and recorded by using the software provided by OMEGA.
10. The current inlet pressure is recorded when the difference between the inlet pressure and the confining pressure drops near 100psi. Then, the ISCO pump is converted to the constant pressure mode with the setting pressure as the pressure just recorded. This can avoid the sudden inlet pressure increase caused by the fluid pushed out due to the increase of the confining pressure.
11. Increase the confining pressure and wait until the inlet flowrate is relatively stable to 0.
12. Change the inlet pump to the constant flow rate mode and set the flowrate the same as before. Continue the pressure recording.
13. Steps 9 and 10 are repeated until the water breakthrough is observed or the max working pressure of the Swagelok connections is reached.
14. The weight of the sample is recorded after the experiment.
15. The sample is wrapped in a wet cotton towel and stored in a plastic seal bag.
16. The permeability is calculated based on Darcy's Law.

This section discusses only water permeability measurement on the saturated cement samples. The water permeability measurement on the dry cement sample is not recommended as the rewetting (Kjellsen & Jennings, 1996; Feldman, 1974) will cause the error on the cement permeability.

## A.2.2 Steady-state permeability measurement on cement samples by Nitrogen

This section describes the procedure of steady-state nitrogen permeability measurement on both dried and saturated samples. The experimental system is the same as the setup of the water permeability measurement.

The procedure is created by modifying ASTM D4525 13E2, as there is no standard procedure for measuring the cement permeability approved by either API or ASTM. Besides, the constant pressure method is used in the study. In the nitrogen outlet, the flowline is connected to the bubble flowmeter shown in Figure A-12.

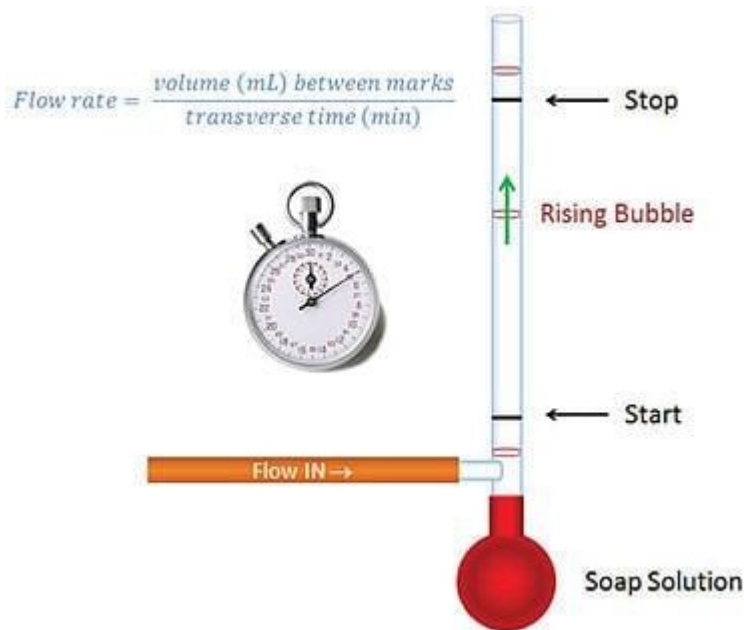


Figure A- 12 Working mechanics of the bubble flowmeter (Solutions, 2021)

The measurement procedure is the same as the water permeability measurement procedure in steps 1-5. Steps starting from step 6 were described below:

6. The valve connected to the Nitrogen is opened, and the valve connected to the water is closed.
7. Constant inlet pressure is set by controlling the regulator attached to the nitrogen tank.
8. Check the bubble flowmeter to see if there is a gas flow. If no flow happens, increase the inlet pressure and increase the confining pressure if needed.
9. The inlet pressure is monitored by using the software provided by OMEGA to see if the flow reaches the steady state indicated by dynamically constant pressure.
10. After the steady state is reached, the flow rate under the inlet pressure is recorded using the bubble flowmeter.
11. Increase the inlet pressure and repeat steps 8-10 until at least five flowrates are measurement.
12. The sample is removed from the core holder, and the weight of the sample is recorded.
13. The saturated sample is wrapped with a wet cotton towel and stored in a plastic seal bag, while the dried cement sample is directly stored in a plastic seal bag.
14. The average inlet pressure during the steady state is used to calculate the nitrogen permeability.
15. The Klinkenberg correction is applied to obtain the liquid permeability of the cement samples.

## Appendix B Procedure for porosity measurement by drying

The weight loss of the cement calculated the porosity of the cement. The process of obtaining the weight loss of the cement is the same as the procedure of getting the dried cement sample. The method is described below.

1. Preheat the oven to 60°C.
2. Fill the pan to ~ 1-inch depth with 20/40 sand or equivalent at room temperature.
3. Place cured cement samples in the pan with sand ensuring that there is a minimum of 1-inch separation from the sides and bottom and a 2-inch gap between the samples (Figure B-1)
4. Fill with 20/40 sand until samples are covered, and there is a minimum of 1 inch of sand covering the top of the samples (Figure B-1).
5. Place the pan into the oven.
6. Weight samples periodically until samples reach constant weight.
7. Ensure that samples after weighing are positioned such that the above gaps are still intact.
8. The dried sample was stored in a plastic sea bag.
9. The porosity is calculated from the weight loss of the cement. The detailed calculation procedure is shown in the parts of the results in this chapter.

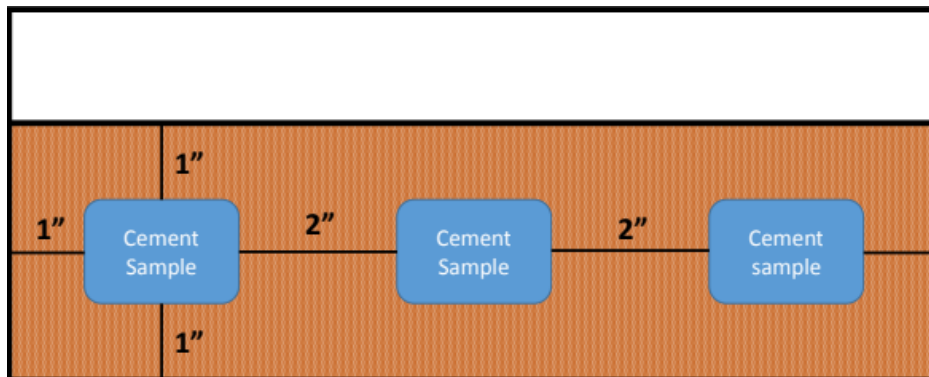


Figure B- 1 Schematic of sand bath for drying the cement

# **Chapter 4 Design and Development of the Physical Wellbore Simulator for Evaluating Oil Well Cement Performance under In-Situ Pressure and Temperature Conditions**

## **4.1 Summary**

To give the capacity of simulating the downhole condition to the wellbore simulator system, a strict design process needs to be followed. In this chapter, the design and development process of the wellbore simulator system, including the wellbore simulator main body, the flowline of the system, the wellbore simulator stand, and the heating source of the system, was explained. The design of the main body was further divided into the selection of inner and outer casing from the regular schedule pipes and API P110 casing by using Hoop Stress calculation compared with the field data, the design of caps, fittings and sealings, and Finite Element Analysis (FEA) assisting design process. Two designs with three different materials were compared based on the FEA result in the wellbore simulator stand part. For the flowline part, the author demonstrated how the design fitted the function of the system.

After all, the results showed:

- The standard schedule pipe cannot be used as the inner casing and outer casing due to the high thickness of the wall and low strength of the material.
- For the FEA of the wellbore simulator main body, increasing the diameter of the holes on the caps and flanges was the most efficient method to increase the safety factor.
- Compared with two designs of the wellbore simulator stand among three materials, the larger hole design was selected with the ANSI 4130 steel.
- FEA was an efficient way of analyzing the design. It can fasten the design cycle with less cost but higher precision compared with the traditional method.

## 4.2 Introduction

Gas leakage from the wellbore has been recognized as one of the most critical problems in the petroleum industry (Bonrtrt & Pafitis, 1996). The gas leakage can be further divided into two categories, Surface casing vent flow (SCVF) and gas migration (GM). SCVF is the gas, liquid, or both coming out on the surface area inside the wellbore area. GM is detectable gas flow at the surface area outside the wellbore area (Alberta Energy Regulator, 2021). The statistics from Alberta Energy Regulator also showed an increasing trend of unrepaired wells with SCVF, GM, or both. In 2019, the unrepaired wells with SCVF, GM, or both reaching the highest number since 2000, 10324 wells reported gas leakage. Khalifeh and Saasen (2020) stated the importance of maintaining well control by using sufficient barriers in the well, and one of the critical barriers in the wellbore is cement. In 2011, Hefley et al. stated that the average cost for a Marcellus shale gas investment was \$7.6 million, and 5% of the total investment of the well went to the cost of primary cement, while an additional 12% cost of the entire well investment would be added if the squeezing is needed. Besides, the remediation job needs to follow the policy and be approved by the local policy and regulation, which can be time-consuming (Bol et al., 1991). Therefore, to reduce the gas leakage from the wellbore, the evaluation of cement is the critical part.

Since the 1960s, to study the gas leakage mechanism from the cement system and to evaluate the performance of the cement system from a fundamental level. Varieties of gas migration experimental apparatus known as the wellbore simulators have been developed to study the effect of different parameters on the gas tightening of the cement system. The gas leakage happens due to the permeability of the cement system. Therefore, the study of gas migration can be viewed as permeability in the cement system. Although many wellbore simulators have been developed, the disadvantages of the wellbore simulators from previous studies are apparent. The main disadvantages include a large volume of needed cement (Carter and Slagle, 1972; Garcia and Clark, 1976; Levine et al., 1979), lack of migration gas flow rate control (Tinley et al., 1980), limited pressure and temperature capacity for simulating the downhole conditions (Bannister et al., 1984), none even heat exchange (Cheung & Beirute, 1985), and complicated maintenance of the system due to the complex set up (Li et al., 2018). Therefore, there is no universal procedure or apparatus recognized for analyzing the gas migration through the cement

system, especially in the annulus of the wellbore. Besides, the lack of API standards for measuring cement permeability does not exist.

This study demonstrates developing a bench-type or small-scale physical wellbore simulator assisted by finite element analysis and stress simulation. The physical validation and the operation process of the physical wellbore simulator are proposed. The newly designed wellbore simulator overcomes the disadvantages summarized in the last paragraph from previous studies. It has a much higher pressure and temperature capacity to simulate the downhole condition better. Furthermore, the improved cyclic stress simulation using the physical wellbore simulator is performed to study the effect of cyclic temperature stress and cyclic mechanical stress on the permeability of the casing annular cement system scaled down based on the field casing dimension.

### **4.3 The development process of the physical wellbore simulator system**

The wellbore simulator system contains four sections, the wellbore simulator main body, the wellbore simulator stand, the heat source, and the flowline part for the wellbore simulator system. The design of the wellbore simulator main body was assisted by the finite element analysis and CAD drawing from Fusion 360. The main body was the most critical component in the whole system. It was the apparatus that would hold the cement slurry and be under the majority thermal and mechanical stress. The primary function of the wellbore simulator stand was to hold the wellbore simulator, which had a mass of 70 kgs. The balance between the self-weight and the strength of the stand was considered to be a critical parameter during its design. The 31-350ERS DIGITAL BENCH OVEN was used as a heat source with the essential modifications to fit the wellbore simulator stand. As for the flowline part, the primary function of the flowline was to ensure the fluid during the test could be delivered to the desired place successfully. The flexibility and the construction structure of the flowline needed to be considered carefully due to the limited space of the oven and the working bench. The detailed design processes for each section were demonstrated in the following four parts.



### 4.3.1 The development of the wellbore simulator main body

The function of the wellbore simulator determined the structure of the wellbore simulator. The purpose of the wellbore simulator was to study the change of the cement integrity based on the permeability measurement on the cement, which would be exposed to the in-situ stress conditions. Therefore, the wellbore simulator should have at least an inner and outer casing to simulate the casing-cement-casing case. Same as the casing design process before the drilling of the petroleum well, the selection of inner casing and outer casing was the first part of the designing process. Besides, to apply enough high pressure to simulate the in-situ conditions, sealing was the second step in the design. Furthermore, the cement slurry should be appropriately separated from the system's sealing to avoid the contamination of the flowline and unwanted bonding of cement to other parts in the system. Therefore, the following schematic (Figure 4-1) for the wellbore simulator was proposed.

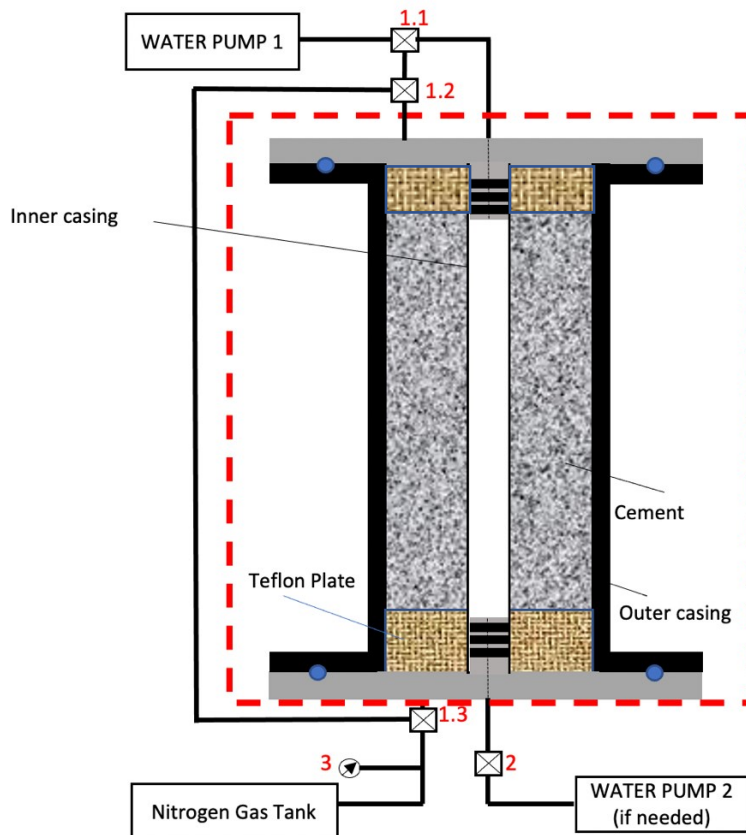


Figure 4- 1 wellbore simulator schematic

The wellbore simulator main body contains an inner casing to generate the Hoop stress by applying the water pressure inside, an outer casing to simulate the casing-cement-casing case, cement sheath between the inner and outer casing, top and bottom caps to provide proper seals, among inner casing, annulus and environment. The overall design process followed the cycle (Figure 4-2).

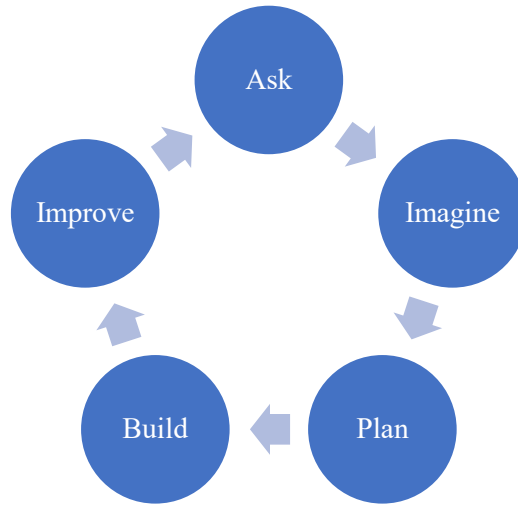


Figure 4- 2 Design cycle for the wellbore simulator

The process started with imagining based on the functions that were wanted to be achieved. Then the plan or a schematic of the product was made. The CAD drawing was prepared, the physical wellbore simulator was built in the Fusion 360. The simulation was run under the desired static thermal stress and mechanical stress. The improvement of the design was made based on the simulation results. The final step was to ask the manufacturer to produce the model to ensure practical design. If the question still existed, the cycle should be further followed until the problem was resolved. Overall, the wellbore simulator should be reusable, with a simplified structure and less cement volume needed, while it should also simulate the downhole conditions.

#### 4.3.1.1 The selection of the inner casing and outer casing

The inner and outer casing selection was started from the standard schedule pipes as they were easy to obtain and replace. Besides the regular schedule pipe, the API tubings were considered another option. Based on the Hoop stress that the pipes could generate, the casing could be selected. Another criterion was the do/di ratio between the inner and outer casing. The ratio of do/di, known as the inner diameter of the outer casing divided by the outer diameter of the inner casing, was a critical parameter during the drilling and casing design procedure. It was also considered an important parameter during selecting the inner casing and outer casing as the ratio also represented the overall cement sheath width to the casing diameters. To simulate the actual wellbore, the do/di ratio of the wellbore simulator should be similar to the field data. The do/di ratio should be close to 1.26, based on the field data from Sanjel.

The Hoop stress calculation for the standard schedule pipes was based on equation 4-1 (Wilcox et al., 2016):

$$\sigma_H = (P_i r_i^2 - P_o r_o^2) / (r_o^2 - r_i^2) - r_i^2 r_o^2 (P_o - P_i) / (r^2 (r_o^2 - r_i^2)) \quad (\text{Equation 4 - 1})$$

Where,

$\sigma_H$  is the Hoop stress, in psi.

$P_i$  is the pressure inside the pipe, in psi.

$P_o$  is the pressure outside the pipe, in psi.

$r_i$  is the inner radius of the pipe, in inches.

$r_o$  is the outer radius of the pipe, in inches.

The pressure inside the pipe was equal to the working pressure of the pipe. The Hoop stress was calculated based on the maximum working pressure of the pipe and the working pressure with a 25% reduction separately to give the safety margin. The calculation results for the inner casing were listed in Table 4-1 and 4-2 separately.

INNER CASING SELECTION								
Nom. Size	OD	ID	Schedule	Work pressure	Work pressure with 25% reduction	Burst pressure	Hoop Stress	Hoop Stress
INCH ES	INC HES	INC HES	-	psi	psi	psi	psi	MPa
1	1.315	1.049	40	2100	1575	12100	7350	51
1	1.315	0.957	80	3500	2625	15900	7882	54
1	1.315	0.815	160	5700	4275	22300	7110	49
1	1.315	0.599	xxs	9500	7125	32700	4975	34
1.25	1.66	1.38	40	1800	1350	10100	8054	56
1.25	1.66	1.278	80	3000	2250	13900	8732	60
1.25	1.66	1.16	160	4400	3300	18100	8398	58
1.25	1.66	0.896	xxs	7900	5925	27700	6496	45
1.5	1.9	1.61	40	1700	1275	9100	8658	60
1.5	1.9	1.5	80	2800	2100	12600	9265	64
1.5	1.9	1.338	160	4500	3375	17700	8854	61
1.5	1.9	1.1	xxs	7200	5400	25300	7260	50
2	2.375	2.067	40	1500	1125	7800	9369	65
2	2.375	1.939	80	2500	1875	11000	9994	69
2	2.375	1.689	160	4600	3450	17500	9414	65
2	2.375	1.503	xxs	6300	4725	22100	8417	58
2.5	2.875	2.469	40	1900	1425	8500	10677	74
2.5	2.875	2.323	80	2800	2100	11500	10532	73
2.5	2.875	2.125	160	4200	3150	15700	10115	70
2.5	2.875	1.771	xxs	6900	5175	23000	8439	58
3	3.5	3.068	40	1600	1200	7400	10616	73
3	3.5	2.9	80	2600	1950	10300	11389	79
3	3.5	2.626	160	4100	3075	15000	10561	73
3	3.5	2.3	xxs	6100	4575	20500	9273	64
3.5	4	3.548	40	1500	1125	6800	11069	76
3.5	4	3.364	80	2400	1800	9500	11598	80
4	4.5	4.026	40	1400	1050	6300	11230	77
4	4.5	3.826	80	2300	1725	9000	11999	83

4	4.5	3.438	160	4000	3000	14200	11217	77
4	4.5	3.152	xxs	5300	3975	18000	10210	70
5	5.563	5.047	40	1300	975	5500	12097	83
5	5.563	4.813	80	2090	1567.5	8100	12443	86
5	5.563	4.313	160	3850	2887.5	13500	11603	80
5	5.563	4.063	xxs	4780	3585	16200	10930	75
6	6.625	6.065	40	1210	907.5	5100	12526	86
6	6.625	5.761	80	2070	1552.5	7800	12840	89
6	6.625	5.189	160	3760	2820	13000	11935	82
6	6.625	4.897	xxs	4660	3495	15000	11225	77

Table 4- 1 Hoop Stress calculation for normal schedule pipes with maximum working pressure

INNER CASING SELECTION								
Nom. Size	OD	ID	Schedule	Work pressure	Work pressure with 25% reduction	Burst pressure	Hoop Stress	Hoop Stress
INCH ES	INCH ES	INCH ES	-	psi	psi	psi	psi	MPa
1	1.315	1.049	40	2100	1575	12100	5512	38
1	1.315	0.957	80	3500	2625	15900	5911	41
1	1.315	0.815	160	5700	4275	22300	5333	37
1	1.315	0.599	xxs	9500	7125	32700	3731	26
1.25	1.66	1.38	40	1800	1350	10100	6041	42
1.25	1.66	1.278	80	3000	2250	13900	6549	45
1.25	1.66	1.16	160	4400	3300	18100	6299	43
1.25	1.66	0.896	xxs	7900	5925	27700	4872	34
1.5	1.9	1.61	40	1700	1275	9100	6494	45
1.5	1.9	1.5	80	2800	2100	12600	6949	48
1.5	1.9	1.338	160	4500	3375	17700	6641	46
1.5	1.9	1.1	xxs	7200	5400	25300	5445	38
2	2.375	2.067	40	1500	1125	7800	7026	48
2	2.375	1.939	80	2500	1875	11000	7496	52
2	2.375	1.689	160	4600	3450	17500	7060	49
2	2.375	1.503	xxs	6300	4725	22100	6313	44
2.5	2.875	2.469	40	1900	1425	8500	8007	55
2.5	2.875	2.323	80	2800	2100	11500	7899	54
2.5	2.875	2.125	160	4200	3150	15700	7586	52
2.5	2.875	1.771	xxs	6900	5175	23000	6329	44
3	3.5	3.068	40	1600	1200	7400	7962	55
3	3.5	2.9	80	2600	1950	10300	8541	59
3	3.5	2.626	160	4100	3075	15000	7921	55
3	3.5	2.3	xxs	6100	4575	20500	6955	48
3.5	4	3.548	40	1500	1125	6800	8302	57
3.5	4	3.364	80	2400	1800	9500	8698	60
4	4.5	4.026	40	1400	1050	6300	8423	58

4	4.5	3.826	80	2300	1725	9000	8999	62
4	4.5	3.438	160	4000	3000	14200	8413	58
4	4.5	3.152	xxs	5300	3975	18000	7657	53
5	5.563	5.047	40	1300	975	5500	9073	63
5	5.563	4.813	80	2090	1567.5	8100	9332	64
5	5.563	4.313	160	3850	2887.5	13500	8702	60
5	5.563	4.063	xxs	4780	3585	16200	8197	57
6	6.625	6.065	40	1210	907.5	5100	9395	65
6	6.625	5.761	80	2070	1552.5	7800	9630	66
6	6.625	5.189	160	3760	2820	13000	8951	62
6	6.625	4.897	xxs	4660	3495	15000	8419	58

Table 4- 2 Hoop Stress calculation for normal schedule pipes with 75% working pressure

The pipes that yielded the six most significant numbers were selected as inner casing (Table 4-3 and 4-4).

INNER CASING SELECTION								
Nom. Size	OD	ID	Schedule	Work pressure	Work pressure with 25% reduction	Burst pressure	Hoop Stress	Hoop Stress
INCH ES	INCH ES	INCH ES	-	psi	psi	psi	psi	MPa
4	4.5	3.826	80	2300	1725	9000	11999	83
5	5.563	5.047	40	1300	975	5500	12097	83
5	5.563	4.813	80	2090	1568	8100	12443	86
6	6.625	6.065	40	1210	908	5100	12526	86
6	6.625	5.761	80	2070	1553	7800	12840	89
6	6.625	5.189	160	3760	2820	13000	11935	82

Table 4- 3 Selected casing based on the maximum working pressure

INNER CASING SELECTION								
Nom. Size	OD	ID	Schedule	Work pressure	Work pressure with 25% reduction	Burst pressure	Hoop Stress	Hoop Stress
INCH ES	INCH ES	INCH ES	-	psi	psi	psi	psi	MPa
4	4.5	3.826	80	2300	1725	9000	8999	62
5	5.563	5.047	40	1300	975	5500	9073	63
5	5.563	4.813	80	2090	1568	8100	9332	64
6	6.625	6.065	40	1210	908	5100	9395	65
6	6.625	5.761	80	2070	1553	7800	9630	66
6	6.625	5.189	160	3760	2820	13000	8951	62

Table 4- 4 Selected casing based on the 75% working pressure

Then, the inner diameter of the outer casing was calculated based on the do/di ratio of 1.26 and 1.27. The nearest diameter to the calculated result was selected as the outer casing (Table 4-5).

OUTER CASING SELECTION						
ID (1.26)	ID (1.27)	Chosen ID	OD	Nominal Size	Schedule	DO/DI
INCHES	INCHES	INCHES	INCHES	INCHES	-	-
5.670	5.715	5.761	6.625	6	80	1.28
7.009	7.065	6.875	8.625	8	xxs	1.24
7.009	7.065	6.875	8.625	8	xxs	1.24
8.348	8.414	8.5	10.75	10	160	1.28
8.348	8.414	8.5	10.75	10	160	1.28
8.348	8.414	8.5	10.75	10	160	1.28

Table 4- 5 Outer casing selection based on inner casing from table 4-3 and 4-4

Then, the gap size between the inner casing and outer casing and the length of the cement column were calculated based on the max required cement volume of 1litter (Table 4-6).



OVERALL CALCULATION			
Gap	Annulus Area	Max Length	Cement Volume
in	ft <sup>2</sup>	in	L
0.6305	0.0706	6.000	1.00
0.656	0.0890	4.761	1.00
0.656	0.0890	4.761	1.00
0.9375	0.1547	2.740	1.00
0.9375	0.1547	2.740	1.00
0.9375	0.1547	2.740	1.00

Table 4- 6 Overall annulus gap and cement column length calculation based on the cement volume of 1 litter

The selection procedure differed slightly from the regular schedule pipes for the API tubing and casing as the field data was received. Therefore, the working pressure and the Hoop stress can be first calculated. Based on the calculated result, the casing size can be selected. The working pressure was calculated based on the equation 4-2 ("Barlow's Formula - Internal, Allowable and Bursting Pressure", 2021):

$$P_a = \frac{2S_y F_d F_e F_t t}{d_o} \quad (\text{Equation 4 - 2})$$

Where,

$P_a$  = maximum allowable design pressure or the max working pressure (psig).

$S_y$  = yield strength (psi).

$F_d$  = design factor, typical 0.72 for liquid pipeline ("Barlow's Formula - Internal, Allowable and Bursting Pressure", 2021).

$F_e$  = longitudinal joint factor, 1 for seamless pipe (2021).

$F_t$  = temperature derating factor 0.9 at 200 Celsius ("Steel Pipes - Temperature Derating", 2021).

The Hoop stress calculation was followed Equation 4-1. The field data gave the yield strength, downhole temperature, pressure applied outside the casing, casing ID and OD. Based on the information, the working pressure was calculated, and the Hoop stress can be determined. The results are listed in Table 4-7.

Calculation with P <sub>o</sub>									
OD	ID	r <sub>o</sub>	r <sub>i</sub>	Wall Thickness	Criterion	Thin Wall or Thick Wall	Work pressure	P <sub>o</sub>	Hoop Stress
in	in	in	in	in	-	-	psi	psi	psi
4.5	3.826	2.25	1.913	0.337	5.68	Thick Wall	12038	4641	33949
							83MPa	32MPa	234MPa

Table 4- 7 Hoop stress calculation based on the field data

Then the inner casing was selected based on the maximum Hoop stress that could be generated. The small diameter pipe was not considered as it would take a very long length to reach the 1-litre cement volume. Therefore, the starting point was set to be 3.5inch P110 tubing. The calculation results are listed in Table 4-8, 4-9.

Calculation with P <sub>o</sub> , API P110 Tubing, OD 3.5in, t=0.375in									
OD	ID	r <sub>o</sub>	r <sub>i</sub>	Wall Thickness	Criterion	Thin Wall or Thick Wall	Work pressure	P <sub>o</sub>	Hoop Stress
in	in	in	in	in	-	-	psi	psi	psi
3.5	2.75	1.75	1.375	0.375	3.67	Thick Wall	10000	0	32267
							MPa	MPa	MPa
							69	0	223

Table 4- 8 Hoop stress calculation for API P110 tubing 3.5in\*0.375in

Calculation with P <sub>o</sub> , API P110 Tubing, OD 3.5in, t=0.254in									
OD	ID	r <sub>o</sub>	r <sub>i</sub>	Wall Thickness	Criterion	Thin Wall or Thick Wall	Work pressure	P <sub>o</sub>	Hoop Stress
in	in	in	in	in	-	-	psi	psi	psi
3.5	2.992	1.75	1.496	0.254	5.89	Thick Wall	10353	0	56205
							MPa	MPa	MPa
							71	0	388

Table 4- 9 Hoop stress calculation for API P110 tubing 3.5in\*0.254

Then the working pressure was back determined by using the function of excel by inputting the field Hoop stress number. The calculated result was summarized in Table 4-10.

Hoop Stress Calculation with P <sub>o</sub> , API P110 Tubing, OD 3.5in, t=0.254in									
OD	ID	r <sub>o</sub>	r <sub>i</sub>	Wall Thickness	Criterion	Thin Wall or Thick Wall	Work pressure	P <sub>o</sub>	Hoop Stress
in	in	in	in	in	-	-	psi	psi	psi
3.5	2.992	1.75	1.496	0.254	5.89	Thick Wall	6250	0	33930
							MPa	MPa	MPa
							43	0	234

Table 4- 10 Work pressure calculation based on the field Hoop stress for API P110 3.5in\*0.254in tubing

Furthermore, the inner diameter of the outer casing was calculated based on the 1.26 do/di ratio. The summary of the inner and outer casing with the Hoop stress and working pressure results is listed in Table 4-11.

Schedule of Inner pipe	API P110 Tubing
Schedule of outer pipe	P110 Casing
Hole (Outer casing) OD, in	5
Hole (Outer Casing) ID, in	4.408
Inner Casing OD, in	3.5
$D_o/D_i$	1.26
Maximum Length, in	10
Annular Volume, L	0.92
Cement sheath thickness, in	0.45
Inner Casing ID, in	2.992
$r_o$ (inner casing), in	1.75
$r_i$ (inner casing), in	1.496
Pipe Thickness, in	0.254
Inner Pipe Working Pressure, psi	9874.5
Burst Pressure, psi	13330
$P_i$ , psi	6249.9
$P_o$ , psi	0
hoop stress, psi	33930
Hoop stress, MPa	234

Table 4- 11 inner and outer casing, working pressure and Hoop stress summary for API tubing selection

#### 4.3.1.2 The design of caps, fittings and sealings

The development of the caps and sealings was inspired by the cement curing cell in our lab (Figure 4-3). Three EPDM o-rings sealed the inner space with the piston seal, and the larger o-ring sealed the space between the cell and the environment. The material of the o-ring can be changed to fit the desired temperature rating. Therefore, in our case, the piston seal with three o-rings can be used to seal the inner casing to avoid the fluid exchange between the inner casing and outer space. The flange seal was used to avoid the leakage of annulus pressure to the outer environment of the wellbore simulator. The main body uses the screws and threads drilled into the outer casing body to connect the caps and cement curing cell. This design could affect the pressure rating of the outer body. Therefore, due to the higher operating pressure for the wellbore simulator than the cement curing cell, the design was changed to the screws and nuts with holes drilled on the flange (Figure 4-4). The o-ring selection was done by using the o-ring calculator from Parker Hannifin®. The detailed calculation process was described on its website ("Parker's O-Ring Selector App", 2021). Besides, to avoid the cement bond with the top and bottom cap of the simulator, two Teflon rings were designed to be placed between the cement and caps during the curing of the cement. The detailed CAD drawings are listed in Appendix D.



Figure 4- 3 1Cement curing cell with piston seal and flange seal

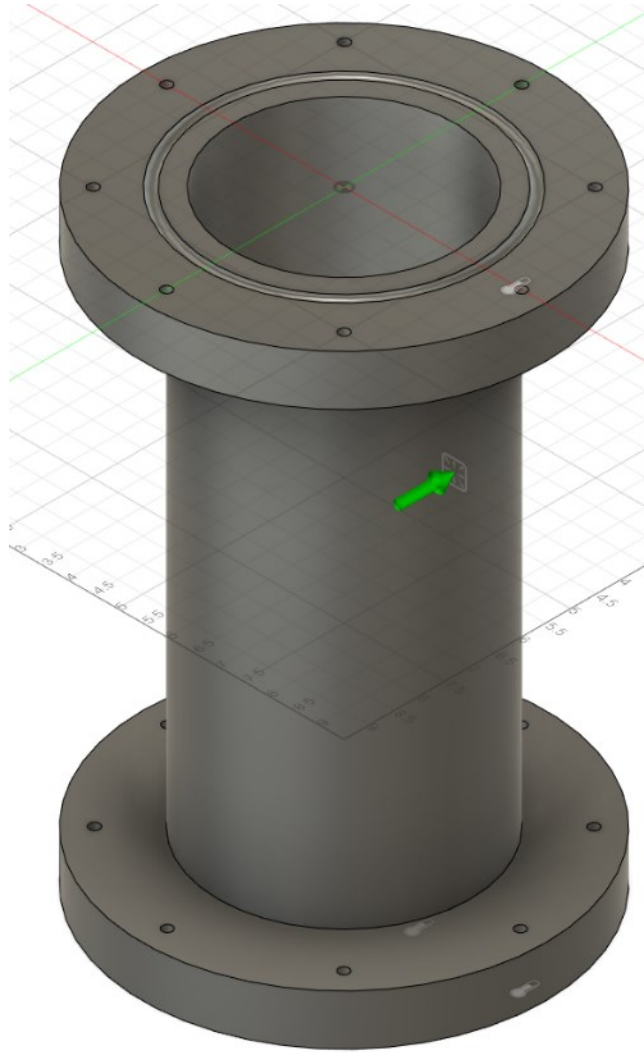


Figure 4- 4 Connection first design - holes drilled on flanges

#### 4.3.1.3 Finite element analysis on the wellbore simulator assisting the design process

The finite element analysis, known as FEA, has been widely used in the design process during these years. It can make the design process more precise, faster, and more affordable than the conventional method. Therefore, the Finite element analysis was used in the designed process of the wellbore simulator. The whole process was done using Fusion 360. The start point was the first design of the wellbore simulator, where the drawings for the different parts were listed below, Figure 4-3 to 4-6, where the green arrows represent the pressure applied to the pointing

surface. The grid or the finite elements had 10% of the overall volume of the interested body and was auto-generated by the software.

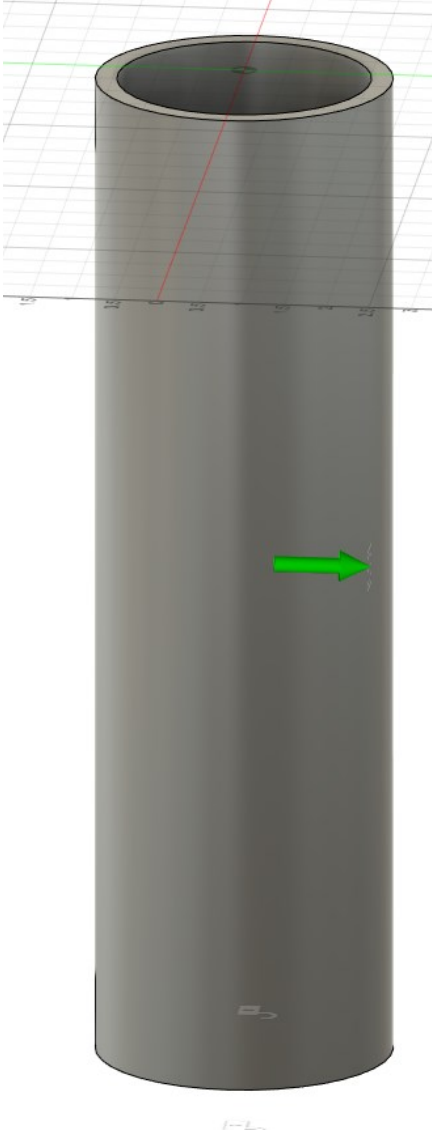


Figure 4- 5 Drawing for the inner casing with applied pressure



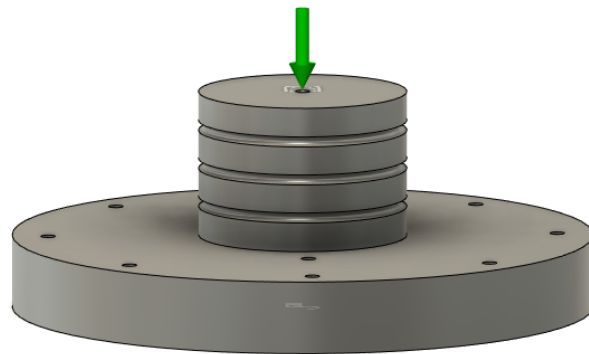
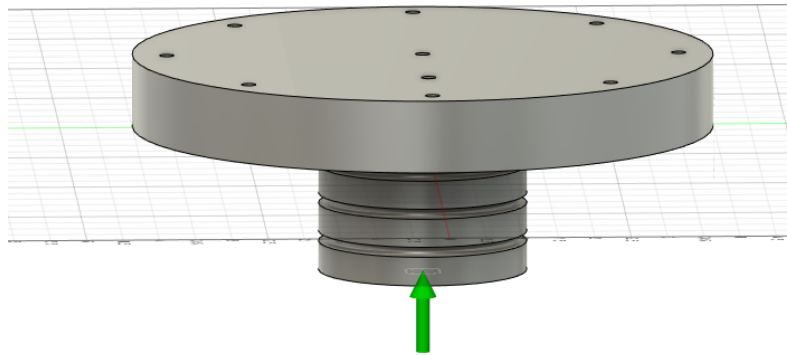


Figure 4- 6 Drawing for the caps with applied pressure

Before the running of the simulation, several assumptions and constraints were made. Firstly, the pressure applied to each surface was assumed to be uniformly distributed over the surface. Besides, the bottom surface for the inner casing and outer casing was assumed to be fixed as these two surfaces would be set on the wellbore simulator stand. Moreover, the holes on the flanges were assumed to be pinned as the threads and nuts would hold the connection between the caps and flanges. Furthermore, to simulate the worst-case scenario, the pressure applied to

the inner and outer casing was the same, 43Mpa. Besides, the pressure applied to the top and bottom cap was considered the maximum pressure, 43Mpa.

Moreover, all parts were set to expose under the temperature of 120 Celsius degrees, the maximum temperature of the wellbore simulator. The material for all parts above was ANSI 4140, the same material as the P110 casing. The overall setup before running the simulation was in Figure 4-7.

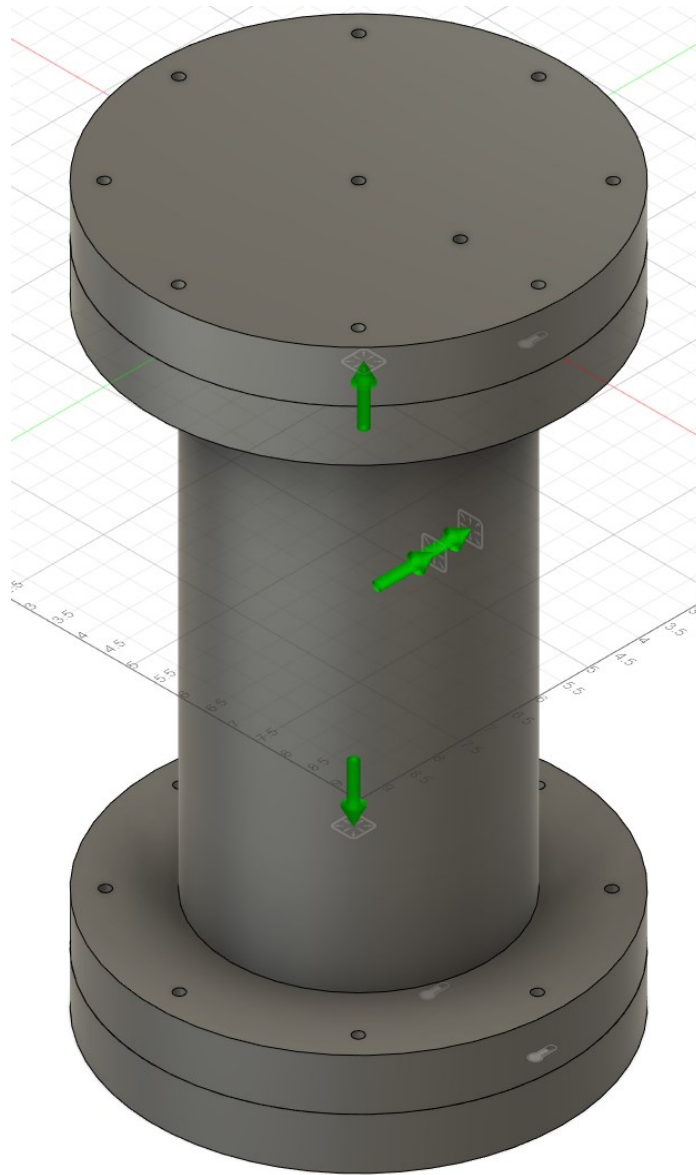


Figure 4- 7 Overall set up of first design before simulation

The safety factor was the critical output for the simulation. It is the ratio of yield strength of the material to the overall applied strength calculated based on the applied pressure. The design aimed to have the safety factor at least above one. Figure 4-8 shows the simulation result of the first design. The safety factor was below one, and the lowest safety factor occurred at the holes on the caps. Therefore, based on the simulation result, two improvement methods for the holes on the caps were tested, increasing the numbers of the holes and increasing the hole diameter of

the holes. Both of them were designed to decrease the stress on each hole. The same percentage of increase was made for each approach, and the efficiency of each approach was compared. Further improvement was made based on the comparison. The results will be discussed in the result and discussion section.

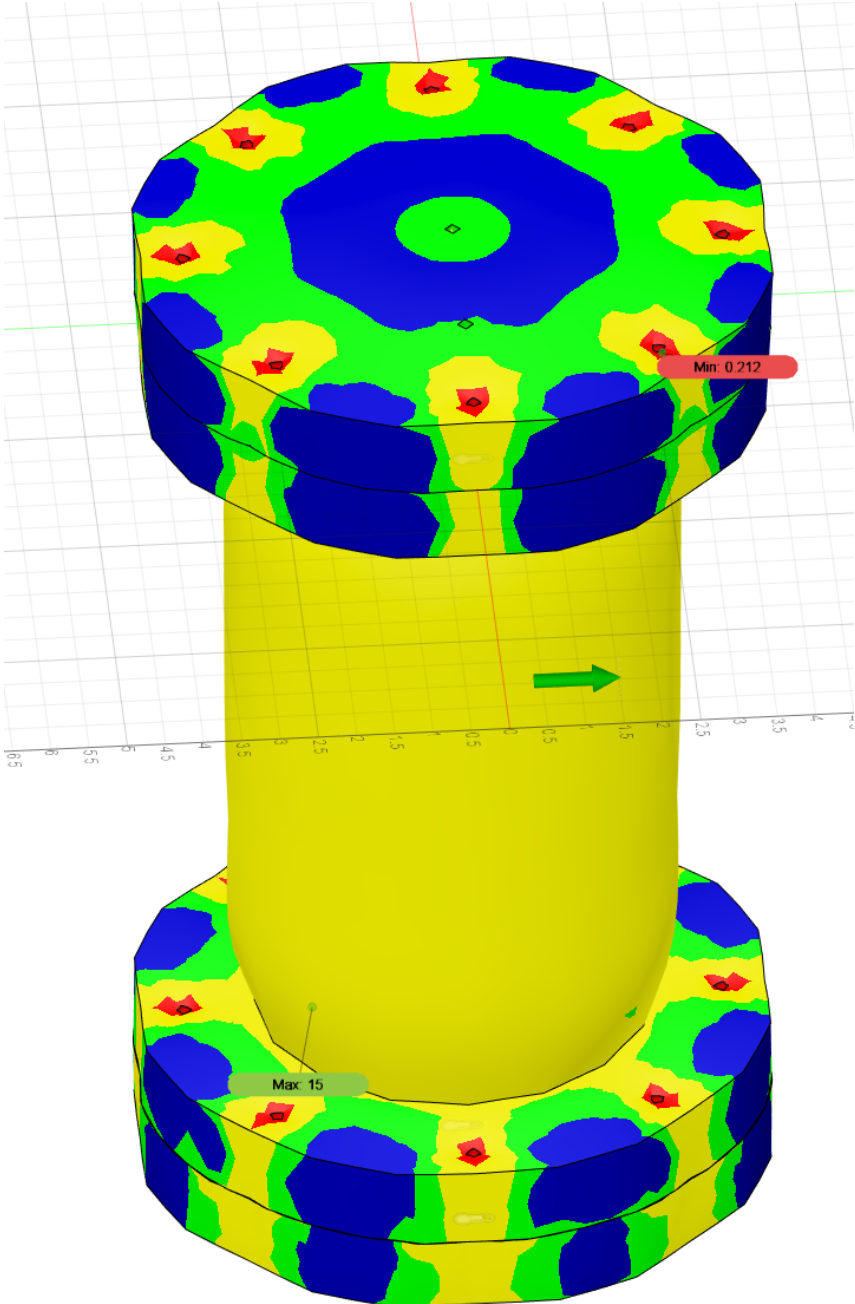


Figure 4- 8 FEA safety factor for the first design

### **4.3.2 The design of the wellbore simulator stand**

The design of the wellbore simulator stand follows the same logic as the main body design. The simulator stand was designed to hold the wellbore simulator, and it needs to have a balance between the self-weight and strength of the material. Besides, due to the limited height in the oven, the wellbore simulator has to be height efficient. Moreover, due to the load limit of the oven, the wellbore simulator had to sit on the workbench rather than the oven. Therefore, the stand's legs needed to be as small as possible to minimize the cutting area on the oven while still holding the weight of the system. Based on the manufacturer, the legs will be circular for easy manufacturing. There were two different designs with three different materials considered for the wellbore simulator stand. The first design was the bolt-in design, where the head of bolts was designed to sit in the holes on the stand. In this case, the contact surface between the bolt heads and stand will hold significant stress. The advantage of this design was that the bolts are parts that can be easily changed while being damaged. The other design was to have a giant hole on the wellbore simulator stand so that the flange would sit on the stand. This case increased the contact area significantly and thus decreased the stress on the surface. However, the flange part was hard to change if there was any damage. The simulation constraints were that there was no movement for the wellbore simulator in any direction as it would be placed on the stand. Gravity and static 120 Celsius were the only force and the temperature during the simulation. The simulation results will be explicitly discussed in the results and discussion part.

### **4.3.3 The design of flowline**

The design of the flowline should fit the function of the wellbore simulator system. The three-way valve was placed where the splitting of the flow or two-fluid flows was needed. The two-way valve was the control of turn on and off for the single flowline. The pressure transducer was placed where the pressure measurement was needed. Therefore, the starting point of the flowline design will be the starting of the experiment, curing of the cement. To cure the cement in the annulus, both pressures applied in the annulus and inner casing should be considered. Therefore,

a three-way valve, Valve 1.1 in Figure 4-9, was placed to control the inner casing and annulus flow from water pump 1. The bottom cap should be connected with the backup pump, water pump 2. Therefore, a two-way valve, Valve 2 in Figure 4-9, was enough.

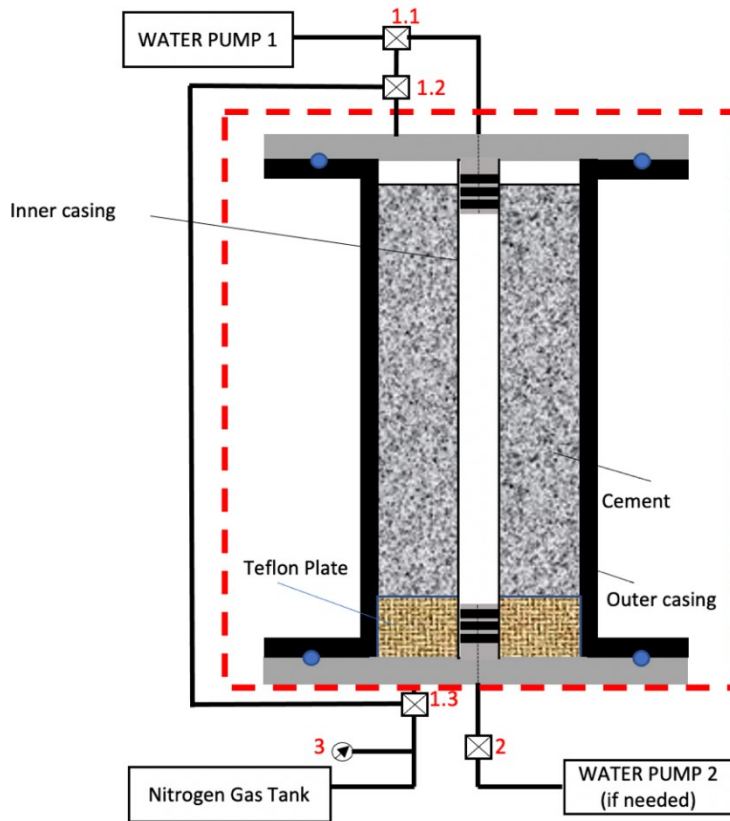


Figure 4- 9 Flowline Schematic for Curing Cement

After curing, the system would measure the permeability of the cement (Figure 4-10). The inlet pressure needs to be measured starting from the inlet, either one or two nitrogen gas tanks. Therefore, pressure transducer three was placed. The flowline should be able to apply the inlet pressure and backup pressure. Thus, the three-way valve, Valve 1.3, was placed to split the nitrogen to control the backup and inlet pressures. Finally, for the outlet side, the nitrogen should be controlled either to apply the backup pressure at the end of the cement column or the outlet of the whole flow system. Therefore, the three-way valve, Valve 1.2, was placed. As for the tubing of the flowline, 1/8in tubing was used for the major part of the flowline as it was easy to bend

and cut, which would give the higher flexibility and installing tolerance to the system. The 1/4in tubing was used to connect the gland to the female connection on the caps as 1/4in was the minimum size for HIP taper type connection. The schematics for curing cement and cement permeability measurement are shown in Figures 4-9 and 4-10.

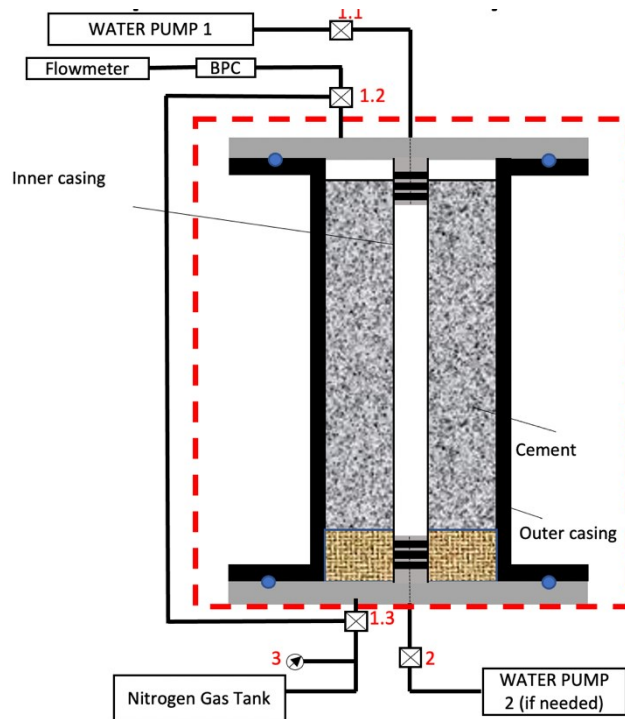


Figure 4- 10 Flowline Schematic for Nitrogen Permeability Test

#### 4.4 Results and discussion

For the design of the wellbore simulator main body, the results for Hoop stress calculation of inner and outer casing selection were listed through Table 4-1 to Table 4-10. Table 4-1 to 4-6 shows that the material was regular schedule pipes. Based on the results, among regular schedule pipes, the highest Hoop stress generated was 89MPa, which was still smaller than the Hoop stress needed, 234MPa. Therefore, the standard schedule pipes were rejected. Based on the calculation result, the API P110 casing with 3.5in OD and 0.254in thickness was selected as the

inner casing. Then the outer casing was selected based on the do/di ratio of 1.26. Therefore, the API P110 casing with 5in OD and 4.408in ID was selected as the outer casing.

As for the simulation part of the wellbore simulator, the base case of the simulation result is shown in Figure 4-8. The safety factor was only 0.212. The weakest part was the holes in the caps and flanges. Therefore, two methods, increasing the numbers of the holes and increasing the hole diameter of the holes, were raised and tested. The results were shown in Figures 4-11 and 4-12 separately. By increasing the number of holes by 25%, from 8 to 10 holes, the safety factor increased from 0.212 to 0.249, 17.45% increment while by increasing the same percentage, 25% of the diameter of the holes, from 0.25in to 0.3125in, the safety factor increase from 0.212 to 0.3029, 42.88% increment. Therefore, increasing the diameter of holes was the most efficient way to raise the safety factor. Based on this, the diameter was increased to 1.5in where the safety factor was 1.229 (Figure 4-13).



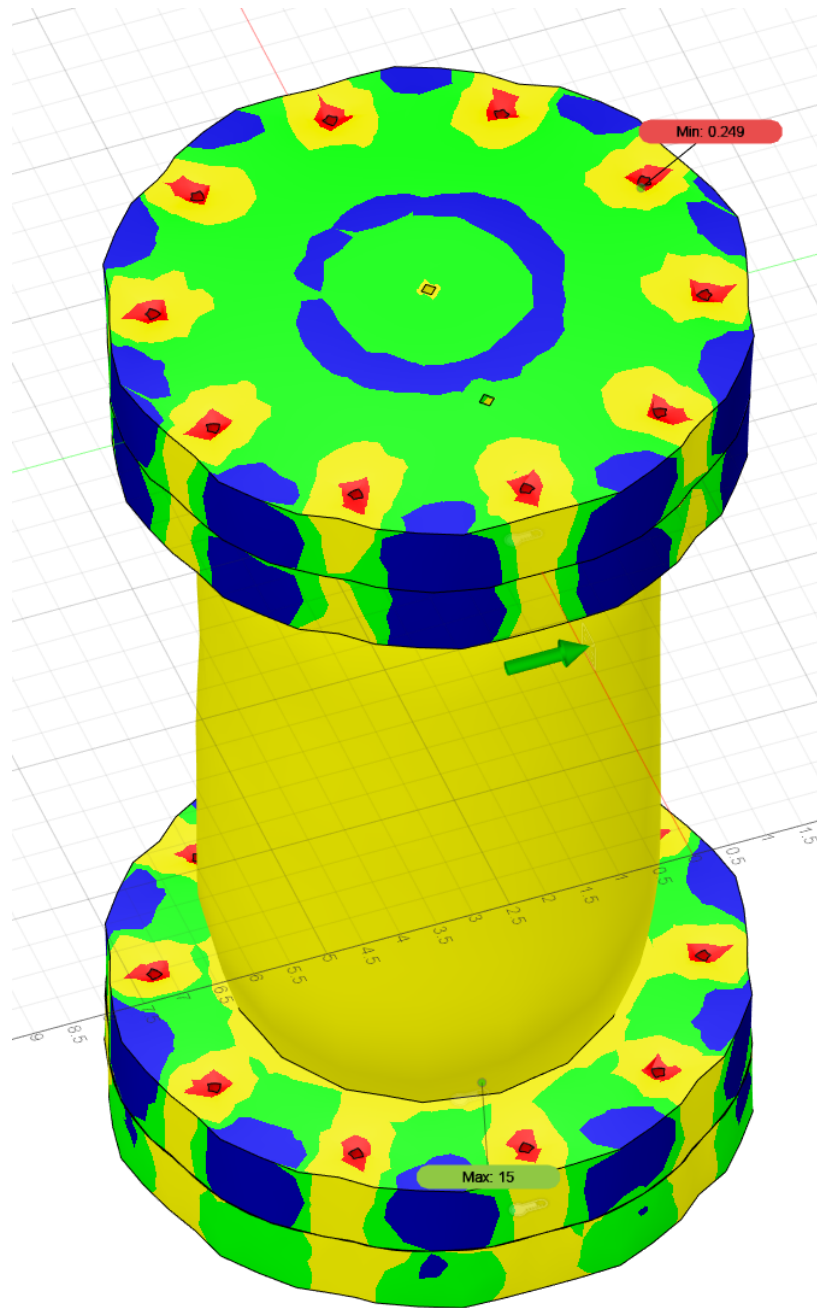


Figure 4- 11 FEA safety factor result for increasing the number of holes

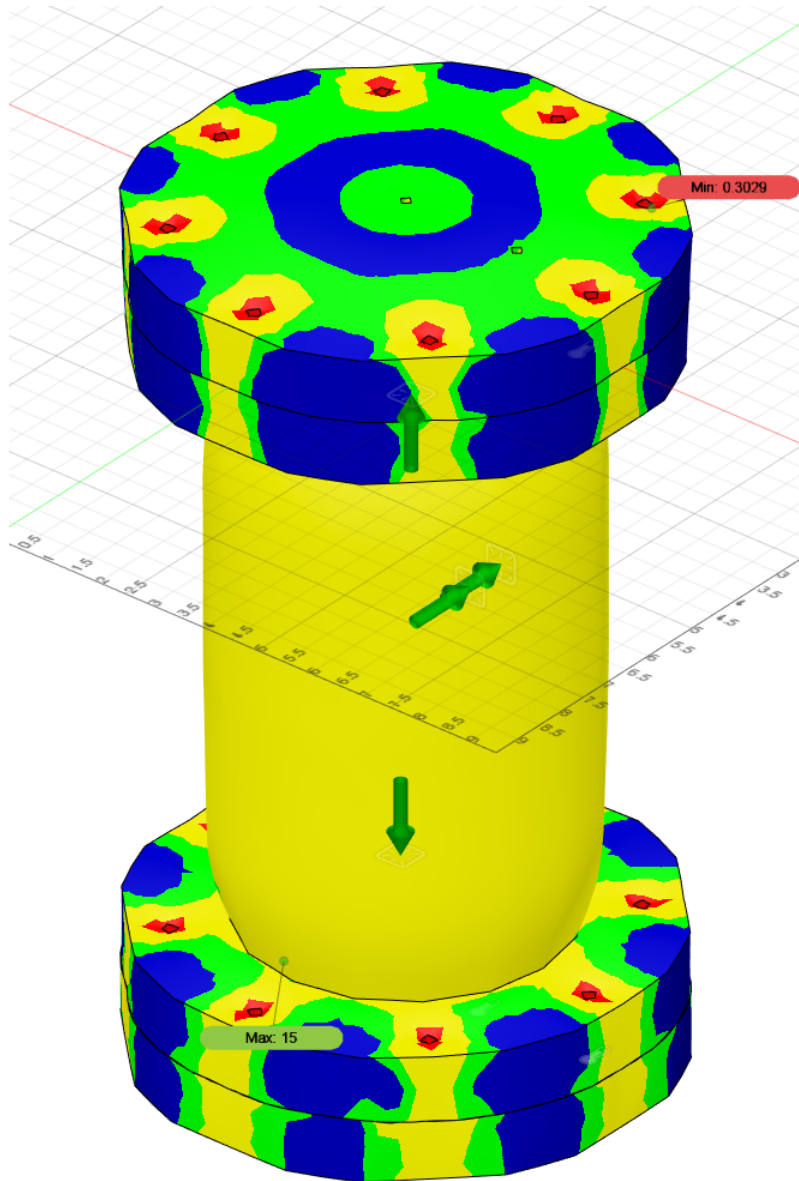


Figure 4- 12 FEA safety factor result for increasing the size of holes

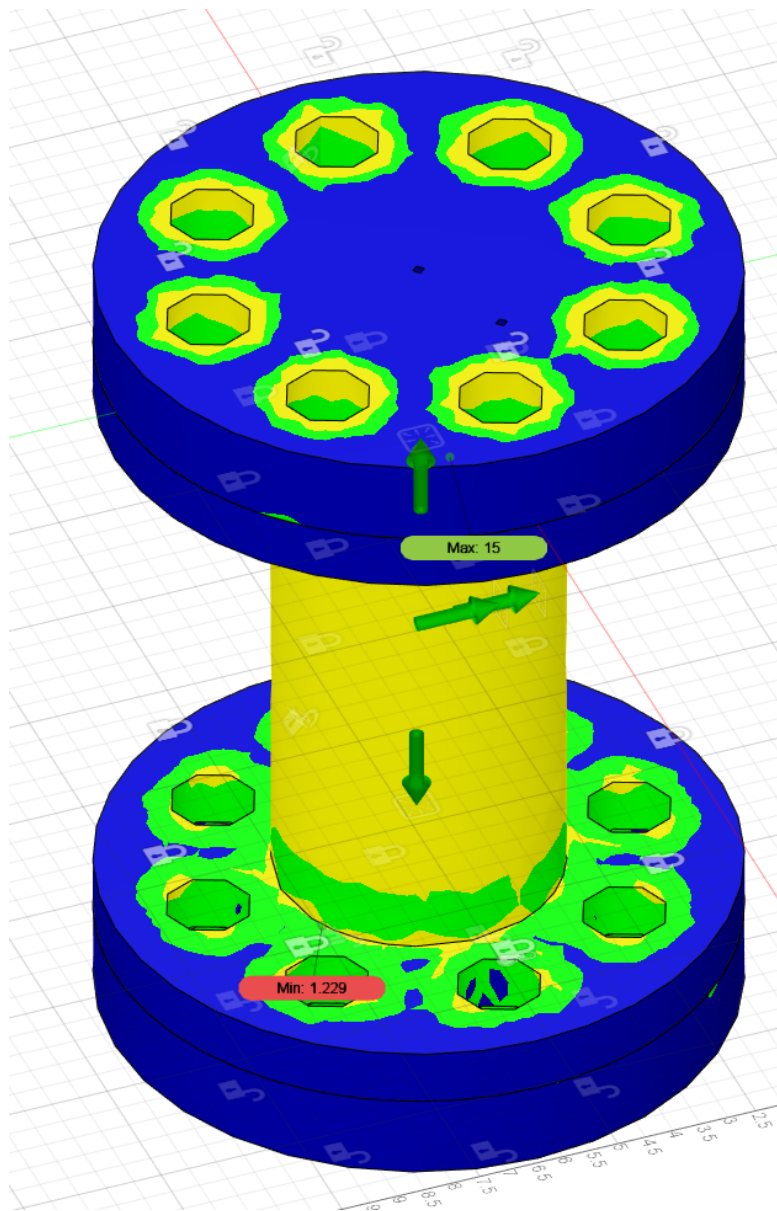


Figure 4- 13 FEA safety factor result for the final design

There were two different designs with three different materials considered for the wellbore simulator stand. The description of the design was in 4.3.2. Three different materials were Grade 60 Iron, ANSI 4130 steel, and ASTM A48 steel. The first step was to compare the design with the same material. For Grade 60 iron, the bolt-in design had the safety factor of 0.4948 (Figure 4-14), while the larger hole design had the safety factor of 0.8171 (Figure 4-15). Therefore, the design with the larger hole was accepted. Among all the materials, ANSI 4130 has the maximum

safety factor of 1.256 (Figure 4-16). However, as shown by Figure 4-17, the thickness of the stand top and the diameter of the legs were too high as the safety factor was over 15. Therefore, the thickness of the stand top and diameter of the legs was reduced. The final drawing of the stand is shown in Figure 4-18.

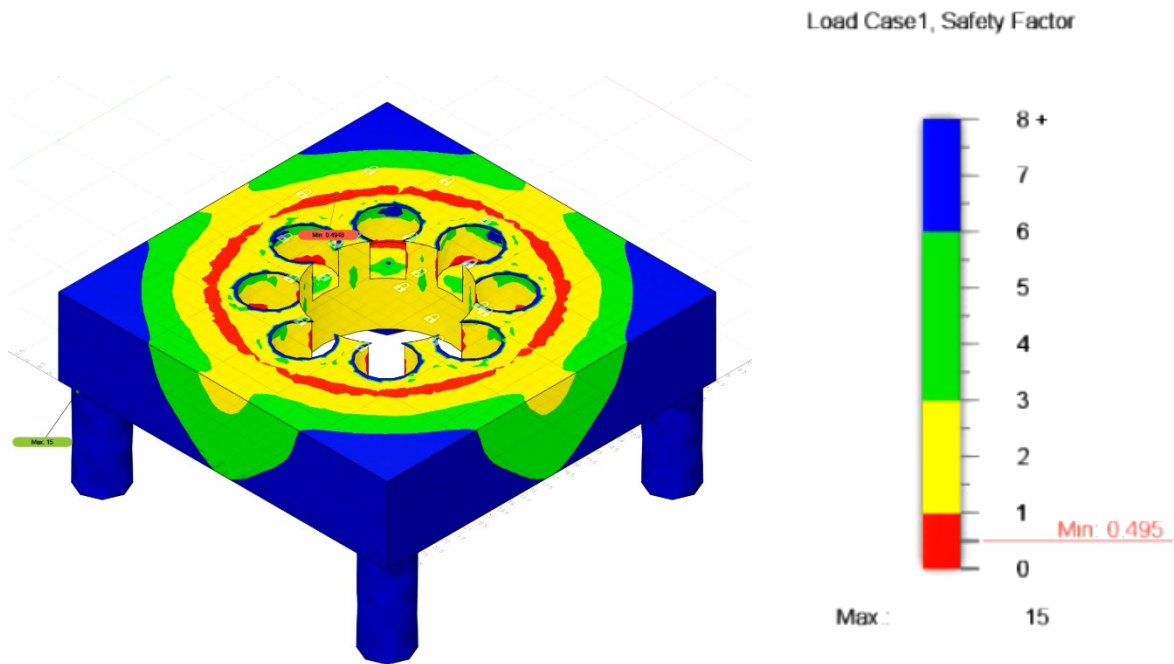


Figure 4- 14 FEA safety factor result for bolt-in design with Grade 60 iron

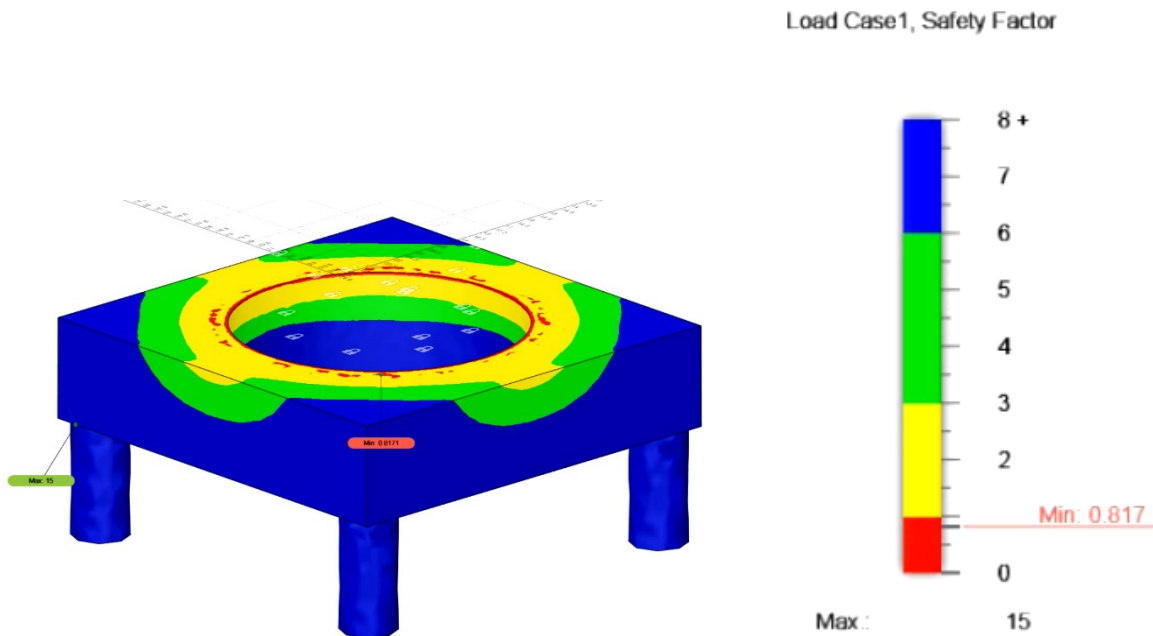


Figure 4- 15 FEA safety factor result for larger hole design with Grade 60 iron

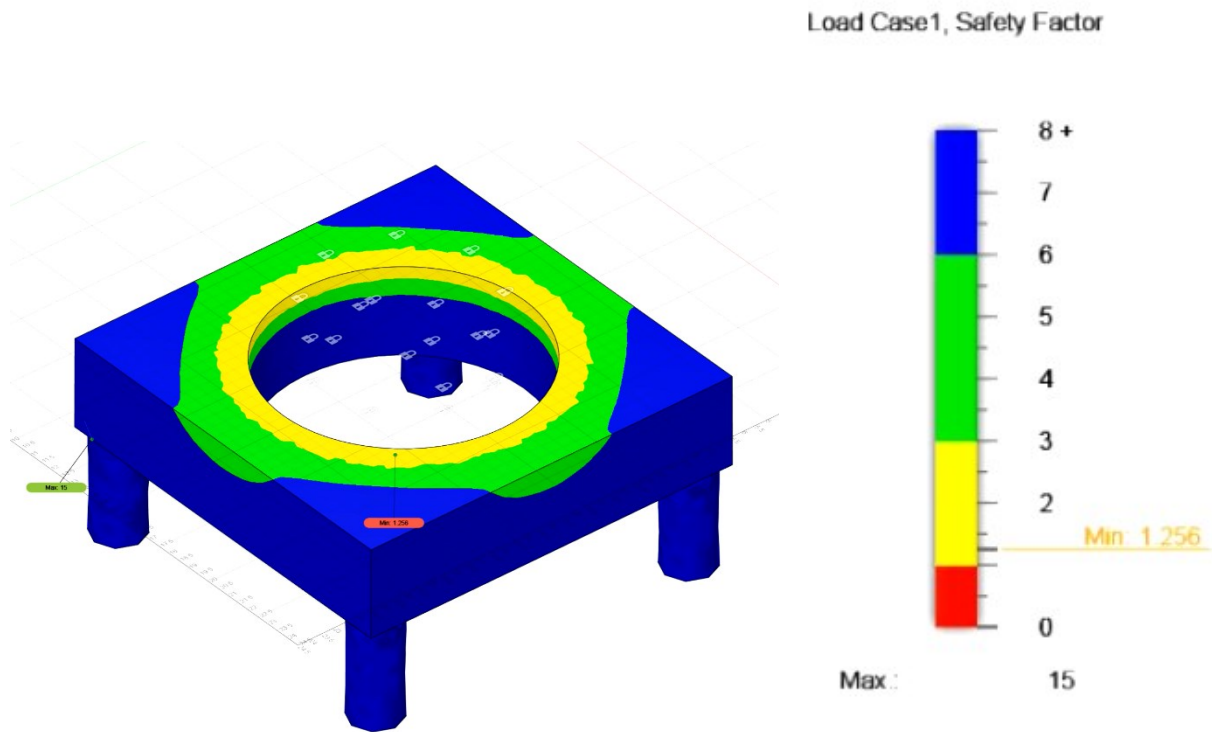


Figure 4- 16 FEA safety factor result for wellbore simulator stand final design with ANSI 4130 steel

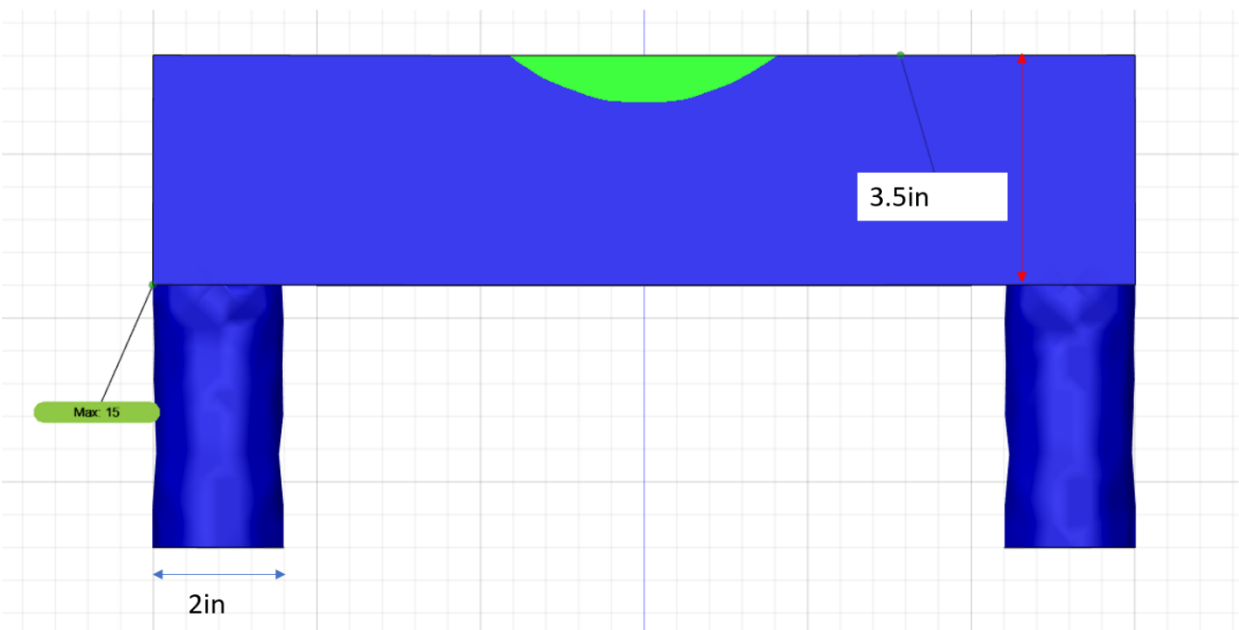


Figure 4- 17 Dimension of the stand with the simulation result

The final CAD drawings for the wellbore simulator main body are shown in Figures D-1 to D-5.

## 4.5 Conclusions

In this chapter, the design and development process of the wellbore simulator system was described. The procedure of casing selection, design of the caps, fittings and seals, wellbore simulator stand design, and flowline design was explicitly explained. Based on the results, the following conclusions can be offered:

- The standard schedule pipe cannot be used as the inner casing and outer casing due to the high thickness of the wall and low strength of the material. API P110 casing with 3.5in OD and 0.254in thickness casing was selected as the inner casing, and 5in OD and 0.296in thickness casing was selected as the outer casing.
- For the FEA of the wellbore simulator main body, increasing the diameter of the holes on the caps and flanges was the most efficient method to increase the safety factor.
- Compared with two designs of the wellbore simulator stand among three materials, the larger hole design was selected with the ANSI 4130 steel. The larger hole increased the contact area and thus decreased the stress on the surface.
- The safety factor was a critical factor during the design. It can indicate where the design needs to be reinforced or weakened. It can also help with saving the raw material before manufacturing the product.
- FEA was an efficient way of analyzing the design. It can fasten the design cycle with less cost but higher precision compared with the traditional method.

The wellbore simulator design still needs to be validated by physical experiments after manufacturing, which will be discussed in the next chapter.

## **Appendix C Protocol for operating the wellbore simulator system**

Before the assembly process, all the O-rings should be removed from the metal parts of the wellbore simulator. Then, the O-rings should be scrutinized. If the plastic deformation or the cuts are found on the O-ring, the O-ring cannot be used as the O-ring may not achieve the sealing of the fluid properly under the high-pressure operation. The assembly process can be further split into four parts: Cleaning, Installation, flowline connection, pressure application.

### **Cleaning**

1. All the O-ring(s) that can be reused, Teflon parts and metal parts, including top cap, bottom cap, inner casing, outer casing, screws, nuts, should be wiped with a wet clean paper towel to remove particulate matters if there is any. The inspection of the particulate matters should be applied again at the time of assembling each part, especially before the installation of each O-ring, as the particulate matter(s) can be the main reason that causes the scratch(es) or cut(s) on the O-Ring. In addition, the wiping process for the O-rings should be carried under more attention as the particulate matter tends to adhere more easily to the grease applied to the O-ring from the previous experiment.
2. The metal parts should be placed on a flat surface. The shafts on the top and bottom caps should be faced upward without touching the ground.
3. After wet wiping off the metal parts, the dry wiping is applied to reduce further the particulate matters left on the metal surfaces and O-rings and speed up the drying after the wet wiping.

### **Installation**

1. The flange side (figure C-1) of the bottom cap is placed on the flat surface.



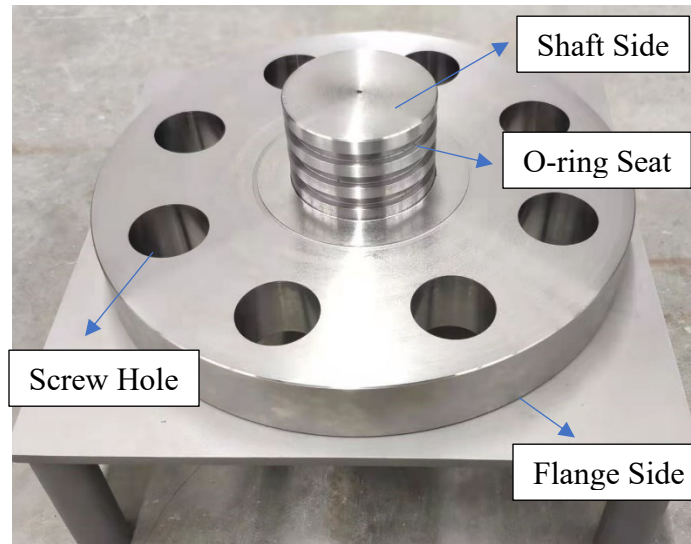


Figure C- 1 Bottom/Top Cap

2. The screws are placed through the screw holes on the bottom caps.
3. The O-ring seats on the shaft of the bottom cap are adequately inspected. The residual particulate matter(s) should be removed if there is any.
4. The grease is applied to the O-ring after ensuring the O-ring is cleaned thoroughly.
5. Place the O-ring onto the most upward O-ring seat.
6. Repeat steps three and four until all the O-rings are properly installed.
7. Inspect the inner casing, especially for the surfaces that will contact O-rings and caps to ensure they are properly cleaned and no chip on the casing body. The installation of the O-rings for the Teflon ring should follow the same process described above, from inside to outside. The assembled Teflon ring is then placed at the bottom of the inner casing. Then the compression is applied parallel to the longitudinal direction of the inner casing on the top surface of the inner casing. Finally, the Teflon ring is installed in the inner casing.
8. The inner casing is then placed on the top surface of the shaft. After ensuring the inner casing is concentric with the shaft, slowly lower down the inner casing. If this step is done properly, the inner casing should move down smoothly until it touches the first O-ring.

9. The compression is applied to the top circular surface (figure C-3) of the inner casing. The compression should be applied parallel to the longitudinal direction (figure C-4) of the inner casing.

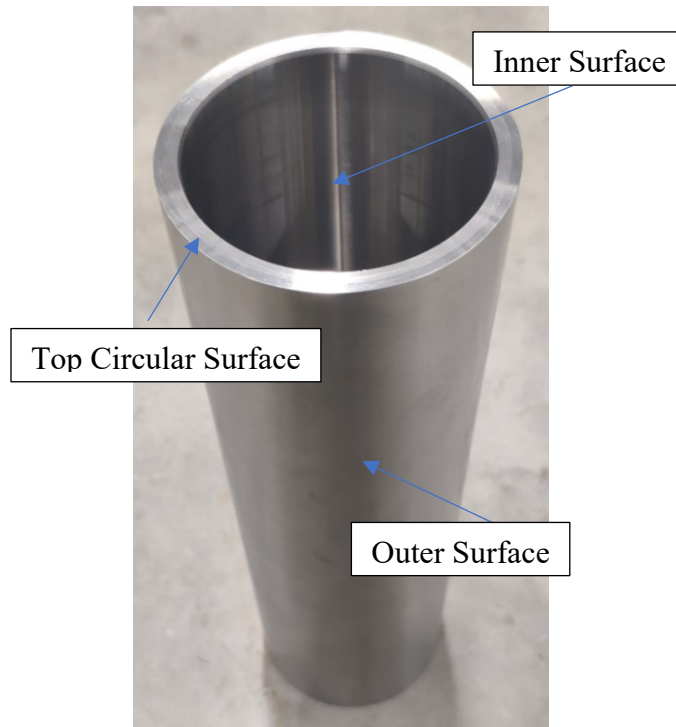


Figure C- 2 Inner casing with surface labels

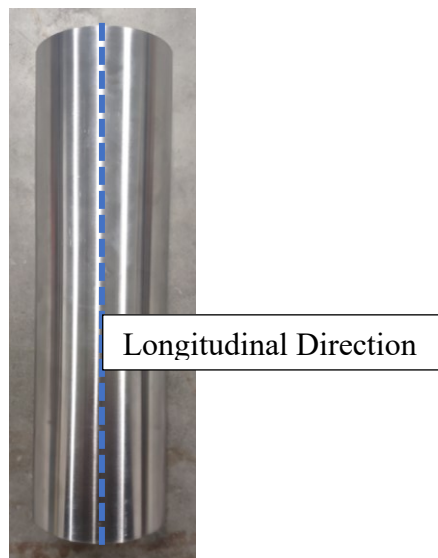


Figure C- 3 Longitudinal direction on the inner casing

10. Install the 1/4in HIP connection BA, BC (Figure C-4) onto the wellbore simulator bottom cap. The two characters on the connection mean the area on the wellbore simulator that the connection is connected to. BA means bottom annulus; BC bottom center; TA, top annulus; TC, top center.
11. The desired fluid, in our case, cement, is poured into the annulus between the inner casing and outer casing until the cement level reaches 1in below the top surface of the outer casing. Slightly vibrate the wellbore simulator during the cement filling process to make the cement level homogeneous. After pouring the cement, use the soft material, such as rubber, flapping the wellbore simulator gently to get rid of the air bubble, if any, in the cement.
12. The other Teflon ring is assembled based on the same procedure described in step 7. The install procedure is also similar to step 7, except that the compression is applied to the Teflon ring this time.
13. The bottom and inner surfaces of the outer casing are inspected and placed onto the flange of the bottom cap. The screw holes on the outer casing and the bottom cap are aligned.
14. The process of O-ring installation for the top cap is the same as that for the bottom cap.
15. The shaft of the top cap is then placed on the center of the inner casing. After ensuring the inner casing is concentric with the shaft, slowly lower down the top cap. If this step is done properly, the top should move down smoothly until the first O-ring is touched by the top circular surface of the inner casing.
16. The compression is applied to the flange side of the cap with a parallel direction to the shaft's longitudinal direction.
17. TC and TA are connected to the top cap of the wellbore simulator.



Figure C- 4 1/4 HIP connection connected with wellbore simulator main body

If the inner casing is used to cure the cement, the procedure will still be similar to what is described above, except that the Teflon rings will switch to Teflon plates, and Teflon plates will be installed in the inner casing.

### **Flowline Connection**

This part only includes the procedure of connecting the wellbore simulator cap to the overall entrance and exit of the flowline wherein daily experiment these two connections will be the most often parts that will be connected and disconnected to connect the wellbore simulator to the flowline before the starting of the experiment and disconnect the wellbore simulator to move the wellbore simulator body after the experiment. The standard procedure of connecting the two-piece sleeves to the tubing is described on the High-pressure equipment website. The URL: <https://www.highpressure.com/products/valves-fittings-tubing/taper-seal-valves-fittings-and-tubing/assembly-procedure/>

1. Before the connection of the gland (figure C-5) and the female opening (figure C-6), both parts need to be inspected for the complete removal of the particulate matters, especially the threads on the female part and the inner surface of the sleeves, because these parts will be the main parts of sealing function under the high pressure. In addition, the particulate matter will create an ultra-high pressure once it sticks between two connecting surfaces as the surface area between the connecting surface(s) and the particulate matter(s) is ultra-small.

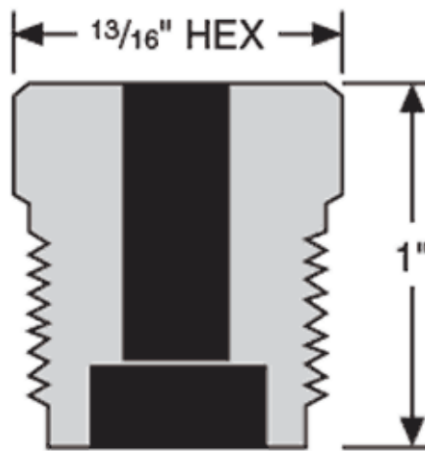


Figure C- 5 1/4 in gland ("Taper Seal Connections | High Pressure Company", 2021)

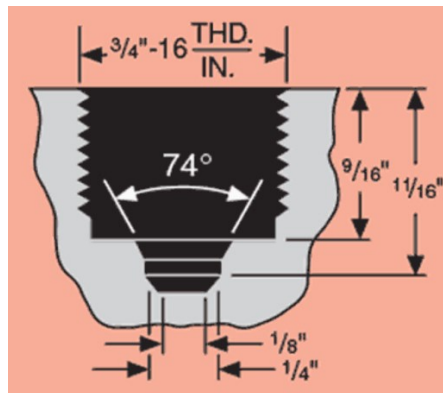


Figure C- 6 Female opening schematic ("Taper Seal Connections | High Pressure Company", 2021)

2. The tubing is pushed through the gland from the non-threaded side to the threaded side.

3. The two-piece sleeve is installed on the tubing. For the correct assembly process, please visit the website of High-Pressure Equipment:  
<https://www.highpressure.com/products/valves-fittings-tubing/taper-seal-valves-fittings-and-tubing/assembly-procedure/>
4. After the gland and two-piece sleeve assembly, hold the gland and sleeve and put them on the top of the female opening on the wellbore simulator cap and ensure the sleeve goes into the female opening. Next, rotate the gland counterclockwise until the gland is fully tightened.
5. Follow the same procedure for the connections.

### **Pressure Application**

Before applying the pressure, inspect the whole flowline and compare the connection to one of the schematics below. The flowline connection must be the same as figure 4-9 for curing cement and figure 4-10 for conducting the nitrogen permeability test.

#### **For Curing Cement:**

1. Turn Valve 1.1 opening to Valve 1.2.
2. Open Valve 1.2 to the annulus or the cement sheath.
3. Apply 20psi pressure and check if there is any leakage on the flowline.
4. Ramp up the pressure to the desired level. Note the pressure should be increased by 100psi each time. Wait for the flowrate on the pump screen to be relatively stable before further increasing pressure.

#### **For Nitrogen Permeability Test:**

1. Turn Valve 1.3 opening to Valve 1.2.
2. Apply the pressure slightly higher than 50psi.
3. Turn Valve 1.3 opening first to cement sheath and then to the backpressure control part. Wait until the 50psi pressure reading is reached.
4. Turn Valve 1.3 to the annulus or the cement sheath.
5. Apply 20psi pressure. Check if there is any gas leakage through the flowline by using soap water.

5. Ramp up the inlet pressure to the desired level. Note the pressure should be increased by 100psi each time. Wait for the pressure reading to be relatively stable before the further increase of pressure.

**For Water Permeability Test:**

From previous experience, the water permeability test is not a practical way for cement permeability, especially when the traditional steady-state method is used, as the pressure build-up process is extremely slow under the low flow rate for the low permeability material such as cement. Therefore, in the case of water permeability being applied, the procedure is similar to the Nitrogen permeability except changing the nitrogen tank to the ISCO pump.

# Appendix D CAD drawing for the wellbore simulator system

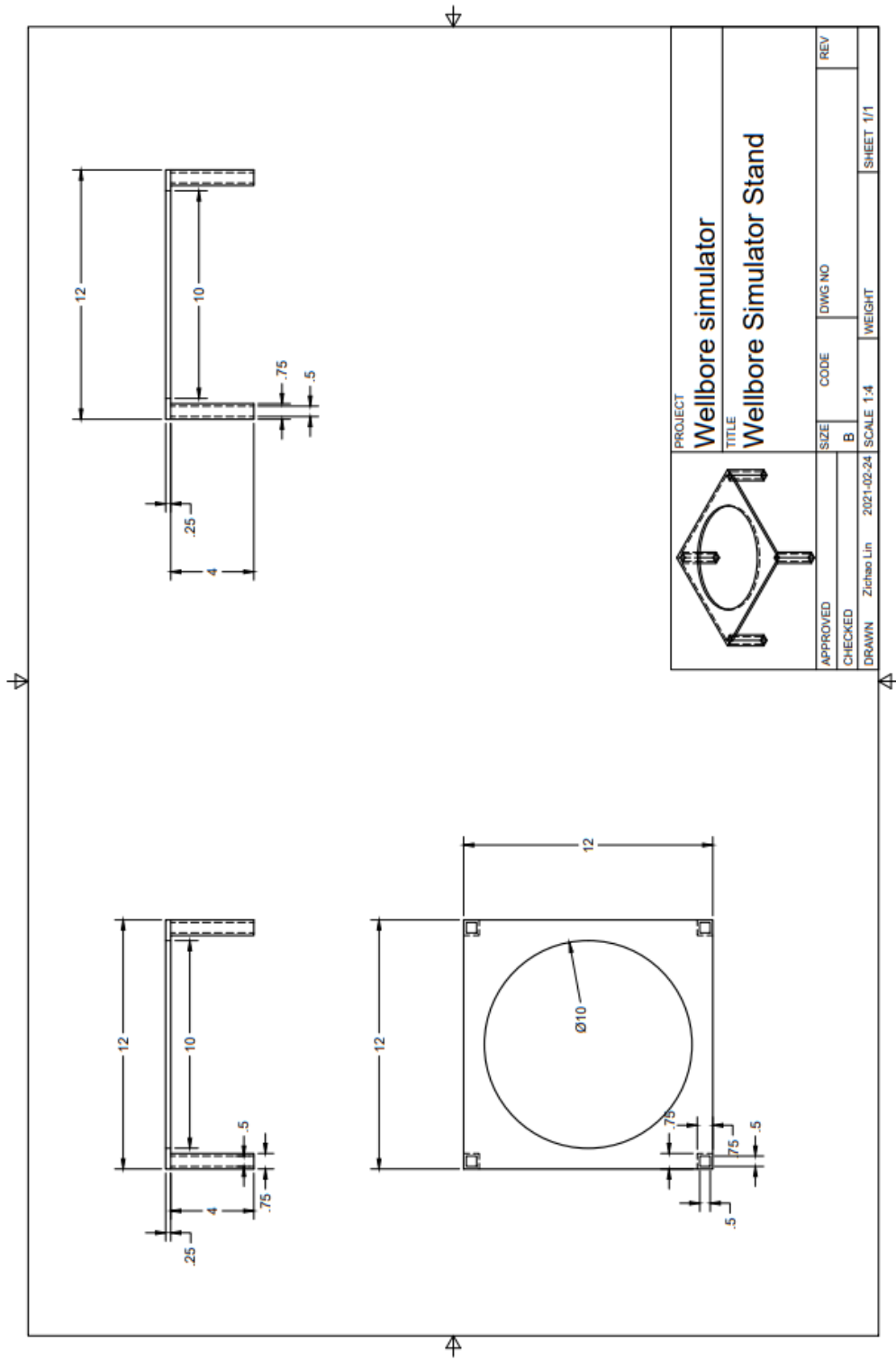


Figure D- 1 Final CAD drawing for the wellbore simulator stand



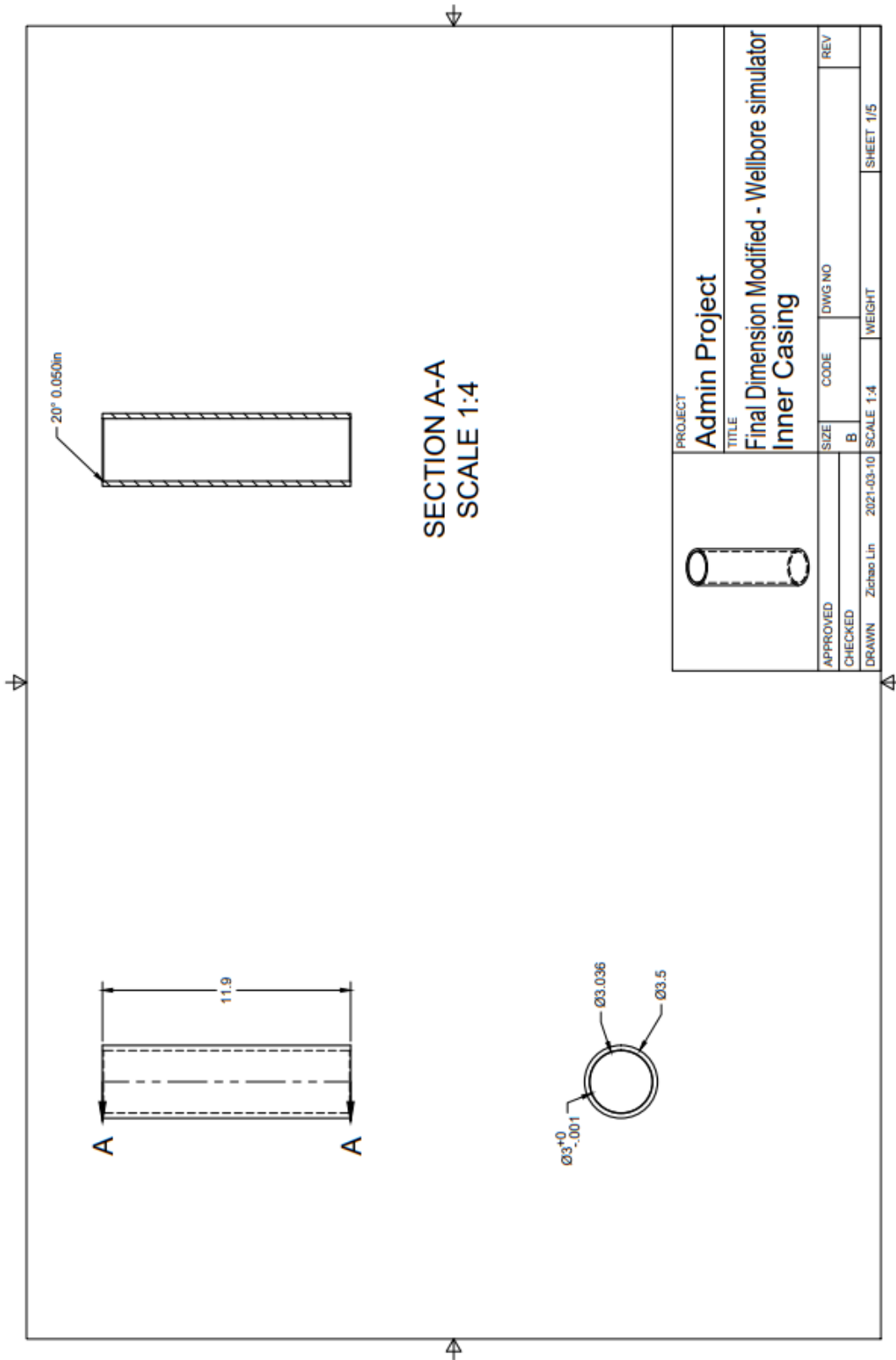
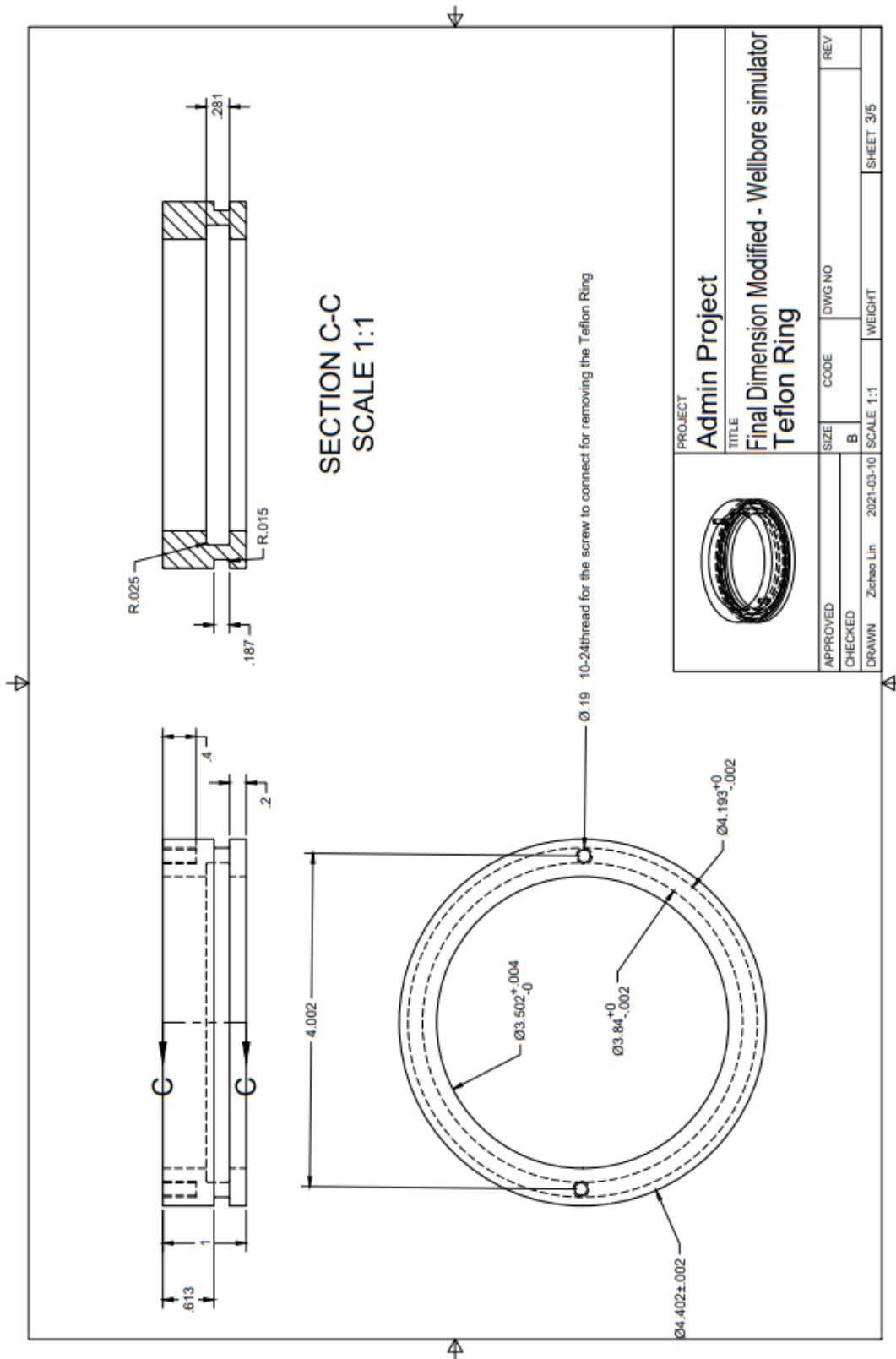


Figure D- 2 Final CAD drawing for inner casing




		<b>PROJECT</b> Admin Project	
<b>TITLE</b> Final Dimension Modified - Wellbore simulator Teflon Ring		<b>SIZE</b> B	<b>DWG NO</b> 
<b>APPROVED</b> 	<b>CODE</b> 	<b>SCALE</b> 1:1	<b>REV</b> 
<b>CHECKED</b> 	<b>SCALE</b> 1:1	<b>WEIGHT</b> 	<b>SHEET</b> 3/5
<b>DRAWN</b> Zichao Lin	<b>DATE</b> 2021-03-10		

Figure D- 3 Final CAD drawing for Teflon ring

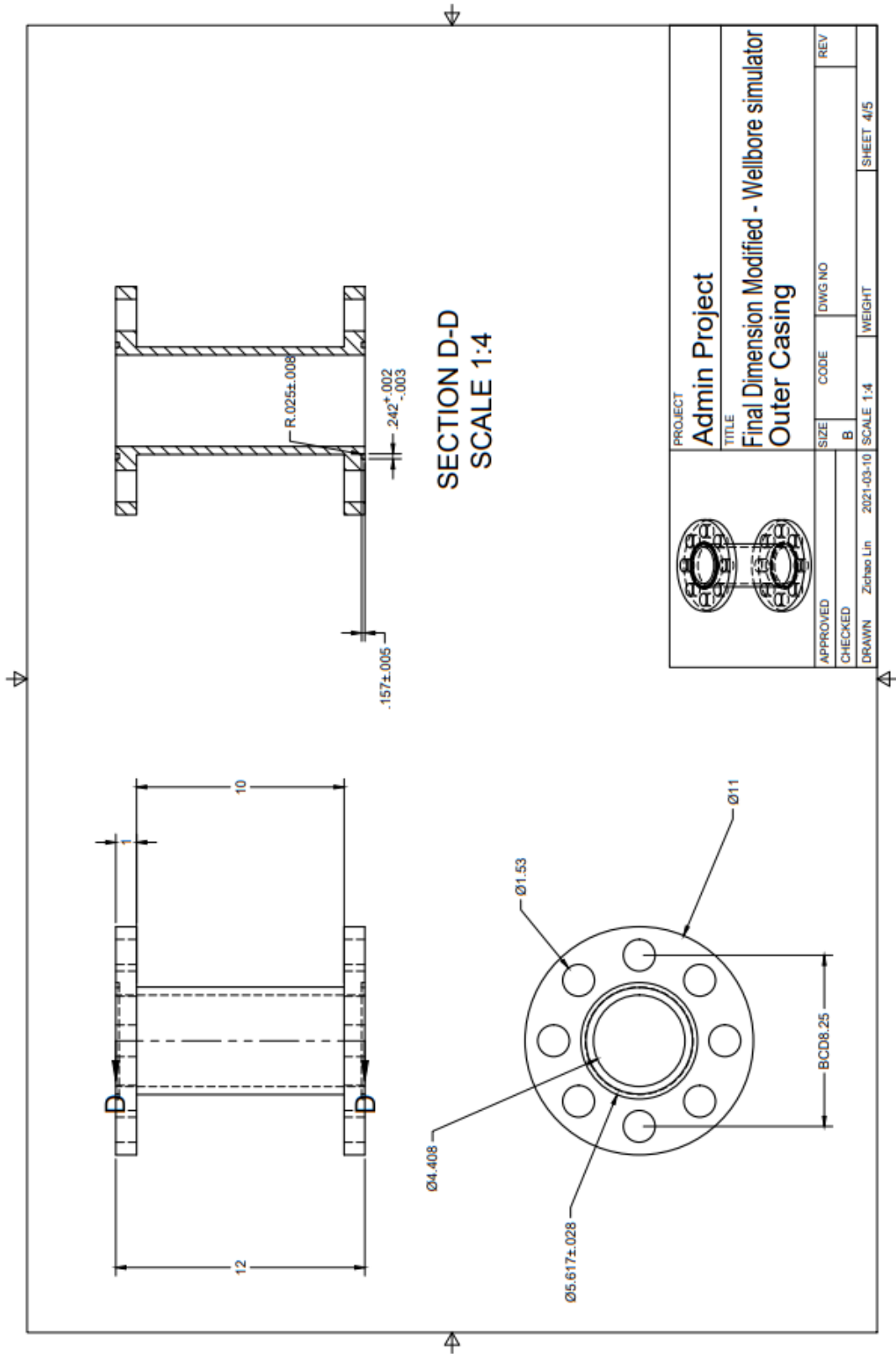


Figure D- 4 Final CAD drawing for outer casing and flange

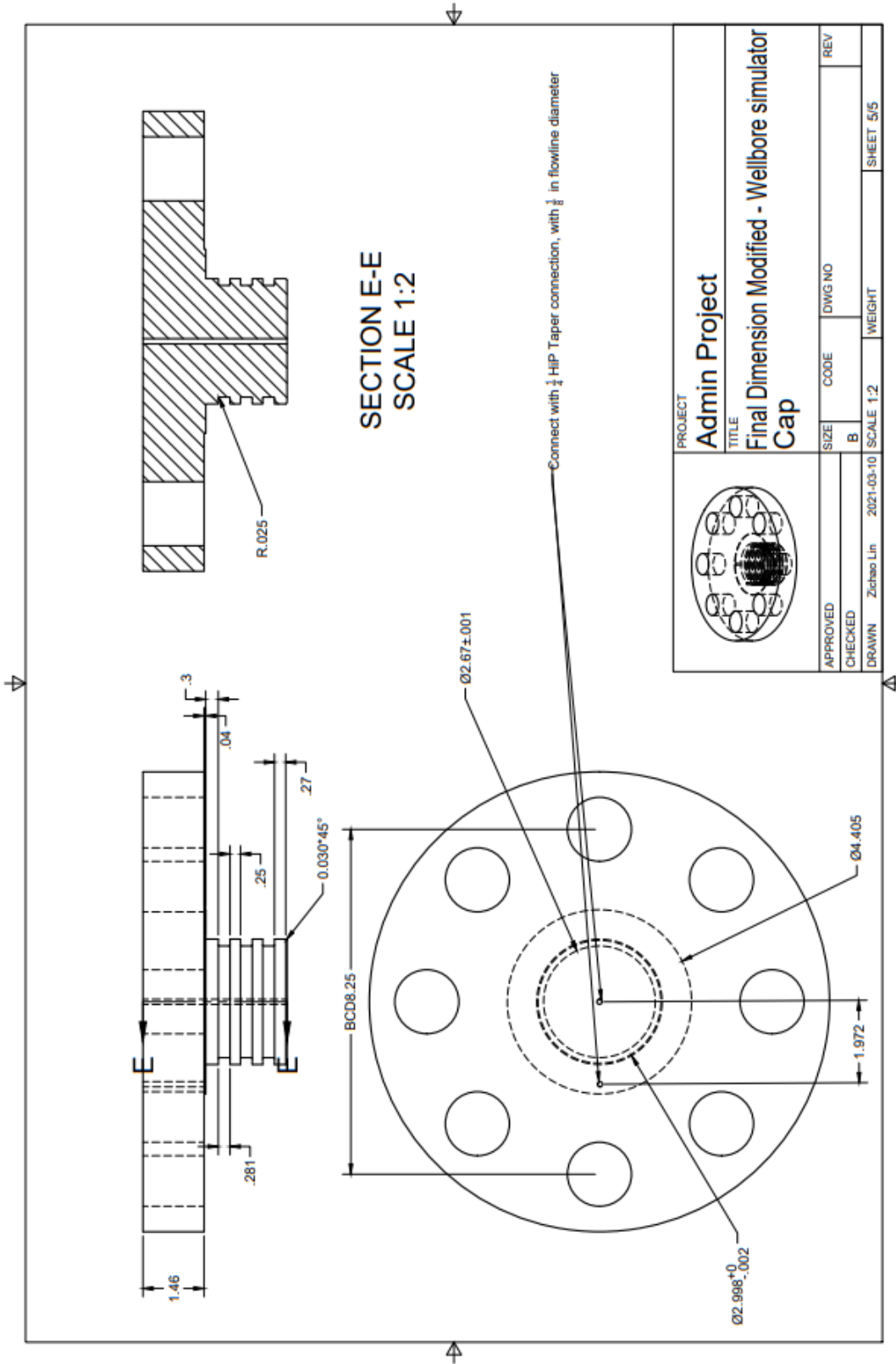


Figure D- 5 Final CAD drawing for caps

# **Chapter 5 Assessment of the Permeability of the Cemented Wellbore Sections Under Elevated Temperature and Cyclic Pressure Conditions**

## **5.1 Summary**

With the development of advanced well stimulation techniques, wells can be exposed to high cyclic mechanical and thermal stress. These continuously changing, loading and unloading pressure and temperature conditions can cause the loss of zonal isolation for the cement (Zhao et al., 2019; Zeng et al., 2019; Kuanhai et al., 2020). In this chapter, the newly designed wellbore simulator was used to study the nature of the loss of zonal isolation of the cement by measuring the permeability change during the static pressure and temperature, the cyclic pressure and constant temperature conditions.

The chapter started with the validation experiments of the newly designed wellbore simulator, confirming the pressure and temperature rating and the cement removal method. Both validations were successful.

Then, the real-world-use production cement, ECOprime, was used for the constant pressure and temperature, cyclic pressure and constant temperature experiments. The slurry volume of 0.92L was injected into the annulus between the inner casing and outer casings made from ANSI 4140 steel, the same material as API P110 casing. The slurry was cured under 80°C, 25MPa, (simulating the field curing conditions provided by the service company) for one week. The wet nitrogen permeability measurements were conducted under the static pressure of 0MPa, 10MPa, 25MPa, 43MPa and static temperature of 50°C, 80°C to demonstrate the effect of changing static pressure and temperature on the permeability or zonal isolation of the cement. Moreover, three cyclic pressures and constant temperature experiments were conducted to study the effect of cyclic pressure varying within the range of 3MPa to 43MPa, under constant temperature.

After the permeability measurements, the leakage pathways were detected visually by applying the nitrogen pressure at the bottom surface of the cement while putting water or soap water on the top surface of the cement. The leakage pathways were identified as the sections where the gas bubbles came out.

The shear bonding tests using the hydraulic press were then conducted to analyze the shear bonding strength between the inner casing and cement.

By changing the pressure rating and the temperature of the system, this s wellbore simulator can be conveniently used for other petroleum and geothermal wells.

## 5.2 Introduction

As the main component of natural gas and Greenhouse Gas (GHG), methane has a global warming potential of more than 70 times greater than carbon dioxide (CO<sub>2</sub>) over 20 years (Government of Canada, 2021) or 25 times greater than carbon dioxide over 100 years (Alberta Energy Regulator, 2021). The oil and gas sectors are also the most significant industrial methane emitters, contributing 44% of total methane emissions in Canada (Government of Canada, 2021). To control methane emission from the wellbore, cement plays an essential role as zonal isolation is the most critical objective of primary cement (Kuanhai et al., 2020). However, even if the cement was appropriately placed initially, zonal isolation may still be lost during the time. One of the reasons is that modern petroleum wells are subjected to very high mechanical and thermal stress, for example, the multistage hydraulic fracturing operation (Garnier et al., 2008). These continuously change, the loading and unloading of the pressure and temperature can cause the loss of zonal isolation for the cement (Zhao et al., 2019; Zeng et al., 2019; Kuanhai et al., 2020). Therefore, it is critical to study the leakage nature of the cement under cyclic pressures and temperatures to increase the wellbore safety (Vrålstad et al., 2019).

From time to time, various ways were designed to analyze cement integrity. They can be mainly divided into three categories based on the tool used. The first method was to scale down the sample size to be scanned under the X-ray computed tomography (Opedal et al., 2014; De Andrade et al., 2015). This method could answer if the potential leakage pathways were caused

by the cement's debonding, cracking, or mechanical failure as it can observe the inner structure of the samples. However, during the scanning of the sample, the stress applied to the cement cannot be maintained. Therefore, the size of the micro annulus or the shape of the internal structure may not be the same as the pressure was applied. Besides, the ageing of the cement during the scanning cannot be negligible.

Another way is to theoretically analyze and predict the cement failure mechanism (Lecampion et al., 2013; Thiercelin et al., 1997; Bois et al., 2012). The advantage of this method was that it could provide theoretical support for the simulation and study the relationship between the different factors by making proper assumptions. However, this method cannot show the critical number of the cyclic pressure or the temperature and therefore miss the effect caused by the cyclic load. The result is also a lack of support of the experimental data.

The author preferred the experimental method as it can clearly show the effect of cyclic load. Besides, the stress applied to the cement can be maintained during the process of analyzing cement. The experimental method can be traced back to 1992 when Goodwin and Crook studied the effect of pressure and temperature on the cement sheath failure on a specially designed shear-bonding test device. By evaluating the shear bonding stress, they observed that the cyclic temperature significantly affected the quality of shear bonding between the cement and casing (Goodwin & Crook, 1992). In 2004, Boukhelifa et al. used a specially designed device that can expand and contract to observe the crack on the cement. After that, in 2017, Therond et al. applied a significant scale testing and modelling in a water injection well. However, all the studies above did not consider the accumulative effect of the cyclic and believed that the cement failure was mainly caused by the single cycle of the pressure and temperature. In the most recent study, Kuanhai et al. considered up to 18 cycles in the experiment. However, it is still not enough to simulate the filed case. In this chapter, up to 50 cycles were considered, based on the actual field data. The whole experiment was also separated into four parts, the validation of the wellbore simulator, the constant pressure and constant temperature experiment, the constant temperature and cyclic pressure experiment, which will be discussed in further sections.

There are also various physical apparatuses designed to analyze the properties of the cement, which were discussed in Chapter two and Chapter four. Based on these experiences and studies, a physical wellbore simulator was designed to simulate the downhole conditions and study the

nature of the development of the cement leakage pathway by measuring the permeability of the cement sheath. The experiment started from the validation of the newly designed wellbore simulator. The validation process contains two-part, the validation of pressure and temperature rating and the validation of cement removal. Then, to control the variables, the further experiments were divided into two parts, the constant pressure and constant temperature experiment, the constant temperature cyclic pressure test. The details will be discussed in the next section.

### **5.3 Materials, equipment, and methods**

In this section, the cement, equipment, and the methodology of each experiment are discussed. As mentioned in the introduction, the experiment contains three parts: the validation of the wellbore simulator, the constant pressure and constant temperature experiment, and the constant temperature cyclic pressure experiment. The validation part was further divided into two parts, the validation of pressure rating and the validation of cement removal.

#### **5.3.1 Validation of the newly designed physical wellbore simulator**

The pressure and temperature rating test was conducted when the wellbore simulator and its stand were received to confirm the pressure and temperature rating from the design was achieved. Besides, the cement removal test was conducted by using two pipes that had the similar dimension with the wellbore simulator to validate the cement removal process and to give the rough information on the shear bonding stress needed to remove the cement so that the hydraulic press with the correct capacity of load could be purchased for the lab.



### **5.3.1.1 Validation of the pressure and temperature rating**

The experiment was aimed to simulate the worst-case scenario in the lab, where the maximum inner casing pressure, 43MPa, the maximum applied temperature, 80 °C, were applied with the empty annulus between the inner and outer casing. However, from the safety perspective, the process started with ramping up the pressure first. After no leakage was detected for one week, which was the standard curing duration of the cement in our case, the temperature was then ramped up, and the conditions were held for another one week. The pressure and temperature rating was accepted if there was no leakage detected. The leakage can be detected by the flow rate on the pump. If there was no leakage after pressure stabilized, the flow rate on pump one should be zero. The detailed operating procedures were listed in Appendix E.1.1.

### **5.3.1.2 Validation of cement removal**

This experiment used two pipes with similar dimensions with the wellbore simulator inner and outer casing. The pipe used in this experiment was 3in schedule 40 pipe and 5in schedule 160 pipe with the length of 10in for each of them. The neat Class G cement with the w/c ratio of 0.45 was used to fill the annulus. The procedure of preparing the sample was described in Appendix E.1.2.1. After curing, the sample was placed on the bottom holder of the loading frame. Then a top 6061T6 aluminum displacement bar with the same diameter as the OD of the inner casing was put on the top of the sample (Figure 5-1). The compression was applied, and the maximum shear bonding strength to move the cement was recorded.

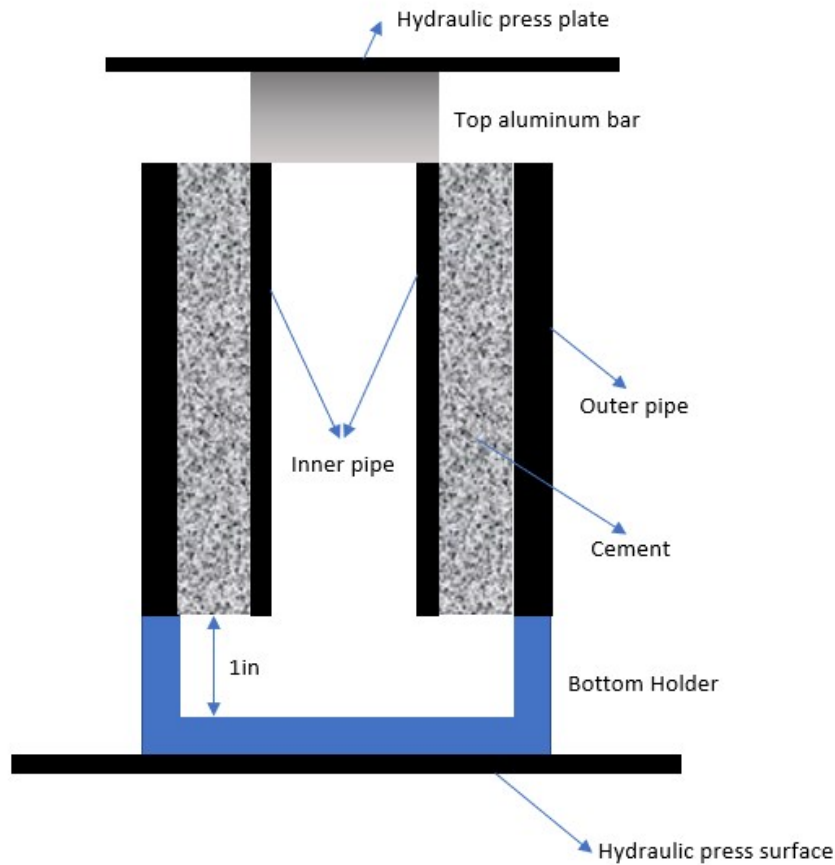


Figure 5- 1 Schematic for the set up of cement removal validation experiment

This experiment would give rough information on the load needed to remove the cement. The hydraulic press in our lab was purchased based on this number. After the hydraulic press was purchased, another cement removal test was conducted using the sample prepared following the same process. However, the 2nd experiment aimed to remove all the cement in the sample besides measuring the shear bonding strength of the cement and inner casing. The reason for conducting this experiment was that the cement was still hard to remove even after moving the cement column, and it took over two weeks to remove all the cement by drying. In the second experiment, three types of displacement 6061T6 aluminum bars were used to remove all the cement. The displacement bars were two 3.0in bars, two 3.5in bars, and two 4.0in bars with 8in length for all of them. The 3.5in bars were used to displace the inner casing; The 3in bars were used to displace the 3.5in bars in case the bars got stuck by the cement. The 4.0in bars were used

to remove the cement by sitting on the top of the cement column while the compression was applied. The detailed procedure was demonstrated in Appendix E.1.2.2

The calculation of the shear bonding strength between the inner casing and cement used the equation below:

$$\sigma_{bonding} = \frac{\sigma_{compression} * A_{top}}{A_{contact}} \quad (\text{Equation 5 - 1})$$

Where,

$\sigma_{bonding}$  is the shear bonding strength between inner casing and cement, in psi.

$\sigma_{compression}$  is the compressive stress applied by the loading frame or the hydraulic press in psi.

$A_{top}$  is the cross-sectional area of the cement sheath in square inches.

$A_{contact}$  is the contact area between the inner casing and cement in square inches.

### **5.3.2 Constant temperature and constant pressure experiment**

In this section, the constant temperature and constant pressure experiment was demonstrated. The cement blend used in this and further experiments was different. As the final goal was to study the effect of the cyclic stress, for example, the multistage fracturing process, on the cement zonal isolation or the permeability of the cement, the production cement used in the real world, named ECOprime, was used to simulate the field case. The water-cement ratio was 0.76. The cement was cured one week under 25MPa and 80 °C. The mixing procedure of the cement was described in Appendix E.2. Then, the sample was prepared, and the experiment was conducted based on the description in Appendix E.3.

There were two variables: the cycle numbers and the pressure or temperature of each cycle during the application of cyclic stress. For example, during the cyclic pressure, the cycle number was one variable. However, each cycle would have different pressure levels. Whether the cycle number or the different pressure levels causing the critical effect on the cement was unknown if the experiment was conducted simply by applying the cyclic pressure and for cyclic temperature

similarly. Therefore, the experiment should start with the application of static pressures and static temperatures. In this experiment, the static pressure of 0MPa, 10MPa, 25MPa, and 43MPa, the static temperature of 50°C and 80°C were applied as these temperatures and pressures would also be used in the cyclic pressure and constant temperature experiments. Under each combination of pressure and temperature, the average nitrogen permeability was measured and recorded. The ageing time of the cement was also recorded. The ageing time refers to the time difference between the end of cement curing and the starting of each permeability measurement. The detailed steps for each experiment are shown below (Table 5-1):

1st Constant P constant T experiment		
Step	Inner casing pressure , MPa	Temperature, °C
1	25	80
2	43	50
3	25	50
4	0	50
5	10	50
6	43	80
7	0	80
8	10	80
2nd Constant P constant T experiment		
1	25	80
2	43	80
3	10	80
4	0	80
5	0	50
6	10	50
7	25	50
8	43	50
3rd Constant P constant T experiment		
1	25	80
2	25	80
3	43	80
4	43	80
5	43	80
6	10	80
7	0	80
8	43	50
9	43	50
10	10	50
11	0	50
12	25	50
13	25	50
14	43	50

Table 5- 1 Experiment order for three constant pressure constant temperature experiments

### **5.3.3 Constant temperature and cyclic pressure experiment**

After knowing the pressure and temperature effect on the cement permeability, the pressure cycles were added to the experiment. One permeability measurement was taken at the curing conditions. Then, the setting temperature of the oven was changed from 80°C to 50°C and waited for 30minutes to simulate the cooldown process of the reservoir fluid due to the injection of fracturing fluid. Another permeability was taken at these conditions. Then, the pressure was changed from a cement curing inner casing pressure of 25MPa to 43MPa in 5minutes and held at 43 MPa for one hour. Then, the inner casing pressure was ramped down from 43MPa to 3MPa in 15minutes and held for 15minutes. This was the end of the first cycle. From the second cycle to the fiftieth cycle, the inner casing pressure change followed the description below:

The inner casing pressure was ramped up from 3MPa to 43MPa in 5minutes and held for one hour. The inner casing pressure was then ramped down from 43Mpa to 3MPa in 15minutes and held for 15minutes. The permeability was measured at the end of the 12<sup>th</sup>, 24<sup>th</sup>, 36<sup>th</sup>, and 50<sup>th</sup> cycles. The pressure was changed from 3MPa to 25MPa to make the permeability measurement comparable with the results measured before the pressure cycles. The procedures of sample preparation, the connection of the flowline, and the permeability measurement were the same as the constant pressure and constant temperature experiment.

### **5.3.4 Leakage pathway detect and cement removal**

After the permeability measurement, the inner casing pressure was reduced to 0MPa and ambient temperature. One day was waited for the temperature to stabilize. Then, the top cap of the wellbore simulator was removed. The nitrogen pressure of 50psi was applied from the bottom of the cement sheath. The water or the soap water was poured on the top surface. The leakage pathways were detected as the place where bubbles appeared. After this, the cement was removed by following the procedure in E.1.2.2.

## 5.4 Results and discussions

### 5.4.1 Validation of wellbore simulator

For the validation of pressure rating, the result is shown in Figure 5-2. Then, the pressure and temperature rating result is shown in Figure 5-3. The cement removal validation result is shown in Figure 5-4. The maximum applied force was 36tons. Therefore, based on this number, the hydraulic press with the capacity of 50tons was purchased for the lab. The cement could be successfully moved. Therefore, the whole system was ready for further experiments.

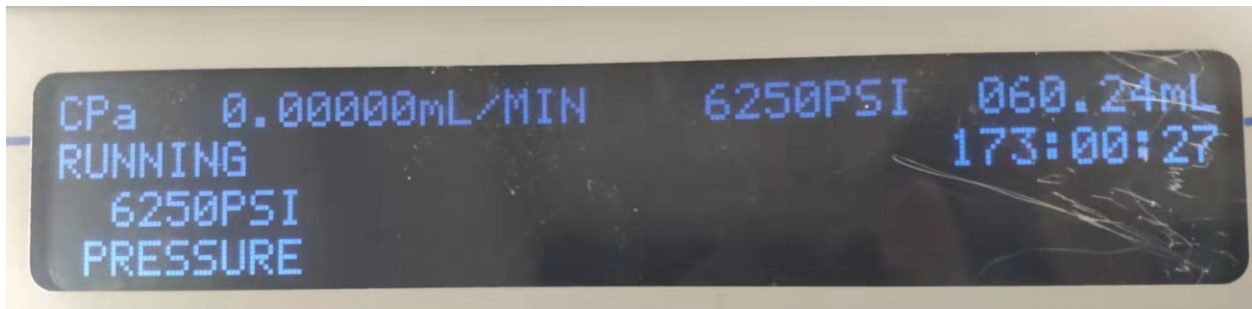


Figure 5- 2 Validation result of the wellbore simulator pressure rating

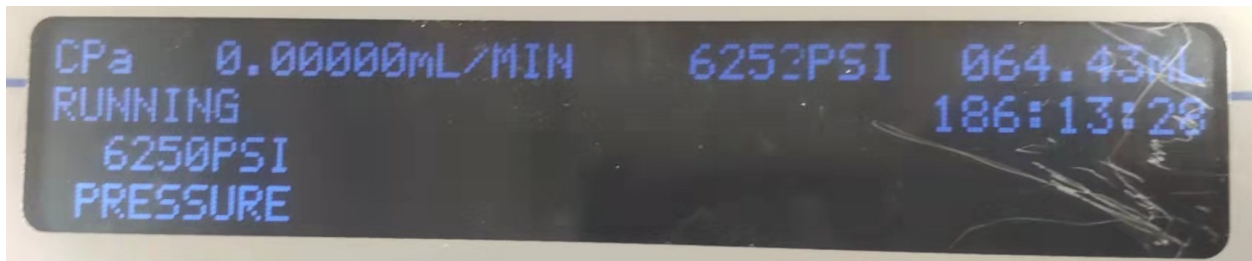


Figure 5- 3 Validation result of the wellbore simulator pressure and temperature rating

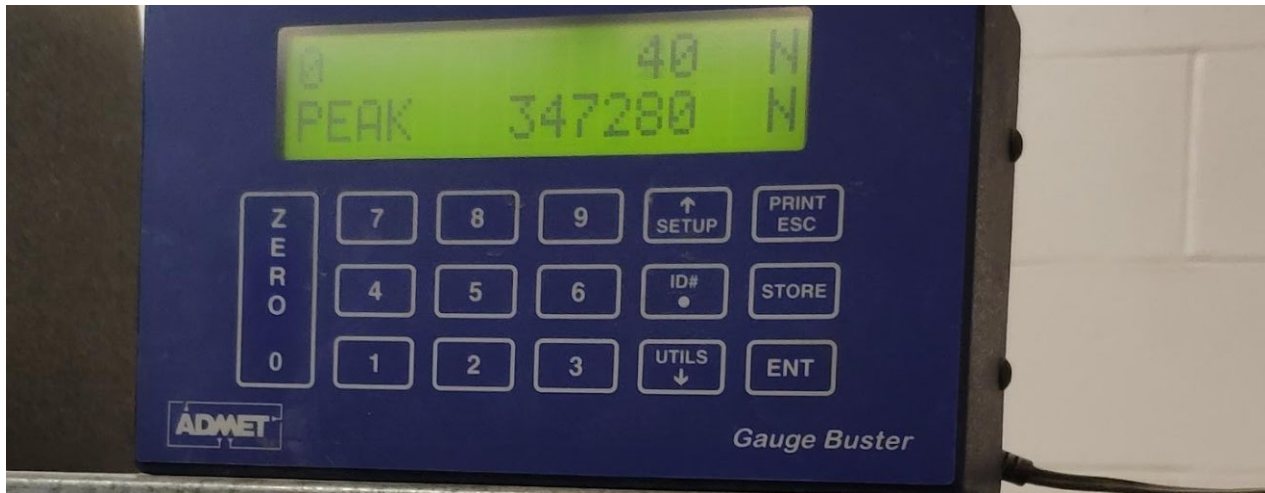


Figure 5- 4 Force applied for cement removal validation using loading frame

#### 5.4.2 Constant pressure and temperature experiments

The permeability measurement results for the first constant pressure and temperature experiment are listed in Table 5-2. Based on the time order, the first permeability measurement result under inner casing pressure of 25MPa and temperature of 80°C was 0.205mD. Then, the increase of inner casing pressure decreased the permeability while the ageing and decrease of temperature increased the permeability. The microannulus was enlarged, resulting in the permeability being increased from 0.205 to 0.27 mD. The pressure was further decreased under the same temperature. Besides, the ageing time of the cement was also increased. Both factors would increase the permeability. The permeability increased from 0.27 to 0.42mD. Then, the inner casing pressure was ramped down from 25MPa to 0MPa under the same temperature, which would increase the permeability, and the ageing would also increase the permeability. This resulted in the permeability increasing from 0.42 to 14.40mD.



<b>1<sup>st</sup> measurement</b>	<b>Average permeability at 50 °C</b>	<b>Time after finishing curing and before each permeability experiment</b>	<b>Average permeability at 80 °C</b>	<b>Time after finishing curing and before each permeability experiment</b>
<b>P, MPa</b>	<b>mD</b>	<b>hrs</b>	<b>mD</b>	<b>hrs</b>
0	14.40	62	19.50	120
10	0.98	68.5	6.97	137
25	0.42	44	0.205	8
43	0.27	26	0.17	100

Table 5- 2 Average permeability results for the first constant pressure and constant temperature experiment

Then, with a tiny ageing difference, i.e. tiny effect on the permeability, the pressure was increased from 0 to 10MPa under the same temperature, which would decrease the permeability. The permeability changed from 14.40mD to 0.98mD, two orders of magnitude difference indicating that the changing of inner casing pressure could significantly affect the permeability of the cement sheath. Then, the increased temperature from 50°C to 80°C and pressure from 10 to 43MPa would decrease the permeability. At the same time, the increase of ageing time would increase the permeability resulting in the decrease of permeability from 0.98mD to 0.17mD. Then, under 80°C, the pressure was decreased from 43 to 0 MPa with increased ageing time. Both of them would increase the permeability. Therefore, the permeability changed from 0.17 to 19.50mD. In the end, the pressure was increased from 0 to 10 MPa under 80°C, which would decrease the permeability with the ageing of 17hours that would increase the permeability. As a result of both effects, the permeability changed from 19.50mD to 6.97mD.

For the second constant pressure and constant temperature experiment, the first permeability measurement result under an inner casing pressure of 25MPa and temperature of 80°C is 0.019mD. Then, the increase of inner casing pressure from 25 to 43MPa under the same temperature decreased the permeability while ageing increased the permeability. The

microannulus was enlarged due to the ageing, resulting in increased permeability one order of magnitude, from 0.019 to 0.15 mD. After that, the decrease of inner casing pressure from 43MPa to 10MPa increased the permeability, while ageing also increased the permeability. The contribution of both effects resulted in the permeability being increased from 0.15 to 0.60 mD (enlarge the microannulus). The decrease of inner casing pressure from 10MPa to 0MPa increased the permeability, while ageing also increased the permeability. The contribution of both effects resulted in the permeability being increased from 0.60 to 6.29 mD (enlarge the microannulus). The further decrease of temperature from 80 to 50°C increased the permeability as the casing and cement shrinkage, while the ageing also increased the permeability. The contribution of both effects resulted in the permeability being increased from 6.29 to 9.38 mD (enlarge the microannulus). Then, the increase of inner casing pressure from 0 to 10MPa decreased the permeability while ageing increased the permeability. The contribution of both effects resulted in the permeability being decreased from 9.38 to 5.90 mD (reduce the microannulus).

Furthermore, increasing inner casing pressure from 10 to 25MPa under the same temperature decreased the permeability while the ageing increased the permeability. The contribution of both effects resulted in the permeability being increased from 5.9 to 6.08 mD (enlarge the microannulus). Finally, the increase of inner casing pressure from 25 to 43MPa under 50°C decreased the permeability while ageing increased the permeability. The contribution of both effects resulted in the permeability being increased from 6.08 to 9.80 mD (enlarge the microannulus). The detailed data for the second constant T and constant P experiment were summarized in Table 5-3.

<b>2<sup>nd</sup> measurement</b>	<b>Average permeability at 50 °C</b>	<b>Time after finishing curing and before each permeability experiment</b>	<b>Average permeability at 80 °C</b>	<b>Time after finishing curing and before each permeability experiment</b>
<b>P, MPa</b>	<b>mD</b>	<b>hrs</b>	<b>mD</b>	<b>hrs</b>
0	9.38	74	6.29	44.5
10	5.90	96	0.60	27.5
25	6.08	119	0.019	5.5
43	9.80	124	0.15	22

Table 5- 3 Average permeability results for the second constant pressure and constant temperature experiment

From the first two experiments, three factors were found that had the most critical effect on the cement permeability, material (cement and casings) shrinkage/expansion caused by the temperature change that would enlarge/reduce the microannulus, thus, increasing/decreasing the permeability, casing shrinkage/expansion caused by the inner casing pressure change that would enlarge/reduce the microannulus, thus, increasing/decreasing the permeability, and cement dehydration caused by ageing time that would enlarge the microannulus and thus increasing the permeability. Several steps were added to the third constant pressure and temperature experiment to separate these three parameters. Besides the standard steps from the previous experiment, step 2 was added to evaluate the effect of ageing under the original curing conditions. Steps 4 and five were added to check the effect of ageing under the conditions with the highest temperature and pressure. The first five steps did not have permeability under the injection pressure of over 2000psi. However, between steps 5 and 6, with tiny ageing, while the inner casing pressure was decreased, the permeability increased to 0.00070mD, which meant that the inner casing pressure had a significant effect on the permeability of the cement. By comparing steps 3, 4, 5, 8, and 14, the permeability started from 0mD, under 2000psi injecting pressure, to 0.01500mD, which indicated that the long ageing time could significantly affect the permeability of cement. The

structure in the cement was permanently changed due to the ageing and changing of pressure and temperature. Therefore, even the inner casing pressure and temperature were changed back to the origin, the same permeability would not be obtained.

Besides, by comparing step 12 with step 13, even with the ageing of 28hours, the permeability could still be decreased up to one order of magnitude, from 0.00545 to 0.01230, increasing 125.68%. This was the result of increased permeability by ageing and decreasing permeability due to the increasing temperature. However, if both factors contributed in the same direction, the permeability change would be more significant. For example, the temperature was changed between step 8 and step 9 from 80 to 50 °C under the same pressure with an ageing effect. Both factors tended to increase the permeability. The permeability increased from 0.00373mD to 0.02000mD, 436.19% increment. These indicated that the decrease of temperature could play a critical role in increasing the permeability of the cement. However, the final permeability was the result of the contribution extent of the three factors listed previously. The data for the third constant T and P experiment were summarized in Table 5-4.

<b>Step number and time interval, hrs</b>	<b>Condition</b>	<b>Permeability (mD), Average value</b>	<b>Step number and time interval, hrs</b>	<b>Condition</b>	<b>Permeability (mD), Average value</b>
1 (5.5)	80°C 25MPa	N/A	8 (117)	80°C 43MPa	0.00373
2 (29.5)	80°C 25MPa (24 hr after starting time of step 1)	N/A	9 (146)	50°C 43MPa	0.02000
3 (32.5)	80°C 43MPa	N/A	10 (167)	50°C 10MPa	0.01770
4 (56.5)	80°C 43MPa (24 hr after starting time of step 3)	N/A	11 (172)	50°C 0MPa	0.03270
5 (70)	80°C 43MPa (just before step 6)	N/A	12 (190)	50°C 25MPa	0.00545
6 (73)	80°C 10MPa	0.00070	13 (218)	80°C 25MPa	0.01230
7 (94)	80°C 0MPa	0.00610	14 (223.5)	80°C 43MPa	0.01500

Table 5- 4 Average permeability results for the third constant pressure and constant temperature experiment

### **5.4.3 Cyclic pressure and constant temperature experiments**

The first, second and third cyclic pressure and constant temperature experiments are shown in Tables 5-5, 5-6, and 5-7 separately. Between steps 1 and 2 for each experiment, the permeability was significantly increased due to cement and casing shrinkage caused by the decrease of temperature. Among the fifty pressure cycles, the permeability was not significantly changed. It even showed a slightly decreasing trend. The reason could be that in the beginning, the large injecting pressures, 1532psi and 1760psi for the first and second experiment separately, were applied to the samples. The microannulus might be opened due to the large injecting pressure. However, due to the elasticity of the cement, once the injecting pressure was turned off during the pressure cycle, the cement would have the trend to turn back to its original shape. Therefore, the microannulus tended to be closed by this deformation. Then after the cyclic pressure, the permeability increased significantly once the permeability was measured under the lower inner casing pressure. The further decrease in both temperature and pressures to the ambient conditions also significantly increased permeability. These proved that the changing of temperature and inner casing pressure at the time of permeability measurement has more influence on the permeability of the cement than the cyclic pressure.

<b>Cycle number</b>	<b>Temperature (°C) and inner casing pressure (MPa)</b>	<b>Time difference after curing and before measurement (hrs)</b>	<b>Average Permeability (mD)</b>
Before cyclic pressure	80 °C, 25MPa	4	0.00231
Before cyclic pressure	50 °C, 25MPa	25	0.14600
After 12 cycles	50 °C, 25MPa	49	0.07310
After 24 cycles	50 °C, 25MPa	73.5	0.07320
After 36 cycles	50 °C, 25MPa	97.5	0.05070
After 50 cycles	50 °C, 25MPa	123	0.05140
After 50 cycles	50 °C, 3MPa	128	1.21000
After 50 cycles	21 °C, 0MPa	167	2.71000

Table 5- 5 Average permeability results for the first cyclic pressure and constant temperature experiment

<b>Cycle number</b>	<b>Temperature (°C) and inner casing pressure (MPa)</b>	<b>Time difference after curing and before measurement, hrs</b>	<b>Average Permeability (mD)</b>
Before cyclic pressure	80 °C, 25MPa	4	N/A
Before cyclic pressure	50 °C, 25MPa	22	0.05860
After 12 cycles	50 °C, 25MPa	46	0.01000
After 24 cycles	50 °C, 25MPa	70	0.00893
After 36 cycles	50 °C, 25MPa	94	0.00929
After 50 cycles	50 °C, 25MPa	120	0.00925
After 50 cycles	50 °C, 3MPa	141.5	0.0391
After 50 cycles	21 °C, 0MPa	165	0.135

Table 5- 6 Average permeability results for the second cyclic pressure and constant temperature experiment



<b>Cycle number</b>	<b>Temperature (°C) and inner casing pressure (MPa)</b>	<b>Time difference after curing and before measurement (hrs)</b>	<b>Average permeability (mD)</b>
Before cyclic pressure	80 °C, 25MPa	4	Lower than 0.000003
Before cyclic pressure	50 °C, 25MPa	23	0.1410
After 12 cycles	50 °C, 25MPa	48	0.0756
After 24 cycles	50 °C, 25MPa	72	0.0830
After 36 cycles	50 °C, 25MPa	96	0.1100
After 50 cycles	50 °C, 25MPa	122	0.1270
After 50 cycles	80 °C, 25MPa	150	0.0543
After 50 cycles	50 °C, 3MPa	178	0.9980
After 50 cycles	21 °C, 0MPa	208	0.7450
After 50 cycles	21 °C, 25MPa	216	0.2810

Table 5- 7 Average permeability results for the third cyclic pressure and constant temperature experiment

#### **5.4.4 Leakage pathway detection and shear bonding strength test**

The results of leakage pathway detection were shown in Figures 5-5 to 5-10 for the three constant temperature and pressure experiments and three cyclic pressure and constant temperature experiments separately. The figures showed that the main leakage pathways were the debonding between the inner casing and cement. These debondings were not evenly

distributed. There was also debonding between the outer casing and cement and radial cracks. However, compared with the debonding between the inner casing and cement, they were minor pathways.



Figure 5- 5 Leakage detection result for the first constant pressure and temperature experiment

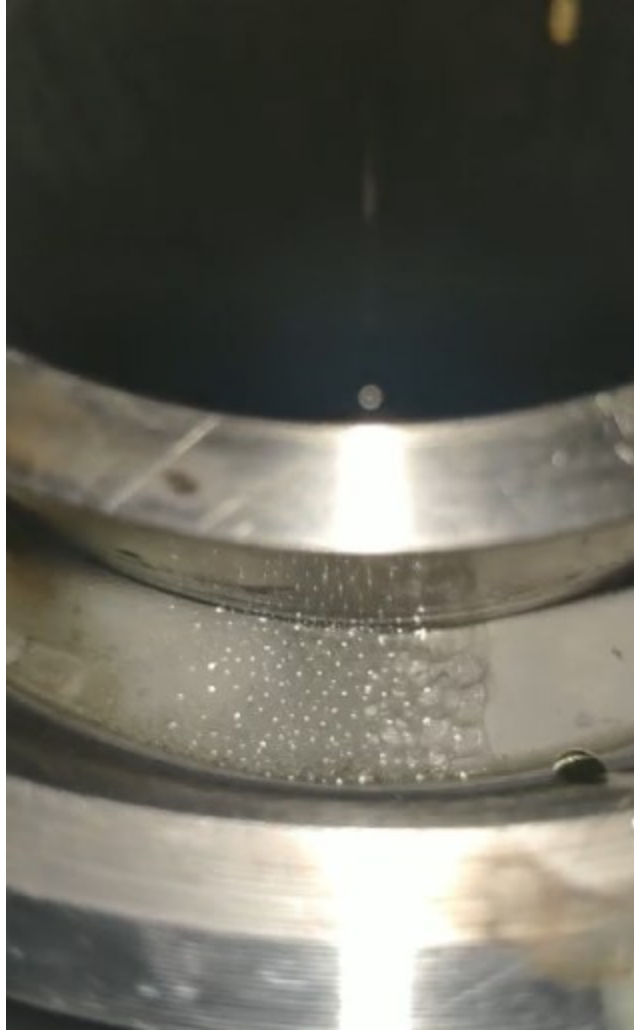


Figure 5- 6 Leakage detection result for the second constant pressure and temperature experiment



Figure 5- 7 Leakage detection result for the third constant pressure and temperature experiment



Figure 5- 8 Leakage detection result for the first cyclic pressure and constant temperature experiment



Figure 5- 9 Leakage detection result for the second cyclic pressure and constant temperature experiment



Figure 5- 10 Leakage detection result for the third cyclic pressure and constant temperature experiment

The results for the shear bonding strength test are listed in Table 5-8. For the first three experiments, with constant pressure and temperature, the shear bonding strength increased with decreasing permeability. However, for the cyclic pressure and constant temperature case, for example, the 1<sup>st</sup> cyclic pressure and constant temperature experiment had lower final permeability than the 1<sup>st</sup> experiment of constant pressure and temperature. However, their shear bonding strengths were the same. Therefore, the cyclic pressure significantly decreases the shear bonding strength.

<b>Experiment</b>	<b>Shear bonding strength, psi</b>	<b>Final permeability, mD</b>
Constant P T 1 <sup>ST</sup>	358	14.4
Constant P T 2 <sup>ND</sup>	471	9.38
Constant P T 3 <sup>RD</sup>	569	0.0327
Constant T cyclic P 1 <sup>st</sup>	358	2.71
Constant T cyclic P 2 <sup>nd</sup>	464	0.135
Constant T cyclic P 3 <sup>rd</sup>	168	0.745

Table 5- 8 Shear bonding strength results



## 5.5 Conclusions

From three experiments of constant pressure and temperature and three experiments of cyclic pressure constant temperature, the following conclusion could be addressed:

- From three constant pressure and temperature experiments, three factors were found that had the most critical effect on the cement permeability. The first is material (cement and casings) shrinkage/expansion caused by the temperature change that would enlarge/reduce the microannulus, thus, increasing/decreasing the permeability. Besides, casing shrinkage/expansion caused by the inner casing pressure change would enlarge/reduce the microannulus, thus, increasing/decreasing the permeability. Finally, cement dehydration caused by the nitrogen injection during each permeability measurement would enlarge the microannulus and thus increase the permeability. The final permeability was determined by the effect or the contribution extent of these factors.
- From three constant temperature and cyclic pressure experiments, the changing of temperature and inner casing pressure at the time of permeability measurement has more influence on the permeability of the cement than the cyclic pressure. Especially in the third constant temperature and cyclic pressure experiments, the temperature was increased from 50 to 80 Celsius after 50 pressure cycles. Even with the effect of ageing, the pressure still decreased significantly. Besides, in the last step of the third constant temperature and cyclic pressure experiment, the pressure was increased back to 25MPa. The permeability decreased from 0.7450 to 0.281 mD, a 62.28% decrease. Compared with the results before and after 50 pressure cycles, from 0.1410 mD to 0.1270 mD, the permeability did not have a significant difference. Besides, in all three constant temperature and cyclic pressure experiments, when the temperature was changed from the curing condition 80 Celsius to 50 Celsius, the permeability increased significantly. Furthermore, the permeability increased significantly when the inner casing pressure was decreased from 25MPa to 3MPa after 50 cycles. These temperature and pressure effects on the constant temperature and cyclic pressure experiments consist with the previous conclusion from the constant pressure and temperature experiments.

- In the shear bonding strength results, for the constant pressure and temperature experiments, the shear bonding strengths for these three experiments are 358psi, 471psi, and 569psi. The shear bonding strength increased significantly between each experiment. As for three constant temperature and cyclic pressure experiments, the results for the first and second experiments showed the increasing trend on the shear bonding strength, from 358psi to 464psi. The shear bonding strength result for the third constant temperature and cyclic pressure experiment was not considered because extra steps were added. This caused the experimental duration to be longer than the previous two experiments and thus not comparable. The increasing trend in the shear bonding strength can be caused by the increase of surface roughness due to the cement removal and pipe cleaning in each experiment.
- It was shown by the shear bonding strength table, especially between the first constant pressure and temperature experiment and the first constant temperature cyclic pressure experiment. The final permeability for the first constant pressure and temperature experiment was an order of magnitude larger than that in the first constant temperature and cyclic pressure experiment. The shear bonding strength was still the same. Therefore, the cyclic pressure significantly decreases the shear bonding strength.

## Appendix E Experimental procedure

### E.1 Experimental procedure for the validation of the wellbore simulator

This section is further divided into two sections, the validation of pressure and temperature rating and the validation procedure for cement removal.

#### E.1.1 Experimental procedure for validating the pressure and temperature rating

1. Follow the procedure in Appendix C. After connecting the flowline, the system should be like:



Figure E- 1 connected wellbore simulator system

1. The top center gland is loosened, and the water pressure of 20psi is set on the pump one to check the flowability of the flowline.
2. The pump is stopped once the water comes out from the top center flowline.
3. Set 20psi water pressure on the pump two to add the water into the inner casing and drive the gas out. If the water is run out in the pump, refilling will be needed before further steps.
4. Pump two is stopped once the water comes out from the top hole on the cap.
5. The top gland is installed.
6. The pressure is applied by using pump one. The pressure is set to 100, 500, 1000, 2000, 3000, 4000, 5000, 6250psi in order. The stabilized pressure or the flow rate close to zero should be observed before increasing the pressure between each step.
7. The pressure is held for one week while the flow rate of the pump is monitored frequently.
8. After one week, if there is no leakage detected, the setting temperature of the oven is increased to 80°C.
9. The temperature and the pressure conditions are held for one week.

## E.1.2 Experimental procedure for cement removal validation

The validation of cement removal is divided into the preparation of the samples and the cement removal using the hydraulic press or loading frame. Both validations are successful as the flowrate is maintained to be zero for more than one week without significant water volume change on the pump.

### E.1.2.1 Preparation of the sample

1. The bottom side of the schedule 160 5in pipe is sealed by the electric tape (Figure E-2).

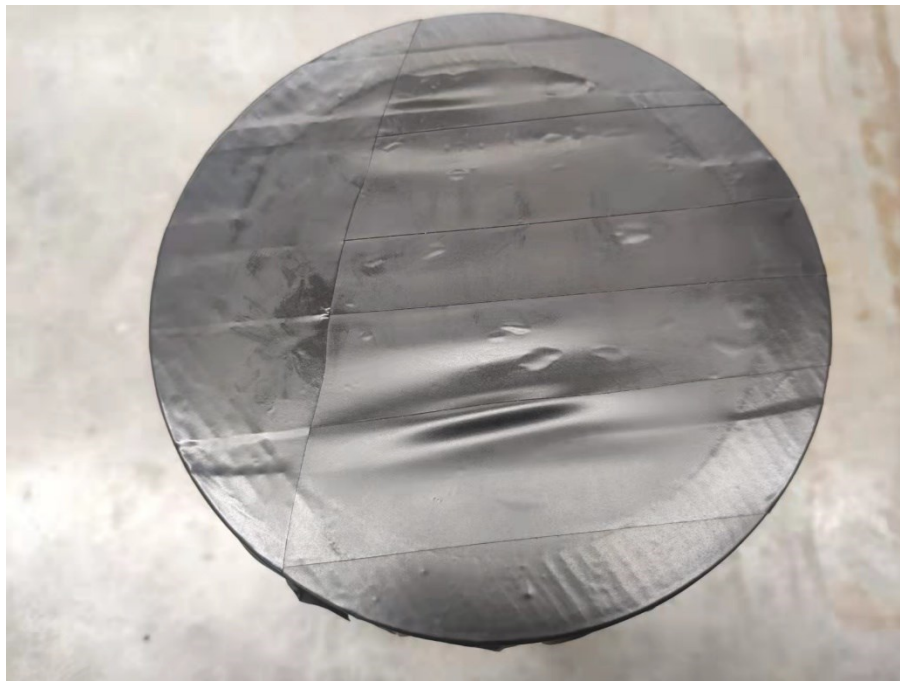


Figure E- 2 Sealing of bottom surface for the outer casing of the cement removal test sample

2. Seal the bottom surface of the inner casing with the electric tape and place the inner casing into the outer casing.
3. Use the calliper to measure the distance to ensure the pipe was centred.
4. Weigh 1311.10g neat Class G and 590ml water.

5. The mixing procedure followed API 10A. The low-speed 150rpm mixer is the same as the one in Chapter 3. The high-speed mixer used is shown below:



Figure E- 3 High-speed mixer for large scale sample preparation

6. The cement slurry is poured into the annulus between the inner and outer casing.
7. The top side of the sample is sealed with electric tape.
8. The temperature of the cement is ramped up to 50 °C with ambient pressure. The sample is cured for one week. After curing, the electric tape is removed.

### **E.1.2.2 procedure for cement removal using hydraulic press and loading frame**

#### **For loading frame:**

1. The bottom holder is placed on the bottom plate of the loading frame (Figure E-4).



Figure E- 4 bottom holder for cement removal using loading frame

2. Then, the sample is placed centrally on the top of the holder. The 3.5in aluminum bar is placed on the top of the inner casing. The setup before the test is shown in Figure E-5.



Figure E- 5 Overall setup for cement removal using loading frame

3. The compression is applied. The maximum compression is recorded.

**For hydraulic press:**

1. The setup of the hydraulic press system is shown in Figure E-6. The sample sits on the bed frame with the bottom holder bar. The hydraulic press is powered by either manual force or a portable air compressor. When the power is applied, the ram assembly will move downward and compress the sample. The pressure gauge will show the compression being applied.



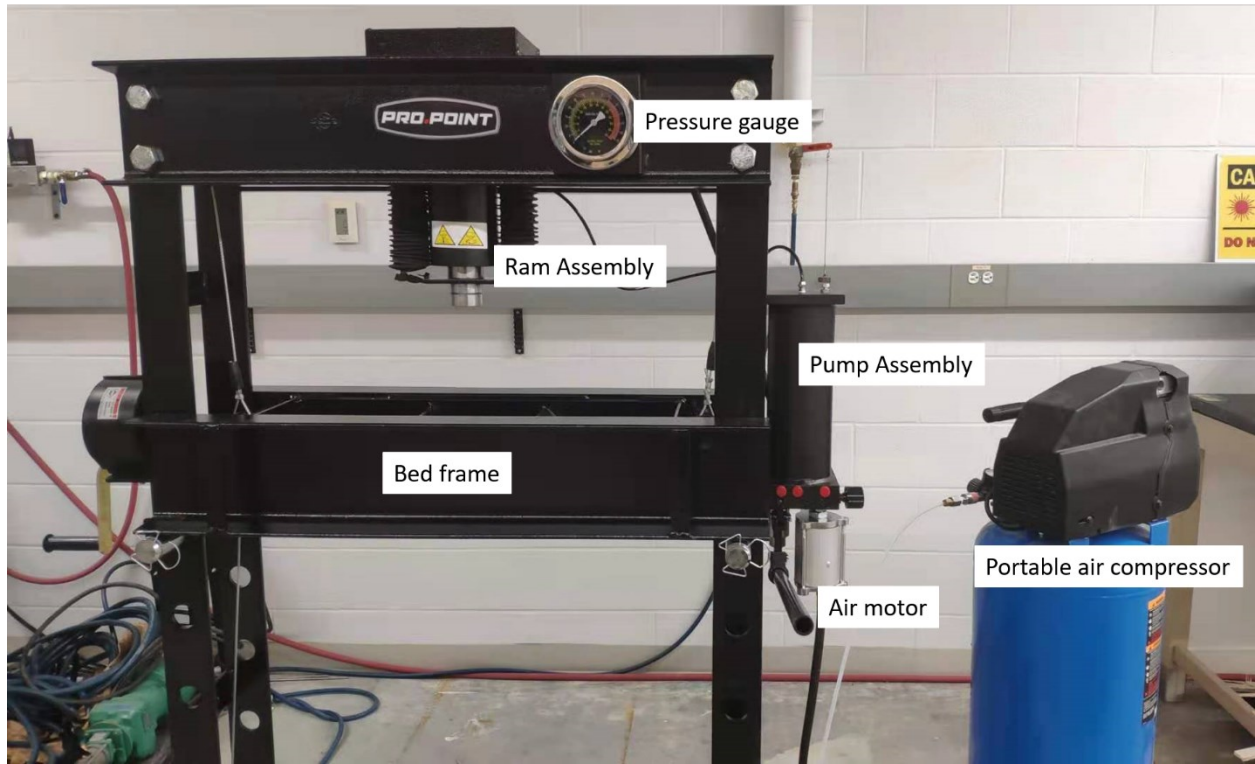


Figure E- 6 Hydraulic press setup

2. The sample is placed on the bed frame, and the 3.5in aluminum bar is placed on the top of the inner casing of the sample (Figure E-7).



Figure E- 7 Overall setup for cement removal using the hydraulic press

3. The air compressor is turned on, and set the output pressure as 110psi.
4. The movement of the pressure gauge is recorded by phone during the application of compression force.
5. Put the second 3.5in bar on the top and further apply the compression until the inner casing is removed.
6. The 3.0in bar is used if the 3.5in bar gets stuck.
7. Put the 4in bar on the top of the cement column and repeat the process until all the cement is removed.

## E.2 Procedure of mixing 1L ECOprime cement slurry for the wellbore simulator experiments

1. Weigh 880.79g ECOprime cement blend and 669.21g water.
2. Add the cement to the water under 4000rpm by using the high-speed mixer.
3. Once all cement is added, increase speed to 12,000 rpm and mix for 35 seconds. With the remaining of 5seconds, a 1mL liquid defoamer is added.
4. The container with the slurry is transferred to the low-speed mixer and placed into the water bath (Figure E-8).



Figure E- 8 Low-speed mixing system with water bath

5. The system is heated from ambient temperature to 80°C for approximately 15 min. Once at 80°C, continue mixing for a further 30 min.

### **E.3 Procedure for constant temperature and constant pressure experiment**

1. The installation procedure of the wellbore simulator followed Appendix C until step 13.
2. The wellbore simulator and the oven are preheated to 50°C.
3. The cement slurry mixed following the procedure in Appendix E.2 is injected into the annulus between the inner and outer casing using a funnel (Figure E-9). One inch gap on the top is left for the Teflon ring.



Figure E- 9 Cement injecting process for wellbore simulator

4. The top Teflon ring and the top cap are placed. The further steps in Appendix C are followed to finish the connection of the flowline.
5. The setting temperature of the oven is increased to 80°C,

6. Ensure the flowline is in the mode of curing cement based on Appendix C. The inner casing pressure is increased to 43MPa. The sample is cured for one week.
7. After curing, the pressure is reduced to ambient pressure, and the water in the inner casing is removed.
8. The wellbore simulator is moved out of the oven. The meshed material replaces the Teflon ring to distribute the nitrogen evenly for further permeability measurement.
9. The wellbore simulator is placed back in the oven and connected to the flowline based on Appendix C.
10. The flowline connection is converted to the mode of permeability measurement. The permeability measurement order for the first, second, and third constant pressure and constant temperature experiments is listed in Table 5-1.
11. The inlet nitrogen pressure is increased by 100psi and waited for five minutes until the flow is observed on the bubble flowmeter.
12. The pressure is monitored on the computer. Once the pressure stabilized, the flow rate was measured. The flow rate is measured following the same procedure in Appendix A.2.2.
13. Five permeabilities are measured under different pressures, and the average permeability is calculated.

## Chapter 6 Conclusions and Recommendations

This chapter aimed to provide a concise summary of the conclusions from the work of the previous chapters as the detailed discussion of data, and experimental procedures have already been demonstrated in the previous chapters. After the conclusion of the work, recommendations for future work were provided.

### 6.1 Conclusions

In chapter 3, the small scale cement samples with 1inch diameter and approximate 1inch length were prepared using neat Class G, G EXP, G Abandonment, and REMEDIALmix EC cement blends. The porosity measurement by drying and by porosimeter was compared. Besides, the proper drying procedure for the cement sample was demonstrated. The permeability measurement techniques, water permeability measurement on the wet samples, water permeability measurement on the dried samples, nitrogen permeability on the wet samples, nitrogen permeability on the dried samples were compared. A suitable permeability measurement technique was selected for further experiments using the physical wellbore simulator. The conclusions of this chapter:

- The drying method is a more accurate way to obtain the porosity of the cement samples.
- For the permeability measurement methods, the nitrogen steady-state permeability measurement for the dried and saturated samples and the water permeability measurement with precise flowrate control for the saturated samples are recommended. Between these three methods, the nitrogen steady-state permeability measurement on the dried sample is faster. It can obtain quantitative results, while the water permeability can only obtain the upper boundary. Besides, the nitrogen permeability measurement on the saturated samples can give the permeability result without significantly changing the structure compared with dry nitrogen permeability measurement while having faster permeability measurement results than water permeability measurement.

- The drying process will change the structure of the cement sample, causing at least three orders of magnitude differences in permeability results. Therefore, the absolute permeability obtained by the nitrogen steady-state permeability measurement can serve as a worst-case scenario permeability result.
- The larger total porosity does not mean the larger permeability. There is no clear positive or negative relationship between the total porosity and absolute permeability.
- The saturated neat Class G plug sample could have a permeability lower than 0.00007mD, far lower than the leakage criterion of 0.1md (Ozyurtkan et al., 2013). This indicates that without the influence of external factors, the cement itself can provide excellent zonal isolation at the beginning even with the neat Class G by appropriately setting the cement.

In chapter 4, the design process of the physical wellbore simulator was demonstrated, including the design of the wellbore simulator main body, the design of the flowline for the wellbore simulator system, and the design of the wellbore simulator stands. The proper design cycle and proper methods of material selection were demonstrated. The design was assisted by the FEA (Finite Element Analysis). The advantages of using FEA in the design were also discussed. The conclusions for this chapter are listed below.

- The standard schedule pipe cannot be used as the inner casing and outer casing due to the high thickness of the wall and low strength of the material. API P110 casing with 3.5in by 0.254in casing was selected as the inner casing, and 5in by 0.296in casing was selected as the outer casing.
- From the FEA of the wellbore simulator main body, increasing the diameter of the holes on the caps and flanges was found to be the most efficient method to increase the safety factor.
- Compared with two designs of the wellbore simulator stand among three materials, the larger hole design was selected with the ANSI 4130 steel. The larger hole increased the contact area and thus decreased the stress on the surface.
- The safety factor was a critical factor during the design. It can indicate where the design needs to be reinforced or weakened. It can also help with saving the raw material before manufacturing the product.

- FEA was an efficient way of analyzing the design. It can fasten the design cycle with less cost but higher precision compared with the traditional method.

Chapter 5 started with the validation of the newly designed wellbore simulator. The validation procedure included the pressure and temperature rating. Besides, in the validation process, the proper way of removing the cement after experiments was demonstrated. Furthermore, three groups of experiments with constant pressures and temperatures were conducted to simulate the static conditions downhole and to study the effect of different static pressure and temperature on the permeability of the cement. Moreover, three groups of experiments with cyclic pressure and constant temperature were conducted to study the effect of cyclic pressure on the permeability of the cement. After the permeability measurements, the shear bonding strength between the inner casing and cement was measured. The conclusions of this chapter are shown below.

- By analyzing the results of the first three groups of experiments, three factors were identified as having the most significant effect on the permeability of the cemented annular (casing/cement/ casing ) wellbore sections: i-) material (cement and casing) shrinkage/expansion caused by the temperature change that would enlarge/reduce the microannulus, thus, increasing/decreasing the permeability, ii-) casing shrinkage/ expansion caused by the nitrogen injection during each permeability measurement would enlarge/reduce the microannulus, thus, increasing/decreasing the permeability, and iii-) cement dehydration caused by nitrogen injection during the permeability measurement would enlarge the microannulus and thus increase the permeability. The final permeability of the cemented annular section was controlled by the combined effects of these three factors.
- Comparison of the permeability test results obtained under cyclic pressure and constant temperature conditions to that of the ones conducted under constant pressure and temperature conditions indicated that once the debonding occurred at the cement/casing interface due to initial change in pressure and/or temperature, applying cyclic pressure does not significantly alter the permeability of the cemented wellbore section.
- Visual observation of the casing surfaces revealed that the surface roughness conditions of the casings changed as more cement permeability tests were conducted, which had a



significant impact on the cement to casing shear bonding strength and the final permeability of the cemented wellbore section.

- The shear bonding strength increased significantly while the permeability of the cemented wellbore section decreased significantly with the increasing casing surface roughness.
- The cyclic pressure tests caused a significant reduction in the cement to casing shear bonding strength and the corresponding increase in the final permeability of cemented wellbore sections.

## **6.2 Recommendations for the future work**

This thesis contributes to leakage pathway analysis of oil and gas well cement. The proper way of preparing cement samples, drying cement samples and proper techniques for measuring the porosity and permeability of cement samples were discussed in the thesis. Moreover, this thesis demonstrated the factors that affect the cement's permeability or zonal isolation under the downhole conditions using a newly designed physical wellbore simulator. Based on the findings of the works, the following suggestions can be made for future research:

- In the future, the small cement samples can be analyzed using the micro-CT scanning technique, which would provide additional information beneficial for the analyses of the results obtained from the wellbore simulator. For example, the same cyclic pressures can be applied to the small-scale cement samples prepared using the same slurry composition and same curing conditions used to prepare the wellbore simulator sample. Such analyses from a micro-CT scan can tell us how the cyclic pressure affects the cement matrix rather than the whole system.
- More variables can be included in the wellbore simulator experiment. Currently, only the static pressure and temperature, cyclic pressure and constant temperature experiments were conducted. The experiments of constant pressure and cyclic temperature, cyclic pressure and cyclic temperature could also be considered in the future to simulate the more realistic conditions. Even considering cyclic pressure and temperature, more

parameters can still be added, such as the effect of drilling fluid contamination while the cement is setting on the permeability of the cemented wellbore sections.

- The expansion of the simulation scenarios will also be worthwhile. In our case, the wellbore simulator only simulated the casing/cement/casing case for the vertical well. The casing/cement case (i.e. plug cement) and formation/cement/casing case for vertical and horizontal wells can also be considered in the future.
- In this study, 50 pressure cycles were considered. In the future, more pressure cycles can be added as required.
- With the current trend of the energy transition concept, geothermal energy has been becoming popular. By changing the pressure rating, temperature rating of the material used for the wellbore simulator construction, similar wellbore simulators can be built to simulate the pressure and temperature conditions of a geothermal well and analyze the cement in the geothermal well.

## Bibliography

- American Petroleum Institute (API). (2019). Cements and Materials for Well Cementing (API SPEC 10A). Retrieved from [https://global.ihs.com/doc\\_detail.cfm?document\\_name=API%20SPEC%2010A&item\\_s\\_key=00128165](https://global.ihs.com/doc_detail.cfm?document_name=API%20SPEC%2010A&item_s_key=00128165)
- 260D Syringe Pump. (2021). Retrieved 18 June 2021, from <https://www.teledyneisco.com/en-us/pumpproducts/Pages/260D.aspx>
- Bachu, S., & Bennion, D. B. (2009). Experimental assessment of brine and/or CO<sub>2</sub> leakage through well cements at reservoir conditions. *International Journal of Greenhouse Gas Control*, 3(4), 494–501. <https://doi.org/10.1016/j.ijggc.2008.11.002>
- Backe, K., Lile, O., Lyomov, S., Elvebakk, H., & Skalle, P. (1997). Characterising Curing Cement Slurries by Permeability, Tensile Strength and Shrinkage. *All Days*. <https://doi.org/10.2118/38267-ms>
- Bannister, C. E. and Lawson, V. M. 1985. Role of Cement Fluid Loss in Wellbore Completion. Presented at the SPE Annual Technical Conference and Exhibition, Las Vegas, Nevada, 22–26 September. SPE-14433-MS. <https://doi.org/10.2118/14433-MS>.
- Bannister, C., Benge, O., & Marcinew, R. (1984). Critical Design Parameters To Prevent Gas Invasion During Cementing Operations. *Annual Technical Meeting*. <https://doi.org/10.2118/84-35-106>
- Barlow's Formula - Internal, Allowable and Bursting Pressure*. Engineeringtoolbox.com. (2021). Retrieved 21 July 2020, from [https://www.engineeringtoolbox.com/barlow-d\\_1003.html](https://www.engineeringtoolbox.com/barlow-d_1003.html).
- Baroghel-Bouny, V., Nguyen, T. Q., & Dangla, P. (2009). Assessment and prediction of RC structure service life by means of durability indicators and physical/chemical models. *Cement and Concrete Composites*, 31(8), 522–534. <https://doi.org/10.1016/j.cemconcomp.2009.01.009>

Basheer, L., Kropp, J., & Cleland, D. J. (2001). Assessment of the durability of concrete from its permeation properties: A review. *Construction and Building Materials*, 15(2–3), 93–103. [https://doi.org/10.1016/S0950-0618\(00\)00058-1](https://doi.org/10.1016/S0950-0618(00)00058-1)

Bauer, S. J., Wilson, J., Matteo, E. N., & Bettin, G. (2019, August 28). Permeability and Deformation Mechanisms During Triaxial Testing of Early-Age Cement. American Rock Mechanics Association.

Beirute, R., & Cheung, P. (1990). Method for Selection of Cement Recipes To Control Fluid Invasion After Cementing. *SPE Production Engineering*, 5(04), 433-440. <https://doi.org/10.2118/19522-pa>

Bentz, D. P., Garboczi, E. J., Haecker, C. J., & Jensen, O. M. (1999). Effects of cement particle size distribution on performance properties of Portland cement-based materials. *Cement and Concrete Research*, 29(10), 1663–1671. [https://doi.org/10.1016/S0008-8846\(99\)00163-5](https://doi.org/10.1016/S0008-8846(99)00163-5)

Bois, A., Garnier, A., Galdiolo, G., & Laudet, J. (2012). Use of a Mechanistic Model To Forecast Cement-Sheath Integrity. *SPE Drilling & Completion*, 27(02), 303-314. <https://doi.org/10.2118/139668-pa>

Bol, G., Grant, H., Keller, S., Marcassa, F., & de Rozières, J. (1991). Putting a Stop to Gas Channeling. *Oilfield Review*, 3(2), 35–43.

Bonett, A., & Pafitis, D. (1996). Getting to the Root of Gas Migration. *Oilfield Review*, 8(1), 36–49.

Boukhelifa, L., Moroni, N., James, S., Le Roy-Delage, S., Thiercelin, M., & Lemaire, G. (2004). Evaluation of Cement Systems for Oil and Gas Well Zonal Isolation in a Full-Scale Annular Geometry. *All Days*. <https://doi.org/10.2118/87195-ms>

Boulin, P., Bretonnier, P., Gland, N. and Lombard, J., 2012. Contribution of the Steady State Method to Water Permeability Measurement in Very Low Permeability Porous Media. *Oil & Gas Science and Technology – Revue d'IFP Energies nouvelles*, 67(3), pp.387-401.

Brace, W., Walsh, J., & Frangos, W. (1968). Permeability of granite under high pressure. *Journal Of Geophysical Research*, 73(6), 2225-2236. <https://doi.org/10.1029/jb073i006p02225>

Carey, J. W, Svec, R., Grigg, R., Zhang, J., & Crow, W. (2010). Experimental investigation of 220 wellbore integrity and CO<sub>2</sub>-brine flow along the casing-cement microannulus. *International Journal of Greenhouse Gas Control*, 4(2), 272–282. <https://doi.org/10.1016/j.ijggc.2009.09.018>

Carles, P., Egermann, P., Lenormand, R., & Lombard, J. (2007). Low permeability measurements using steady-state and transient methods. In *International Symposium of the Society of Core Analysts* (p. 3). Calgary; Institut Français du Pétrole.

Carpenter, R., Brady, J., & Blount, C. (1992). The Effects of Temperature and Cement Admixes on Bond Strength. *Journal Of Petroleum Technology*, 44(08), 936-941. doi: 10.2118/22063-pa

Carter, G., & Slagle, K. (1972). A Study of Completion Practices To Minimize Gas Communication. *Journal Of Petroleum Technology*, 24(09), 1170-1174.

<https://doi.org/10.2118/3164-pa>

Carter, L., Cook, C., & Snelson, L. (1973). Cementing Research in Directional Gas Well Completions. *All Days*. <https://doi.org/10.2118/4313-ms>

CELIA, M., BACHU, S., NORDBOTTEN, J., GASDA, S., & DAHLE, H. (2005). Quantitative estimation of CO<sub>2</sub> leakage from geological storage Analytical models, numerical models, and data needs. *Greenhouse Gas Control Technologies* 7, 663-671. doi: 10.1016/b978-008044704-9/50067-7

Chandler Engineering, Inc. 2015. Instruction Manual for Model 7200 Cement Hydration Analyzer. Part Number 7200-1050, Revision H, June 2015. Broken Arrow, OK: Chandler Engineering.

<http://www.chandlereng.com/media/ametechandlereng/files/pdfs/model%207200%20cement%20hydration%20analyzer%20manual.pdf> (accessed 04 July 2021).

Chandler Engineering, Inc. 2017. Model 7200 Cement Hydration Analyzer, <http://www.chandlereng.com/products/oilwellcementing/gas-migration/cement-hydration-analyzers/model7200> (accessed 04 July 2021).

Cheung, P., & Beirute, R. (1985). Gas Flow in Cements. *Journal Of Petroleum Technology*, 37(06), 1041-1048. <https://doi.org/10.2118/11207-pa>

- Coleman, J., & Corrigan, G. (1941). Fineness and Water-cement Ratio in Relation to Volume and Permeability of Cement. *Transactions Of The AIME*, 142(01), 205-215. doi: 10.2118/941205-g
- CUI, X., BUSTIN, A., & BUSTIN, R. (2009). Measurements of gas permeability and diffusivity of tight reservoir rocks: different approaches and their applications. *Geofluids*, 9(3), 208-223. <https://doi.org/10.1111/j.1468-8123.2009.00244.x>
- Darcy, H. (1856). *Les fontaines publiques de la ville de Dijon*. Paris: Dalmont.
- De Andrade, J., Sangesland, S., Todorovic, J., & Vrålstad, T. (2015). Cement Sheath Integrity During Thermal Cycling: A Novel Approach for Experimental Tests of Cement Systems. *All Days*. <https://doi.org/10.2118/173871-ms>
- Drecq, P., & Parcevaux, P. (1988). A Single Technique Solves Gas Migration Problems Across a Wide Range of Conditions. *All Days*. <https://doi.org/10.2118/17629-ms>
- Energy, I. (2021). What Are The Three Primary Methods Of Well Stimulation?. Retrieved 4 July 2021, from <https://www.infinitysol.net/chemical-toll-blending-blog/what-are-the-three-primary-methods-of-well-stimulation>
- Evans, G., & CARTE, L. (1962). Bounding Studies of Cementing Compositions to Pipe and Formations. In *Drilling and Production Practice*. New York: Onepetro.
- Feldman, R. (1974). Changes to structure of hydrated portland cement on drying and rewetting observed by helium flow techniques. *Cement And Concrete Research*, 4(1), 1-11. doi: 10.1016/0008-8846(74)90061-1
- Fischer, G., & Paterson, M. (1992). Chapter 9 Measurement of Permeability and Storage Capacity in Rocks During Deformation at High Temperature and Pressure. *International Geophysics*, 213-252. [https://doi.org/10.1016/s0074-6142\(08\)62824-7](https://doi.org/10.1016/s0074-6142(08)62824-7)
- Garcia, J., & Clark, C. (1976). An Investigation of Annular Gas Flow Following Cementing Operations. *All Days*. <https://doi.org/10.2118/5701-ms>

Garnier, A., Saint-Marc, J., Bois, A., & Kermanac'h, Y. (2008). A Singular Methodology To Design Cement Sheath Integrity Exposed To Steam Stimulation. *All Days*.  
<https://doi.org/10.2118/117709-ms>

Giot, R., Giraud, A., Auvray, C., Homand, F., & Guillon, T. (2011). Fully coupled poromechanical back analysis of the pulse test by inverse method. *International Journal For Numerical And Analytical Methods In Geomechanics*, 35(3), 329-359.  
<https://doi.org/10.1002/nag.897>

Goode, J. (1962). Gas and Water Permeability Data for Some Common Oilwell Cements. *Journal Of Petroleum Technology*, 14(08), 851-854. doi: 10.2118/288-pa

Goodwin, K., & Crook, R. (1992). Cement Sheath Stress Failure. *SPE Drilling Engineering*, 7(04), 291-296. <https://doi.org/10.2118/20453-pa>

Govinfo.gov. (2021). Retrieved 21 July 2020, from <https://www.govinfo.gov/content/pkg/CFR-2010-title49-vol3/pdf/CFR-2010-title49-vol3-sec192-113.pdf>.

Guyvoronsky, A.A., and Farukshin, L.K.: "Hydrostatic Pressure of Cement Slurry," *Neftyanik* (October 1963) 10, 30–32, translated from Russian.

Hefley, W.E., Seydor, S.M., et al. 2011. The Economic Impact of the Value Chain of a Marcellus Shale Well. Katz Graduate School of Business, University of Pittsburgh. August. Available from: <http://www.business.pitt.edu/faculty/papers/pittmarcellusshaleeconomics2011.pdf> [Accessed 29 June, 2021].

Hsieh P.A., Tracy J.V., Neuzil C.E., Bredehoeft J.D., Silliman S.E. (1981) A transient laboratory method for determination of the hydraulic properties of 'thigh' rocks - I. Theory, *Int. J. Rock Mech. Min. Sci. Geomech. Abstr.* 18, 245-252.

Jung, H. B., Jansik, D., & Um, W. (2013). Imaging wellbore cement degradation by carbon dioxide under geologic sequestration conditions using X-ray computed microtomography. *Environmental Science and Technology*, 47(1), 283–289. <https://doi.org/10.1021/es3012707>

Khalifeh M., Saasen A. (2020) General Principles of Well Barriers. In: Introduction to Permanent Plug and Abandonment of Wells. *Ocean Engineering & Oceanography*, vol 12. Springer, Cham. [https://doi.org/10.1007/978-3-030-39970-2\\_2](https://doi.org/10.1007/978-3-030-39970-2_2)

Kjellsen, K., & Jennings, H. (1996). Observations of microcracking in cement paste upon drying and rewetting by environmental scanning electron microscopy. *Advanced Cement Based Materials*, 3(1), 14-19. doi: 10.1016/s1065-7355(96)90065-6

Klinkenberg, L.J. "The Permeability Of Porous Media To Liquids And Gases." Paper presented at the Drilling and Production Practice, New York, New York, January 1941.

Kranz, R., Saltzman, J., & Blacic, J. (1990). Hydraulic diffusivity measurements on laboratory rock samples using an oscillating pore pressure method. *International Journal Of Rock Mechanics And Mining Sciences & Geomechanics Abstracts*, 27(5), 345-352.  
[https://doi.org/10.1016/0148-9062\(90\)92709-n](https://doi.org/10.1016/0148-9062(90)92709-n)

Kuanhai, D., Yue, Y., Yi, H., Zhonghui, L., & Yuanhua, L. (2020). Experimental study on the integrity of casing-cement sheath in shale gas wells under pressure and temperature cycle loading. *Journal Of Petroleum Science And Engineering*, 195, 107548.  
<https://doi.org/10.1016/j.petrol.2020.107548>

Kwon, O., Kronenberg, A., Gangi, A., & Johnson, B. (2001). Permeability of Wilcox shale and its effective pressure law. *Journal Of Geophysical Research: Solid Earth*, 106(B9), 19339-19353. <https://doi.org/10.1029/2001jb000273>

Lamik, A., Pittino, G., Prohaska-Marchried, M., Krishna, R., Thonhauser, G., & Antretter, T. (2021). Evaluation of Cement-Casing & Cement-Rock Bond Integrity During Well Operations. *Day 3 Thu, May 27, 2021*. doi: 10.2118/202186-ms

Lavrov, A., & Cerasi, P. (2013). Numerical modeling of tensile thermal stresses in rock around a cased well caused by injection of a cold fluid. 47th US Rock Mechanics/Geomechanics Symposium.

Lecampion, B., Abbas, S., & Prioul, R. (2013). Competition Between Transverse And Axial Hydraulic Fractures In Horizontal Wells. *Day 2 Tue, February 05, 2013*.  
<https://doi.org/10.2118/163848-ms>

Levine, D., Thomas, E., Bezner, H., & Tolle, G. (1979). Annular Gas Flow After Cementing: A Look At Practical Solutions. *All Days*. <https://doi.org/10.2118/8255-ms>



Li, J., Su, D., Tang, S., Li, Z., Wu, H., Huang, S., & Sun, J. (2021). Deformation and damage of cement sheath in gas storage wells under cyclic loading. *Energy Science & Engineering*, 9(4), 483-501. doi: 10.1002/ese3.869

Li, Z., Vandenbossche, J., Janssen, D., & Iannacchione, A. (2018). A Newly Developed Wellbore-Simulation Apparatus To Study Performance of Oilwell Cements. *SPE Drilling & Completion*, 33(02), 174-191. doi: 10.2118/191129-pa

Luffel, D., Hopkins, C., & Schettler, P. (1993). Matrix Permeability Measurement of Gas Productive Shales. *All Days*. <https://doi.org/10.2118/26633-ms>

Luping, T., & Nilsson, L. O. (1992). A study of the quantitative relationship between permeability and pore size distribution of hardened cement pastes. *Cement and Concrete Research*, 22(4), 541–550. [https://doi.org/10.1016/0008-8846\(92\)90004-F](https://doi.org/10.1016/0008-8846(92)90004-F)

Maharidge, R., Bottiglieri, A., Dighe, S., Holley, A., Zhang, H., & Koch, A. (2016). Development of Permeability and Mechanical Properties of Class G Cement from Slurry to Set. *SPE Annual Technical Conference And Exhibition*. doi: 10.2118/181512-ms

Morgan, B., & Dumbauld, G. (1952). Measurement of the Permeability of Set Cement. *Journal Of Petroleum Technology*, 4(06), 16-10. doi: 10.2118/952323-g

Muskat, M., & Meres, M. (1936). The Flow of Heterogeneous Fluids Through Porous Media. *Physics*, 7(9), 346-363. doi: 10.1063/1.1745403

Newman, K., & Wojtanowicz, A. (2001). *Improving Gas Well Cementing Through Cement Pulsatio* (p. 8). Conroe: CTES. Retrieved from [http://www.athenaeng.com/Content/publications/1999\\_2001\\_GRI\\_Cement\\_Pulsation\\_Project\\_Report.pdf](http://www.athenaeng.com/Content/publications/1999_2001_GRI_Cement_Pulsation_Project_Report.pdf)

OFI Testing Equipment, Inc. 2014. Laboratory Gas Flow Model, Fluid Gas Migration Analyzer #120-57, Instruction Manual. Version 1.16, updated 19 November 2014. <http://www.ofite.com/publications/instructions/104-120-57-instructions/file> (accessed 04 July 2021).

Opedal, N., Todorovic, J., Torsæter, M., Vrålstad, T., & Mushtaq, W. (2014). Experimental Study on the Cement-Formation Bonding. *Day 2 Thu, February 27, 2014*.

<https://doi.org/10.2118/168138-ms>

Ozyurtkan, M., Altun, G., Mihcakan, I., & Serpen, U. (2013). An Experimental Study on Mitigation of Oil Well Cement Gas Permeability. *All Days*. doi: 10.2523/iptc-16577-ms

*Parker's O-Ring Selector App*. Publish.vidavee.com. (2021). Retrieved 23 October 2020, from [https://publish.vidavee.com/publish/19EBD00875F8FD79A0D54BDC9EC5FEE7.doc?AF\\_deliveryChannel=landingpage&elqTrackId=77FFE797A2368A9A7DD8F604CF810D46&elqaid=10064&elqat=2](https://publish.vidavee.com/publish/19EBD00875F8FD79A0D54BDC9EC5FEE7.doc?AF_deliveryChannel=landingpage&elqTrackId=77FFE797A2368A9A7DD8F604CF810D46&elqaid=10064&elqat=2).

PVC-P vs. PTFE:: MakeItFrom.com. (2021). Retrieved 17 June 2021, from

<https://www.makeitfrom.com/compare/Plasticized-Flexible-Polyvinyl-Chloride-PVC-P/Polytetrafluoroethylene-PTFE>

Rogers, M. J., Dillenbeck, R. L., and Eid, R. N. 2004. Transition Time of Cement Slurries, Definitions and Misconceptions, Related to Annular Fluid Migration. Presented at the SPE Annual Technical Conference and Exhibition, Houston, 26–29 September. SPE-90829-MS.

<https://doi.org/10.2118/90829-MS>.

Sabins, F., Tinsley, J., & Sutton, D. (1982). Transition Time of Cement Slurries Between the Fluid and Set States. *Society Of Petroleum Engineers Journal*, 22(06), 875-882.

<https://doi.org/10.2118/9285-pa>

Scrivener, K. L., Crumbie, A. K., & Laugesen, P. (2004). The interfacial transition zone (ITZ) 234 between cement paste and aggregate in concrete. *Interface Science*, 12(4), 411–421.

<https://doi.org/10.1023/B:INTS.0000042339.92990.4c>

Shenyang Taige Oil Equipment Company Limited. 2017. Fluid (Gas) Migration Analyzer TG-7150. <http://rig123.com/Migration%20Analyzer%20TG-7150.html> (accessed 04 July 2021).

Skorpa, R., & Vrålstad, T. (2018). Visualization of Fluid Flow Through Cracks and Microannuli in Cement Sheaths. *SPE Journal*, 23(04), 1067–1074. <https://doi.org/10.2118/180019-PA>

*Steel Pipes - Temperature Derating*. Engineeringtoolbox.com. (2021). Retrieved 22 July 2020, from [https://www.engineeringtoolbox.com/temperature-derating-factor-steel-pipes-d\\_1744.html](https://www.engineeringtoolbox.com/temperature-derating-factor-steel-pipes-d_1744.html).

Tanikawa, W. and Shimamoto, T., 2009. Comparison of Klinkenberg-corrected gas permeability and water permeability in sedimentary rocks. *International Journal of Rock Mechanics and Mining Sciences*, 46(2), pp.229-238.

Taper Seal Connections | High Pressure Company. (2021). Retrieved 6 April 2021, from <https://www.highpressure.com/products/valves-fittings-tubing/taper-seal-valves-fittings-and-tubing/taper-seal-connections/>

Therond, E., Bois, A., Whaley, K., & Murillo, R. (2017). Large-Scale Testing and Modeling for Cement Zonal Isolation in Water-Injection Wells. *SPE Drilling & Completion*, 32(04), 290-300. <https://doi.org/10.2118/181428-pa>

Thiercelin, M., Dargaud, B., Baret, J., & Rodriguez, W. (1997). Cement Design Based on Cement Mechanical Response. *All Days*. <https://doi.org/10.2118/38598-ms>

Tinni, A., Fathi, E., Agarwal, R., Sondergeld, C., Akkutlu, Y., & Rai, C. (2012). Shale Permeability Measurements on Plugs and Crushed Samples. *All Days*. <https://doi.org/10.2118/162235-ms>

Tinsley, J. M., Miller, E. C., Sabins, F. L. et al. 1980. Study of Factors Causing Annular Gas Flow Following Primary Cementing. *J Pet Technol* 32 (8): 1427–1437. SPE-8257-PA. <https://doi.org/10.2118/8257-PA>.

Torsæter, M., Todorovic, J., & Lavrov, A. (2015a). Structure and debonding at cement-steel and cement-rock interfaces: Effect of geometry and materials. *Construction and Building Materials*, 96, 164–171. <https://doi.org/10.1016/j.conbuildmat.2015.08.005>

Viswanathan, H. S., Pawar, R. J., Stauffer, P. H., Kaszuba, J. P., Carey, J. W., Olsen, S. C., Keating, G. N., Kavetski, D., & Guthrie, G. D. (2008b). Development of a Hybrid Process and System Model for the Assessment of Wellbore Leakage at a Geologic CO<sub>2</sub> Sequestration Site. *Environmental Science & Technology*, 42(19), 7280–7286. <https://doi.org/10.1021/es800417x>

Vrålstad, T., Saasen, A., Fjær, E., Øia, T., Ytrehus, J., & Khalifeh, M. (2019). Plug & abandonment of offshore wells: Ensuring long-term well integrity and cost-efficiency. *Journal Of Petroleum Science And Engineering*, 173, 478-491. <https://doi.org/10.1016/j.petrol.2018.10.049>

Whitaker, S. (1986). Flow in porous media I: A theoretical derivation of Darcy's law. *Transport In Porous Media*, 1(1), 3-25. doi: 10.1007/bf01036523

Wilcox, B., Oyenehin, B., & Islam, S. (2016). HPHT Well Integrity and Cement Failure. *All Days*. <https://doi.org/10.2118/184254-ms>

Yang, X., Kuru, E., Gingras, M., Iremonger, S., Biddle, S., & Lin, Z. (2021). Characterization of the Microstructure of the Cement-Rock Interface Using Environmental Scanning Electron Microscopy and Micro-Computed Tomography Scan. *SPE Journal*, 1-18. doi: 10.2118/205512-pa

Yang, X., Kuru, E., Gingras, M., Iremonger, S., Chase, P., & Lin, Z. (2020). Characterization of the Microstructure of the Cement/Casing Interface Using ESEM and Micro-CT Scan Techniques. *SPE Journal*, 26(03), 1131-1143. doi: 10.2118/204227-pa

Yang, X., Kuru, E., Gingras, M., Iremonger, S., Taylor, J., Lin, Z., & Chase, P. (2020). Quantifying the Impact of 2D and 3D Fractures on Permeability in Wellbore Cement after Uniaxial Compressive Loading. *SPE Journal*, 25(05), 2265-2280. doi: 10.2118/198683-pa

Zeng, Y., Liu, R., Li, X., Zhou, S., Tao, Q., & Lu, P. (2019). Cement sheath sealing integrity evaluation under cyclic loading using large-scale sealing evaluation equipment for complex subsurface settings. *Journal Of Petroleum Science And Engineering*, 176, 811-820. <https://doi.org/10.1016/j.petrol.2019.02.014>

Zhao, C., Li, J., Liu, G., & Zhang, X. (2019). Analysis of the influence of cement sheath failure on sustained casing pressure in shale gas wells. *Journal Of Natural Gas Science And Engineering*, 66, 244-254. <https://doi.org/10.1016/j.jngse.2019.04.003>